



8-2001

Investigation into Schempp-Hirth airbrakes of sailplanes

Ignacio Agramunt

Follow this and additional works at: https://trace.tennessee.edu/utk_gradthes

Recommended Citation

Agramunt, Ignacio, "Investigation into Schempp-Hirth airbrakes of sailplanes. " Master's Thesis, University of Tennessee, 2001.

https://trace.tennessee.edu/utk_gradthes/9549

This Thesis is brought to you for free and open access by the Graduate School at TRACE: Tennessee Research and Creative Exchange. It has been accepted for inclusion in Masters Theses by an authorized administrator of TRACE: Tennessee Research and Creative Exchange. For more information, please contact trace@utk.edu.

To the Graduate Council:

I am submitting herewith a thesis written by Ignacio Agramunt entitled "Investigation into Schempp-Hirth airbrakes of sailplanes." I have examined the final electronic copy of this thesis for form and content and recommend that it be accepted in partial fulfillment of the requirements for the degree of Master of Science, with a major in Aviation Systems.

Uwe Peter Solies, Major Professor

We have read this thesis and recommend its acceptance:

Ralph D. Kimberlin

Accepted for the Council:

Carolyn R. Hodges

Vice Provost and Dean of the Graduate School

(Original signatures are on file with official student records.)

To the Graduate Council:

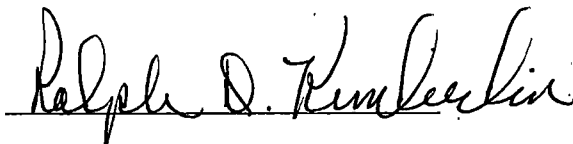
I am submitting herewith a thesis written by Ignacio Agramunt entitled "Investigation into Schempp-Hirth Airbrakes of Sailplanes".

I have examined the final copy of this thesis for form and content and recommend that it be accepted in partial fulfillment of the requirements for the degree of Master of Science, with a major in Aviation Systems.

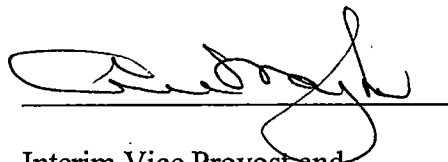


Dr. Uwe Peter Solies, Major Professor

We have read this thesis
And recommend its acceptance:



Accepted for the Council:



Interim Vice Provost and
Dean of The Graduate School

INVESTIGATION INTO SCHEMPP-HIRTH AIRBRAKES OF
SAILPLANES

A Thesis
Presented for the
Master of Science
Degree
The University of Tennessee, Knoxville

Ignacio Agramunt
August 2001

DEDICATION

To my family and friends

ACKNOWLEDGMENTS

The author would like to express his appreciation to several people for their assistance in this work.

He is grateful to the faculty of the Aviation Systems Department of The University of Tennessee Space Institute. Special thanks go to Dr. Uwe Peter Solies, academic advisor, professor, sailplane instructor and friend.

He would also like to extend his thanks to Prof.- Dr.-Ing. Wolfgang Alles and to Dipl.-Ing. Stefan Kirschstein from the Chair of Flight Dynamics of the Technical University of Aachen, for accepting him as a project member for this investigation. Mr. Kirschstein was his primary advisor for this work; his continuous support, patience and guidance in the preparation of the final document are greatly appreciated.

Recognition is given also to the FVA- Akaflieg Aachen members for the opportunity to participate with them in the 2000 Idaflieg Summer Meeting and for providing the test pilots and aircraft for this study.

Finally, for her continuous affective support while at UTSI, special thanks to P.

ABSTRACT

The present thesis is a study of airbrakes control forces and accelerations generated on the LS8 – Standard Class sailplane.

A flight test program was developed and conducted to measure the forces required to operate the Schempp-Hirth airbrakes of the LS 8 sailplane at several airspeeds inside the flight envelope and at several operating speeds. The accelerations produced after this operation were also measured and recorded. Additionally, a computer simulation for the longitudinal motion of the LS 8 was developed and presented.

The flight test program was conducted successfully and representative values for control forces and accelerations generated were recorded. The results from the flight experiments were compared with the current regulations for sailplanes (JAR 22) and, for the case of the accelerations, with the simulation results. For the operating forces, results are available only from the flight experiments. It was found that, in general, the flight test results compared favorably with the flight test data.

Practical procedures are recommended throughout the study.

Where do we come from?
Where are we going?
And...why in such a hurry?

Jean-Jacques Rousseau (1712-1788)

TABLE OF CONTENTS

CHAPTER	PAGE
1. INTRODUCTION	1
Definition	1
Objective	2
Organization of the study	4
Author participation in testing	8
2. BACKGROUND	10
Nomenclature	10
Airbrake aerodynamic characteristics	10
Airbrake Regulations	16
Handle forces human factors	19
3. EQUIPMENT	23
Aircraft	23
Instrumentation	27
4. FLIGHT TEST PROGRAM	33
Data requirements	33
Data recording	34
Instrument calibration and mounting	35
Airspeed calibration	38
Flight test plan	39
Safety considerations and test approach	41
Test conduct	42

CHAPTER	PAGE
5. FLIGHT TESTS RESULTS	45
Control forces	46
Accelerations	54
6. SIMULATION OF THE LONGITUDINAL MOTION	68
Objectives of the simulation	68
Structure of the simulation	69
Derivatives estimation	70
Wind tunnel derivatives scaling	72
Trim program	74
Simulink model	79
7. SIMULATION RESULTS	99
Time histories from simulation and flight tests	99
Results from simulation and flight tests	106
8. CONCLUSIONS AND RECOMMENDATIONS	111
REFERENCES	114
APPENDICES	118
A. Trim program (listing).	119
B. Derivatives look-up tables (listing).	122
C. LS 8 characteristics measured by Idaflieg	127
D. LS 8 airbrake system description	133
E. Examples of time histories obtained from the flight tests	136
VITA	141

LIST OF TABLES

TABLE	PAGE
1-1 Composite-structure Standard Class sailplanes with upper-surface only Schempp-Hirth airbrakes	5
2-1 Design values for male muscle strength of the arm for control forces	21
3-1 LS 8 Technical Specifications	24
4-1 Channels and Parameters in loggers A and B	34
4-2 Weight and balance information	42
4-3 Flight test log	44
6-1 Stability Derivatives	71
6-2 Scaling Factors	73

LIST OF FIGURES

FIGURE		PAGE
1-1	Wing section showing an upper-surface Schempp-Hirth airbrake	2
1-2	Upper-surface Schempp-Hirth airbrakes deployed for landing in a modern sailplane	3
1-3	Airfoil thickness vs year	6
1-4	Airbrake length vs year	6
2-1	Position of the airbrakes on the wings and body-fixed axis system	11
2-2	Axes and angles definition	11
2-3	Lift coefficient versus angle of attack	13
2-4	Speed polar diagram	15
2-5	Lift distribution along the span	15
2-6	Direction of force	22
3-1	LS 8 airbrake over the right wing	24
3-2	Side view of the LS 8 at the Aalen/Elchingen test site	25
3-3	Front view of the LS 8 at the Aalen/Elchingen test site	25
3-4	Detailed drawing of the LS 8	26
3-5	Flight Test Instrumentation	28
3-6	Data Acquisition Package	29

3-7	Accelerometer and rotation sensor	30
3-8	Force gage and wire-pull displacement transducer	31
3-9	Static and dynamic pressure sensors	32
4-1	Instrumentation layout	37
4-2	LS 8 Airspeed Calibration	38
5-1	Flight test data - LS 8 Flt # 3, exp # 5	47
5-2	Flight test data - LS 8 Flt # 3, exp # 5	47
5-3	Time histories for the airbrakes slow deployment at 6 different airspeeds	49
5-4	Force required (N) vs airbrakes height (%) at 6 different airspeeds	50
5-5	Forces vs calibrated airspeed	53
5-6	Gravity force in trim condition	55
5-7	Flight #3, experiment # 6 flight test data	56
5-8	Signals in the "trim" condition	58
5-9	Frequency content of the vertical acceleration and the pitch rate signals	58
5-10	Definition of a_z after the opening and closing maneuvers	59
5-11	Time histories for the airbrakes fast deployment at 6 different airspeeds	61
5-12	X-acceleration vs calibrated airspeed	62
5-13	Z-acceleration vs calibrated airspeed	63
5-14	X-acceleration vs calibrated airspeed	64
5-15	Z-acceleration vs calibrated airspeed	65
6-1	Longitudinal CG location for the simulation	69
6-2	Simulation structure	70

6-3	Balance of forces	76
6-4	Control surfaces scope	78
6-5	Simulink Model Structure	80
6-6	Model Main Screen	81
6-7	Aerodynamic Block	82
6-8	Static Block	83
6-9	Axes and angles	84
6-10	$C_{L\ stat}$ Block	85
6-11	$C_{D\ stat}$ Block	86
6-12	$C_{M\ stat}$ Block	86
6-13	CG location for the simulation	87
6-14	Delta M(s) Block	88
6-15	Dynamic Block	89
6-16	$C_{L\ dyn}$ Block	90
6-17	$C_{M\ dyn}$ Block	90
6-18	Sailplane Dynamics Block	91
6-19	Longitudinal Motion Block	93
6-20	States + Trigonometric Block	94
6-21	Accelerations Block	95
6-22	Atmosphere + Parameter Block	95
6-23	Atmospheric Model	97
6-24	Scheduling Parameters Block	98

7-1	Simulation scope windows	100
7-2	Simulation scope windows	101
7-3	Simulation-Flight test results	102
7-4	Simulation-Flight test results	103
7-5	Simulation-Flight test results	104
7-6	Simulation-Flight test results	105
7-7	Simulation results - Longitudinal acceleration generated after a sudden deployment and retraction of the airbrakes	106
7-8	Simulation results - Longitudinal acceleration generated after a sudden deployment and retraction of the airbrakes	107
7-9	Partial deployments at 53 m/s - Airspeed after 4 seconds vs % of airbrakes deployment	108
7-10	Partial deployments at 53 m/s- Longitudinal and vertical accelerations vs % of airbrakes deployment	109
7-11	Simplified airbrake over the wing surface	110
C-1	LS 8 Glide Ratio vs Calibrated Airspeed	129
C-2	LS 8 Speed Polar	130
C-3	LS 8 Lift Coefficient vs Fuselage Angle of attack Curve	131
C-4	LS 8 Drag Polar	132
C-5	LS 8 Modified Drag Polar	133
D-1	LS 8 Airbrake Control Mechanism - Fuselage	135
D-2	LS 8 Airbrake Control Mechanism - Wing	136

E-1	Flight Test Data – Accelerations and Pitch Rate	138
E-2	Flight Test Data – Airspeed, Accelerations and Airbrakes Position	139
E-3	Flight Test Data – Pitch Rate, Airspeed and Airbrakes Position	140
E-4	Flight Test Data – Airbrakes Control Force and Airbrakes Position	141

NOMENCLATURE

x		longitudinal (body-fixed) axis
y		lateral (body-fixed) axis
z		vertical (body-fixed) axis
X		longitudinal force
Y		lateral force
Z		vertical force
M		pitching moment
V		flight velocity (total)
V _{NE}		Never exceed speed
V _{S1}		Stall speed with flaps/airbrakes retracted
V _{SO}		Stall speed with flaps/airbrakes deployed
V _A		Maneuvering speed
q		pitch rate
α	(alpha)	angle of attack
γ	(gamma)	flight path angle
θ	(theta)	pitch angle
η	(eta)	elevator angle
a _x		longitudinal acceleration
a _z		normal (vertical) acceleration

s	height of airbrake over wing surface
Δ (delta)	increment
l (MAC)	mean aerodynamic chord
S	wing area
alpha_dot	angle of attack rate of change
C_l	lift coefficient
C_d	drag coefficient
C_m	pitching moment coefficient
v_t	total velocity
v_t dot	total velocity rate of change
u	longitudinal velocity
u_dot	longitudinal velocity rate of change
w	vertical velocity
w_dot	vertical velocity rate of change
rho	air density
qbar	dynamic pressure
alt	altitude
table_Cl_alpha1 ($C_L(\alpha)$)	look-up table for lift coefficient depending on angle of attack
table_Cd_alpha2 ($C_D(\alpha)$)	look-up table for drag coefficient depending on angle of attack

table_Cm_alpha3 ($C_M(\alpha)$)	look-up table for pitching moment coefficient depending on angle of attack
table_Cl_eta1 ($\Delta C_L(\eta)$)	look-up table for increment in lift coefficient depending on elevator angle
table_Cd_eta1_alpha1 ($\Delta C_D(\eta, \alpha)$)	look-up table for increment in drag coefficient depending on elevator angle and angle of attack
table_Cm_eta1 ($\Delta C_M(\eta)$)	look-up table for increment in pitching moment coefficient depending on elevator angle
table_Cl_alphadot_alpha1 ($C_{L_{\dot{\alpha}}}(\alpha)$)	look-up table for dynamic derivative $C_{L_{\dot{\alpha}}}$ depending on angle of attack
table_Cm_alphadot_alpha1 ($C_{M_{\dot{\alpha}}}(\alpha)$)	look-up table for dynamic derivative $C_{M_{\dot{\alpha}}}$ depending on angle of attack
Cl_q (C_{L_q})	dynamic derivative C_{L_q}
Cm_q (C_{M_q})	dynamic derivative C_{M_q}
table_Cl_s ($\Delta C_L(s)$)	look-up table for increment in lift coefficient depending on airbrake deployment

table_Cd_s ($\Delta C_D(s)$)

look-up table for increment in drag coefficient depending on airbrake deployment

table_Cm_s ($\Delta C_M(s)$)

look-up table for increment in pitching moment coefficient depending on airbrake deployment

ABBREVIATIONS

AGL	Above ground level
CG	Center of gravity
DLR	German Aerospace Agency
FAA	Federal Aviation Administration of the United States of America
FVA	Akaflieg Aachen (Students flying group)
ILR	Institute for Aeronautics and Astronautics of the Technical University of Aachen
JAA	Joint Aviation Authorities
JAR	Joint Aviation Requirements
MAC	Mean aerodynamic chord
USAF	United States Air Force
UTSI	University of Tennessee Space Institute
ZELL	Electronics Laboratory of ILR

CHAPTER 1

INTRODUCTION

DEFINITION

The airbrakes (also called dive brakes, speed brakes or spoilers) are aerodynamic devices used to prevent an aircraft from going faster than its never-exceed speed (V_{NE}) when it is in a dive. They are also used for approach control, since they allow an airplane to increase its descent angle without building up an excessive amount of speed.

Sailplane airbrakes are typically mounted on the wings. There are several types of airbrakes used in modern sailplanes. Some of these are:

- Schempp-Hirth airbrakes.
- Combination of trailing edge flap and airbrake system.
- Spoiler-type airbrake (hinged over the wing top surface)

The Schempp-Hirth airbrakes are named after the German manufacturer that developed them. They are also called conventional, since they are the most popular. There are two possible configurations for this type of airbrakes: upper/lower or upper-only configuration. The upper-only configuration consists of two flat surfaces extending from the wings and aligned perpendicular to the airflow.

The present study focuses on this type of airbrakes, particularly on the upper-surface only configuration. See figures 1-1 and 1-2.

OBJECTIVE

The objective of this study was to prepare and conduct a flight test investigation in order to evaluate the effectiveness of the Schempp-Hirth airbrakes in the context of the current regulations. The regulations are presented and discussed in Chapter 2.

The specific objectives were to measure the forces required to operate the airbrakes and the accelerations generated, in order to determine:

- 1) The sailplane acceleration (deceleration) as a function of airspeed and airbrakes operating speed.
- 2) The airbrakes operating force as a function of airspeed and operating speed.

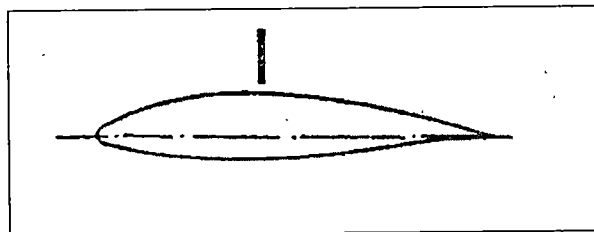


Figure 1-1

Wing section showing an upper-surface Schempp-Hirth airbrake

Modern sailplanes fly considerably faster today than 20 years ago. These higher flying speeds have led to the development of more powerful airbrakes, in order for them to properly accomplish their functions over the entire flight envelope of the sailplane. Nowadays the airbrakes are longer than their predecessors and –another problem- they are placed in thinner wings than before.

Wooden sailplanes designed in the 1950's typically feature Schempp-Hirth airbrakes in both upper and lower wing surfaces. The airbrake length in these sailplanes is about 1.0 m and their maximum flying speeds are about 190 km/h.

Composite materials sailplanes designed after the 1960's feature Schempp-Hirth airbrakes of both upper / lower surface and upper-surface only configurations. After the



Figure 1-2

Upper-surface Schempp-Hirth airbrakes deployed for landing in a modern sailplane

1970's the upper-surface only configuration has become the most popular. And the airbrakes power and dimensions have gradually increased. Table 1-1 shows a comparison of several Standard Class (15 m wingspan) composite-structure sailplanes. All the sailplanes in the table feature upper-surface only Schempp-Hirth airbrakes. The maximum flying speeds of these sailplanes has gradually increased; the latest sailplanes can fly up to 280 km/h.

Figures 1-3 and 1-4 show the present trends in airfoil thickness and airbrake length. It can be seen that the tendency is to produce sailplanes with longer airbrakes and to place them in thinner wings.

ORGANIZATION OF THE STUDY

As part of a research project leading to a more thorough understanding of the airbrakes operation characteristics and effects, the present investigation included the following:

- Planning and preparation of the flight test program
- Support of the flight tests
- Evaluation and discussion of the results
- Simulation of the longitudinal motion of the sailplane
- Assessment and documentation of the results of the flight tests and the simulation

Table 1-1

Composite-structure Standard Class sailplanes with upper-surface only Schempp-Hirth
airbrakes

YEAR (1 st flight)	AIRCRAFT	AIRFOIL THICKNESS (%MAC)	AIRBRAKE LENGTH (m)
1967	LS1c		0.93
1969	Std Cirrus	19.6	1.20
1972	D 38	18.4	1.35
1973	PIK 20D	17.0	1.20
1974	Astir CS	19.0	1.21
1975	ASW 19		1.20
1976	LS 3		1.38
1981	Falcon	17.2	1.30
1983	ASK 23		1.23
1987	DG 600	12.2	1.46
1988	LS 7		1.40
1993	DG 800	13.8	1.46
1994	LS 8		1.41

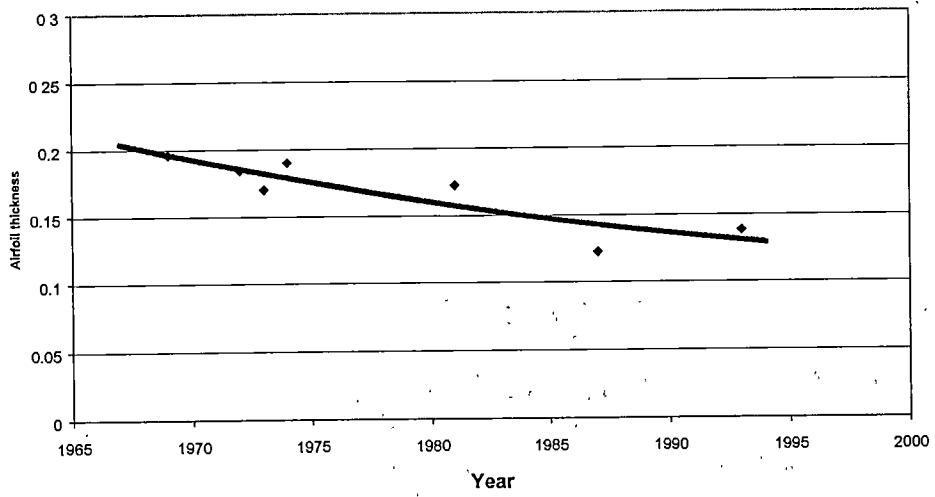


Figure 1-3

Airfoil thickness vs year

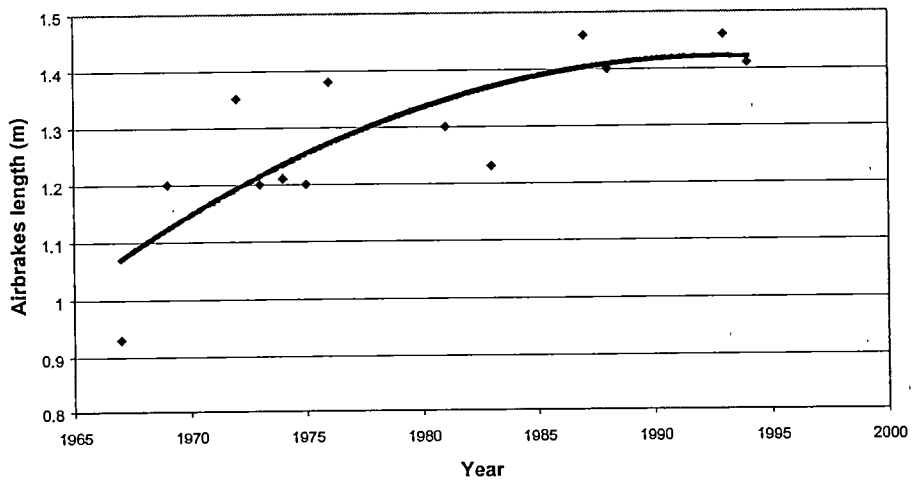


Figure 1-4

Airbrake length vs year

Although the present thesis deals only with the LS 8 sailplane, the flight test program was also developed to test other two modern sailplanes:

- The ASH 25 (open class, double seater)
- The ASK 21 (open class, double seater)

These sailplanes were selected because they are representative of typical sailplanes in the actual market and were readily available for the flight tests.

The flight tests were performed between July and August 2000 in two different locations, Aachen Merzbrück and Aalen-Elchingen, both in Germany. A total of 23 flight tests were conducted, as follows:

- 6 flight tests with the ASH 25
- 7 flight tests with the ASK 21 (including 2 flights with forward CG variation)
- 10 flight tests with the LS8 (including 2 flights with forward and 2 flights with aft CG variations)

This study discusses the results for only one of the sailplanes tested, the LS 8. However, the instrumentation, flight test program, procedures and analysis methods apply to the three aircraft.

A computer simulation using SIMULINK was developed, and is presented in order to help to visualize the sailplane motion caused by the airbrakes operation and to extrapolate some results above permissible flying speeds.

For this computer simulation, the aerodynamic derivatives used in the equations of motion were estimated using the software "Digital Datcom". The airbrakes control derivatives were estimated from wind tunnel experiments.

The results from the flight experiments are compared to those obtained from the simulation, for the case of the accelerations. For the operating forces, results are available only from the flight experiments.

AUTHOR PARTICIPATION IN TESTING

The flight test team consisted of the author, Mr. Stefan Kirschstein from the Institute of Flight Mechanics of the Technical University of Aachen, and Mr. Thomas Brinkmann from the FVA-Akaflieg Aachen (Students Flying Group). The Akaflieg Aachen also provided the test pilots for the experiments.

As a member of the flight test team, the author was directly involved in the calibration and mounting of the instrumentation in the three sailplanes tested, and he supervised all the flight tests. Additionally, as a sailplane pilot, he personally performed

the experiments flying on the back seat of the ASK 21. This helped to gain valuable insights on the peculiarities and limitations of testing the airbrakes, especially at high speeds.

CHAPTER 2

BACKGROUND

NOMENCLATURE

The axes, angles, forces and moments are defined in figures 2-1 and 2-2. Refer to page xiii for a complete listing of the nomenclature used.

Some comments on the nomenclature: "a_x" is defined as the longitudinal acceleration (acting along the x axis) and "a_z" is defined as the normal acceleration (acting along the z axis). The actual height of the airbrake over the wing surface is expressed as a percentage of the maximum height and is denoted by "s".

AIRBRAKE AERODYNAMIC CHARACTERISTICS

The Schempp-Hirth airbrakes are located typically about mid-span, to avoid aerodynamic interference with the tail surfaces or with the ailerons. The airbrakes primarily increase the parasite drag, but they also affect the lift distribution over the wings. The retracted airbrakes cause an irregularity on the wing surface that creates a slight flow disturbance where the airbrake caps fit into the wing. To keep the laminar flow over the wings and to avoid its transitioning to turbulent, the airbrakes are placed at

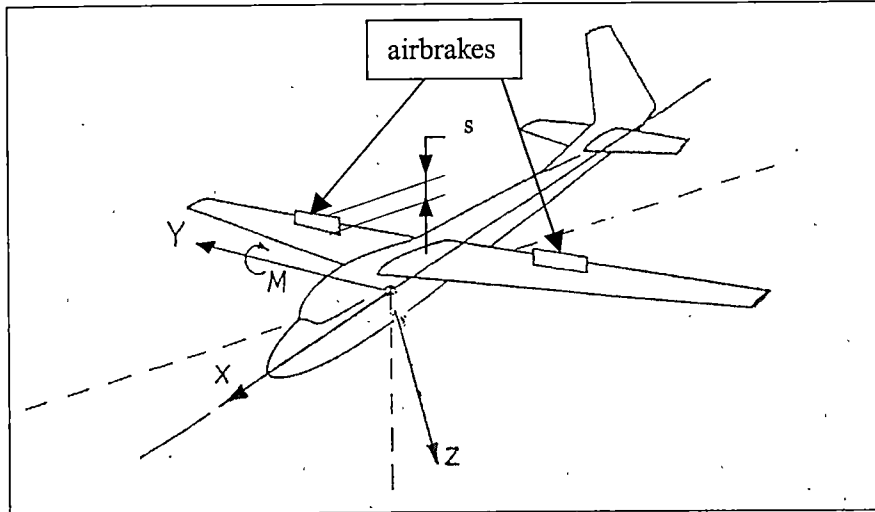


Figure 2-1

Position of the airbrakes on the wings and body-fixed axis system

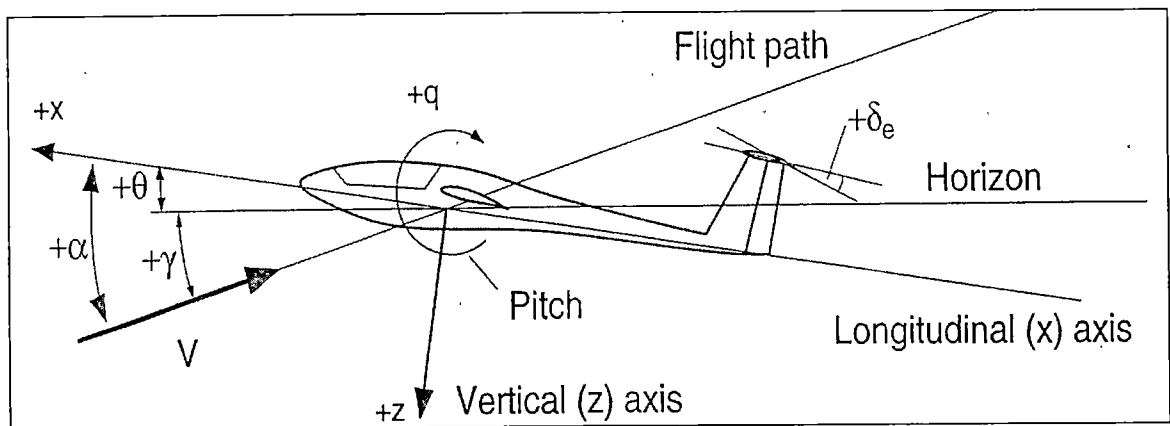


Figure 2-2

Axes and angles definition (from ref. 29)

50% or more of the chord, where the boundary layer thickness is large compared to the surface irregularity.

A wind tunnel study was conducted at the ILR of the RWTH Aachen. An airbrake was placed on a typical sailplane airfoil and the lift, drag and pitching moment characteristics were measured. The results are presented in the form of look-up tables in appendix B. It is interesting to note that, for an airbrake deployment of a certain height, the variation in lift coefficient with respect to the smooth airfoil is quite large when compared to the variation in drag coefficient. As an example, for an angle of attack of 3.6 degrees almost 50% of the total loss in lift coefficient occurs with only 15% deployment. On the other hand, the drag is not so sensitive: For the same angle of attack, to increase the drag by approximately 50%, a 40 % deployment is necessary.

In addition to the wind tunnel study discussed above, several aerodynamic characteristics of the upper surface airbrake are presented in this section to aid the reader to better visualize its effects. These characteristics include lift coefficient vs angle of attack, airspeed vs sink rate and lift distribution along the span. These results have been taken from reference 2.

The lift coefficient vs angle of attack characteristics for a typical sailplane airfoil (FX67 K-170) are shown in figure 2-3. The most important changes introduced into the

airfoil lift characteristics as a consequence of the airbrake extended on the upper surface only are:

small change in the slope of the lift-line: $dC_L/d\alpha$.

large change in the "zero lift" angle.

The airbrake characteristics are:

- position: 60% of chord
- air brake plate height: 11.4% of chord
- slot between the wing surface and the air brake lower edge: 3.6% of chord.

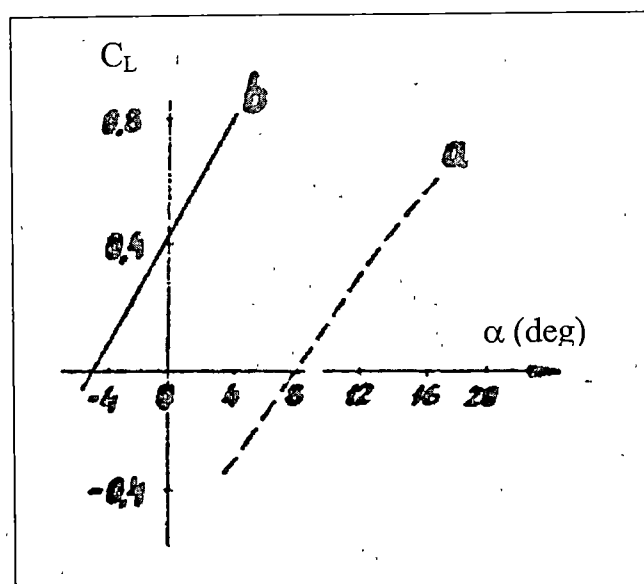


Figure 2-3

Lift coefficient versus angle of attack .

Line "a" is for the upper surface air brake extended configuration.

Line "b" is for the smooth airfoil.

A typical speed polar diagram is shown in figure 2-4. This polar corresponds to a SZD-42 "Jantar 2" sailplane.

The lift distribution along the span is shown in figure 2-5. The upper surface airbrake wing configuration produces greatly modified lift distribution along the span when compared with that of the smooth wing configuration. This modification leads to very serious increment of wing loading. Figure 2-5 yields to the following observations:

- For the smooth wing configuration (line "a") the lift distribution is nearly constant along the wing semi-span. (Note: A more realistic assumption will be to consider an elliptical lift distribution)
- For the air braked configuration (line "b") the lift distribution is considerably hollowed at the airbrake region and reaches a negative value.
- On the outer wing part the lift coefficient for the "air braked" configuration is higher than for the smooth one.
- The total lift of the smooth and air braked wing must be the same (assuming steady flight).

The author of reference 2 has, apparently, extrapolated a two-dimensional result from figure 2-3 to explain the three-dimensional situation of figure 2-5. The author of this thesis believes the lift distribution along the span with the airbrakes extended would present the behavior shown, but should be "smoother" (with no straight edges).

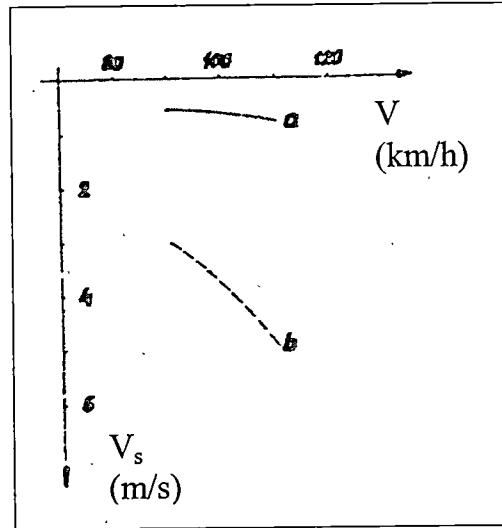


Figure 2-4

Speed polar diagram

Line "a" shows the smooth wing (airbrakes closed)
 Line "b" the upper surface airbrakes extended

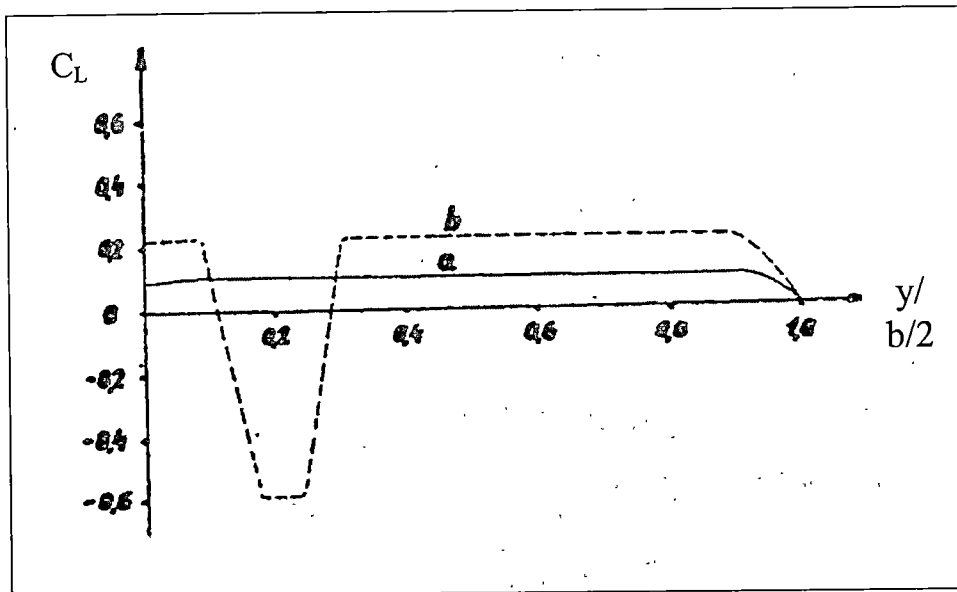


Figure 2-5

Lift distribution along the span

Line "a" shows the smooth wing (airbrakes closed)
 Line "b" the upper surface airbrakes extended

In the same reference cited, Robert T. Lamson wrote an editorial comment where he addressed the possibility of sailplane wings overloading in bending through spoiler (airbrakes) operation at high speeds. In his words: "The airbrakes destroy the lift at those wing stations spanned by them. This requires the generation of additional lift loading on the remaining wing panels (particularly on those outboard of the airbrakes) to maintain a given net lift value. The additional outboard loading transfer can be very abrupt if the airbrakes have a tendency to go full open at high speeds (which is the actual case, as demonstrated by the flight tests). This may lead to rapid increases in wing root bending moments on stiff winged sailplanes".

AIRBRAKE REGULATIONS

Sailplane regulations concerning airbrakes were made several years ago, when the airbrakes power and dimensions were small compared to the ones in present-day sailplanes.

JAR 22 contains regulations for sailplanes and powered sailplanes. According to it, the dive brakes must be sufficiently powerful to prevent the sailplane from exceeding V_{NE} in a dive of 45° (sailplanes certified for aerobatics or cloud flying) or 30° (all others). It must be possible to operate them safely at any speed up to $1.05 V_{NE}$. In addition, the dive brakes must provide a glide angle of 7:1 or steeper at $1.3 V_{so}$.

Other regulations that address airbrakes operation and characteristics are presented below.

Subpart B- Controllability and Maneuverability

JAR 22.143-General

This regulation states the maximum forces allowed at the control handles or pedals. Particularly, for the airbrakes handle and for a temporary force application the maximum limit is 20 daN (45 lbf). For a prolonged application no limit has been established.

JAR 22.145- Longitudinal Control

This regulation states that it must be possible throughout the appropriate flight envelope to change the configuration (landing gear, air brakes, wing-flaps, etc.) without exceptional piloting skills and without exceeding the control forces defined in JAR 22.143.

Additionally, it states that it must be possible, without exceptional piloting skills, to maintain the sailplane in steady straight flight when retraction or extension of the airbrakes is made at speeds between $1.1 V_{S1}$ and $1.5 V_{S1}$, where V_{S1} is the stalling speed with airbrakes retracted or extended, whichever is the higher, for a given flap position.

Subpart C- Control Surfaces and Systems

JAR 22.397-Loads Resulting From Limit Pilot Forces

This regulation states the design forces that the different control systems must withstand for the full range of motion up to and including the stops. For the airbrakes handle, this force is 35daN (79 lbf).

JAR 22.405-Secondary Control Systems.

This regulation states the minimum design loads assumed for structural design. For hand loads on levers and hand-grips, applied by the force of a supported arm or by making use of the body weight (this is the airbrakes handle case) this force is 60daN (135 lbf).

Subpart D- Control Systems

JAR 22.697-Wing-flap And Air-brake Controls

This regulation states that each wing-flap and air brake must be designed to prevent inadvertent extension or movement. The pilot forces and the rate of movement at any approved flight speed must not be such as to impair the operating safety of the sailplane.

Additionally, it states that it must be possible to extend the air brake at any speed up to $1.05 V_{NE}$ without causing structural damage and to retract the device at any speed up to V_A , with a hand force not exceeding 20 daN (45 lbf).

Finally, the time required for extension as well as retraction of the device may not exceed 2 seconds.

HANDLE FORCES HUMAN FACTORS

It is obvious that the maximum handle forces that the pilot needs to exert to operate the airbrakes must be within the ranges of which he or she is capable. As a reference and for comparison purposes, an excerpt from the FAA (Federal Aviation Administration of the United States of America) Human Factors Design Guide is presented here.

Table 2-1 and figure 2-6 show the male muscle strength of the arm for control forces. The values shown represent 80% of the maximum exertion forces for the 5th percentile male. For design, one does not want to deliberately or consistently require maximum exertions. Thus, these source values were reduced by 20% before applying them as design criteria. To estimate female strength, male data should be reduced by 43%.

The numbers presented in this table are for design purposes and do not represent the maximum forces that can be applied. This maximum force will depend on such factors as the type of control, the position of the arm during the control operations, the general position of the body, whether or not support is provided by backrests, and the frequency and time of operation.

For the case of the airbrakes handle operation, a 150° arm position can be assumed. The arm used is the left one. Thus, the following maximum forces for the 5th percentile man are:

- For pulling: 180 N (40.3 lbs)
- For pushing 128 N (28.8 lbs)

These values are only references for design. The real maximum forces that can be exerted should take into account following factors:

- The favorable seating position: having the arm and back well supported.
- The good handle grip.
- The infrequent and short time of operation.

All these factors are favorable and lead to higher maximum applicable forces.

Table 2-1

Design values for male muscle strength of the arm for control forces,
80 % of 5th percentile data, FAA Human Factors Design Guide, 2000.
Values in N (lbs)

<i>Degree elbow</i>	<i>Pull</i>	<i>Pull</i>	<i>Push</i>	<i>Push</i>
<i>Flexion</i>	<i>Left</i>	<i>Right</i>	<i>Left</i>	<i>Right</i>
180	177.6 (40)	184.8 (41.6)	149.6 (33.6)	177.6 (40)
150	149.6 (33.6)	199.2 (44.8)	106.4 (24)	149.6 (33.6)
120	120.8 (27.2)	149.6 (33.6)	92.8 (20.8)	128 (28.8)
90	113.6 (25.6)	132 (29.6)	78.4 (17.6)	128 (28.8)
60	92.8 (20.8)	85.6 (19.2)	78.4 (17.6)	120.8 (27.2)

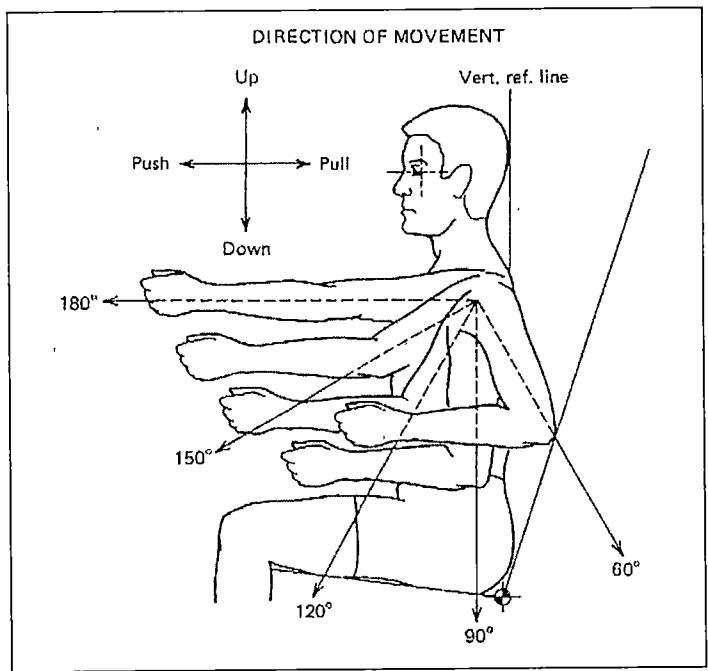


Figure 2-6

Direction of force

CHAPTER 3

EQUIPMENT

AIRCRAFT

The LS 8 is a Standard Class (single seat, 15 m wingspan, no flaps) sailplane. It is manufactured by Rolladen-Schneider Flugzeugbau GmbH in Germany. The model tested (registration number D 4477) belongs to the FVA- Akaflieg Aachen and features winglets. It has a retractable landing gear and a wheel brake controlled by a separate lever on the cockpit (not by the airbrakes handle as in many other sailplanes). It has water ballast tanks in the inner portion of the wings, as well as a vertical tail ballast tank. These characteristics allowed to change the center of gravity to a rear location for the flight tests.

The airbrakes are upper surface Schempp-Hirth, located at 50% of the local airfoil chord. They have a spanwise length of 1.410 m and a maximum height over the wing surface of 150 mm. See figure 3-1.

Several technical specifications are provided on table 3-1, and on the detailed drawing on figure 3-4. See also figures 3-2 and 3-3 for a side and front view of the aircraft.

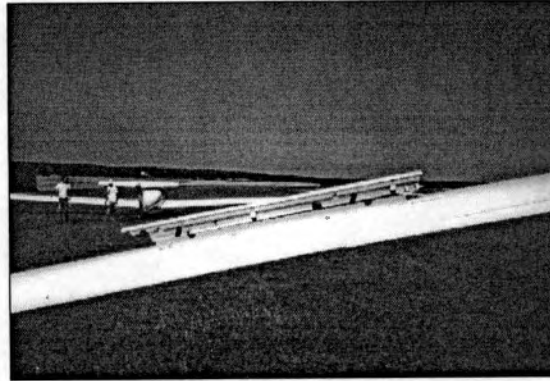


Figure 3-1

LS 8 airbrake over the right wing

Table 3-1

LS 8 Technical Specifications

Span	15 m	Allowed CG travel	280 – 400 mm (from LE wing/fus junction)
Wing area	10.50 m ²	Fuselage length	6.78 m
Wing aspect ratio	21.4	Min wing loading	31.9 daN/m ²
Wing airfoil	FX 81-K-130/148/17	Max wing loading	49.0 daN/m ²
Max. load factor (airbrakes in, 280 km/h)	+ 4.0 g - 1.5 g	Max. speed	280 km/h
Max. load factor (airbrakes out, 280 km/h)	+3.5 g 0 g	Min. speed	65 km/h
Max. load factor (190 km/h)	+5.3 g -2.6 g	Maneuvering speed	190 km/h
Empty mass	263 kg	Minimum sink	0.59 m/s at 82 km/h
Max. take-off mass	525 kg	Best glide ratio	42.5



Figure 3-2

Side view of the LS 8 at the Aalen/Elchingen test site



Figure 3-3

Front view of the LS 8 at the Aalen/Elchingen test site

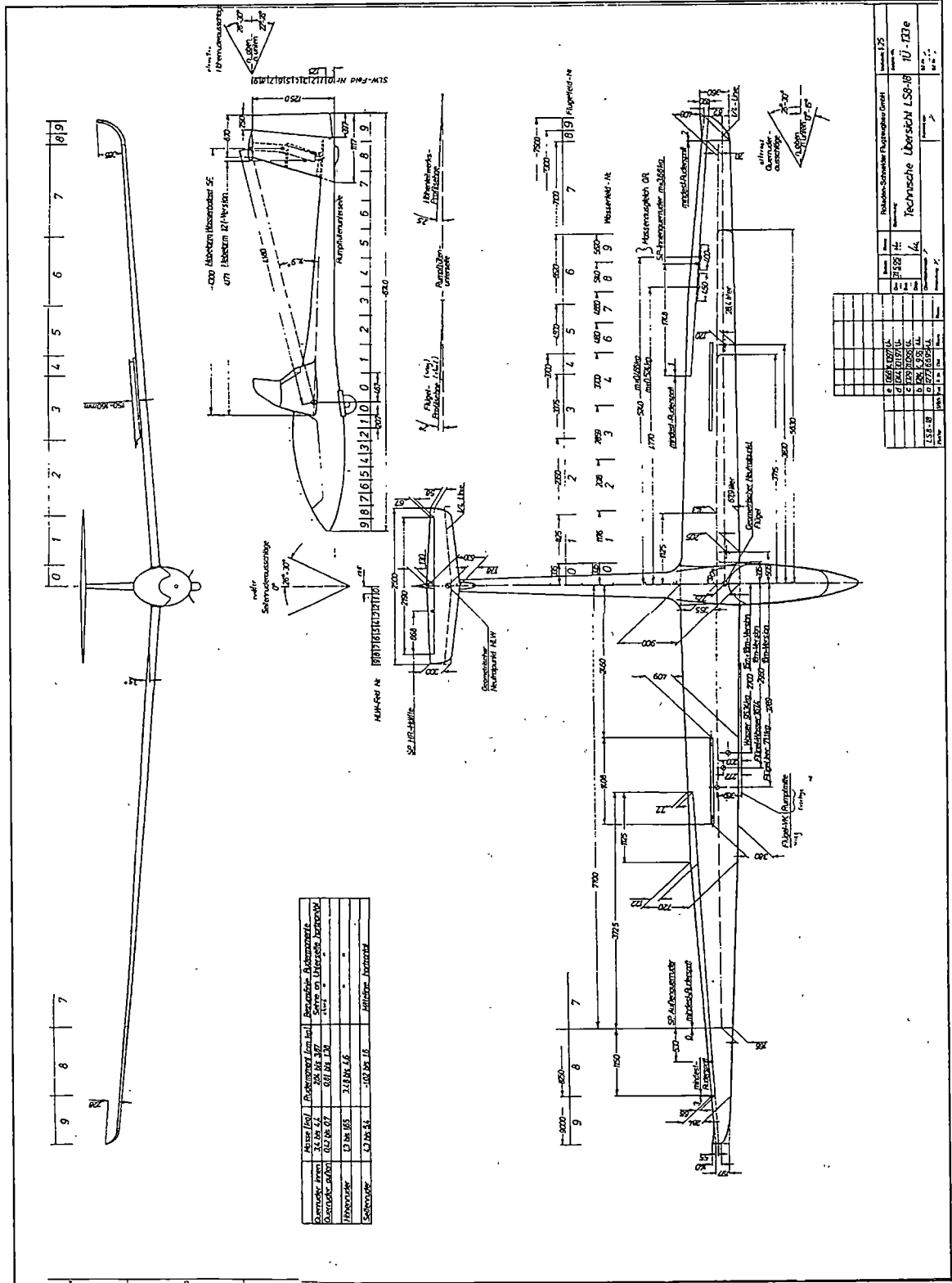


Figure 3-4 - Detailed drawing of the LS 8

INSTRUMENTATION

The instrumentation used in the flight test program was prepared by the Electronic Laboratory (ZELL) of the ILR of the RWTH Aachen. It was designed as a (portable) strap-on package. Figure 3-5 shows a display of the instrumentation used.

The flight test instrumentation included the following items: data loggers, signal conditioning accessories, tri-axial accelerometer, pitch rate sensor, temperature sensor, static and dynamic pressure sensors, wire-pull displacement transducer (with its correspondent amplifier), force measuring device and battery pack. In addition, a portable computer (laptop) was used throughout the process to save the data stored on the data loggers.

The signal conditioning accessories were implemented together with the data loggers and the transducers ports in a small box. These accessories amplify low-level signals, and isolate, filter, excite and bridge complete transducers to produce appropriate signals for the data acquisition hardware and software.

A more detailed description of the principal instrumentation elements-data loggers, tri-axial accelerometer, solid state rotation sensor, force measuring device, draw wire displacement transducer-follows.

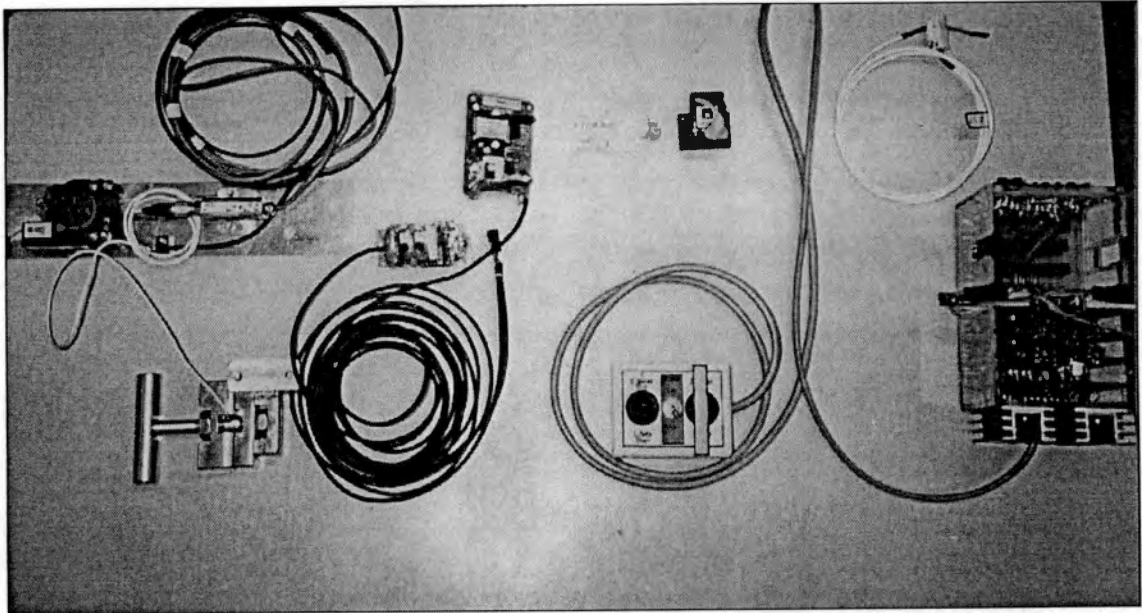


Figure 3-5

Flight Test Instrumentation

DATA LOGGERS (Figure 3-6)

The data loggers for the flight test program had to be installed in a very small space in the sailplanes. Thus, the two main considerations for the selection of the data loggers (and in general for the whole instrumentation package) were weight and size.

Two data loggers were used. The following are their most important features:

- Mass: 16 g
- Dimensions: 28 x 12 x 42 mm
- Operating voltage/current: 5V / 4mA, with 2-4 batteries.
- Storage capacity: 8 bit / 128 kB RAM / 16384 data points

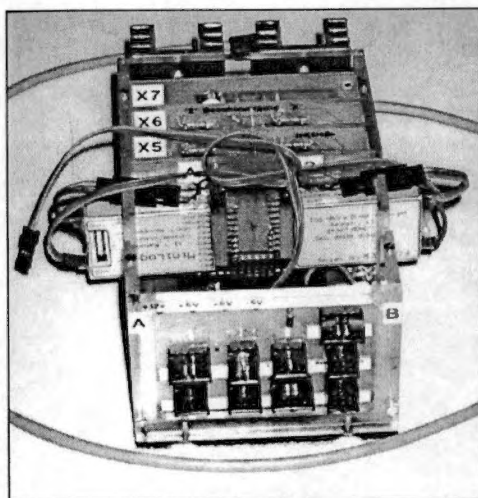


Figure 3-6

Data Acquisition Package showing the 8 transducer connectors, both data loggers and the signal conditioning accessories

TRI-AXIAL ACCELEROMETER (Figure 3-7)

Manufactured by Summit instruments, model 34103A.

Range: +/- 1 g to +/- 7.5 g (full scale measurement).

Sensitivity: 420 mV/g (at 25°C).

For the purposes of this investigation only the x and z sensitive axes were used.

SOLID-STATE ROTATION SENSOR (Figure 3-7)

Manufactured by Systron Donner Inertial Division, model GyroChip II QRS14-00100-102.

Range: +/- 100°/s.

Sensitivity: 15 mV/°/s

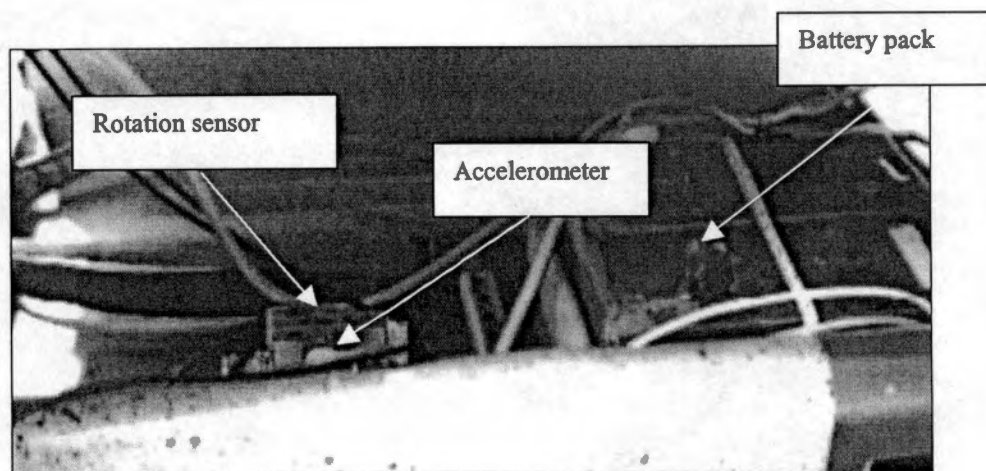


Figure 3-7

Accelerometer, rotation sensor and battery pack behind the pilot's seat

FORCE MEASURING DEVICE (Figure 3-8)

The force measuring device consisted of a clamp (manufactured to fit the airbrakes handle) and a load cell. The force device measured only forces in the direction of the handle motion.

The load cell is manufactured by AMOS Sensoren & Messtechnik, model KALM-170-MKA/1. This transducer is able to measure compression as well as tension loads. It provides an output signal which is linear and proportional to the applied load.

Range: It was adjusted to cover the range from -500 N to 500 N .

Sensitivity: $1.5\text{-}10\text{ mV/V}$ (foil - semiconductor sensor element).

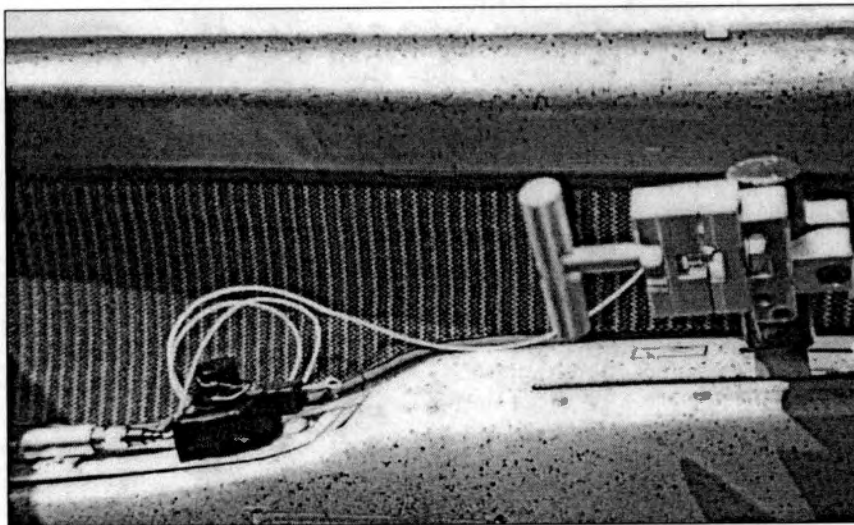


Figure 3-8 - Force gage and wire-pull displacement transducer

DRAW WIRE DISPLACEMENT TRANSDUCER (Figure 3-8)

Manufactured by Waytec Positionsmesstechnik GmbH

Model: LX-PA

Range of measurement: 0 - 700 mm

Weight: 85 g

Figure 3-9 shows the air pressure sensors.

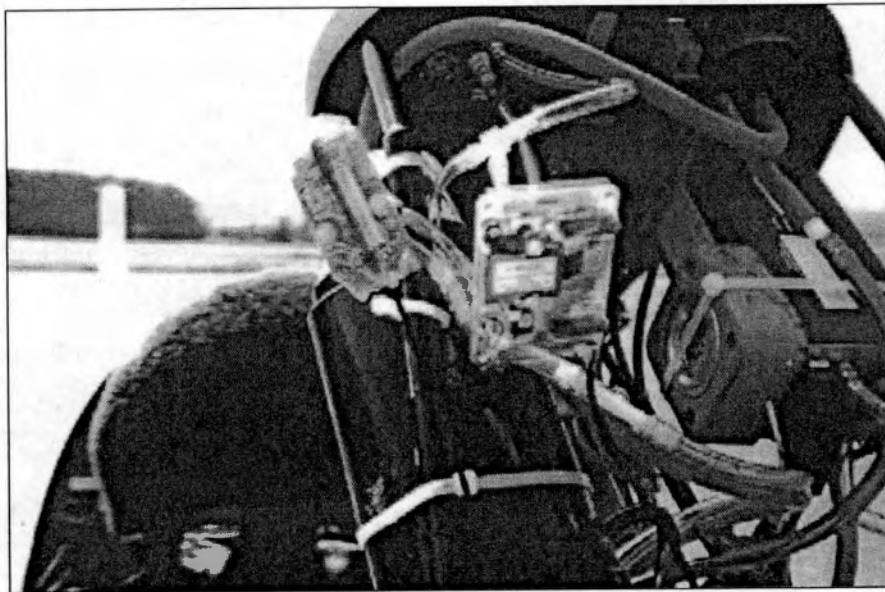


Figure 3-9

Static and dynamic pressure sensors behind the instrument panel

CHAPTER 4

FLIGHT TEST PROGRAM

The flight tests were the essential part of the present investigation. Compliance with regulatory requirements, such as those pertaining to airbrakes operating characteristics, can be demonstrated only by flight tests. This chapter describes the flight test program, with special emphasis on the planning stage and on the procedures followed on the actual flight tests. The flight test results will be discussed in the next chapter.

DATA REQUIREMENTS

In order to meet the specified objectives, the following parameters were collected in each of the test flights:

- Static and dynamic pressure
- Airbrakes position
- Accelerations in x and z directions (longitudinal and vertical body-fixed axes)
- Forces on the airbrakes handle
- Pitch rate
- Temperature

DATA RECORDING

The preceding parameters were recorded in two data loggers, A and B.

Table 4-1 shows the parameters recorded in each of the loggers.

The sampling rate used during the flight experiments was 92 Hz. With this setting the data loggers were able to store 180 seconds of data on each of their four channels.

After every flight the data stored on the loggers was recorded on the portable computer and converted to a spreadsheet file (Excel).

Table 4-1

Channels and Parameters in loggers A and B

CHANNEL	LOGGER A	CHANNEL	LOGGER B
1	dynamic pressure	1	normal acceleration
2	static pressure	2	longitudinal acceleration
3	Temperature	3	position of the handle
4	force in the handle	4	pitch rate

INSTRUMENT CALIBRATION AND MOUNTING

All the sensors used in the flight test program had calibration certificates from the respective manufacturer. In addition, special calibrations were performed for the force-measuring device and for the airbrakes handle position sensor.

Since the force-measuring device consisted of an assembly (clamp, handle and load cell) a calibration curve was obtained using standard weights. The draw wire position sensor was calibrated at the test site after the force-measuring device was mounted on the sailplane control handle. A correlation between the actual airbrake height over the wing and the longitudinal position of the control handle was obtained.

The adequate mounting of the instrumentation on the aircraft was a crucial part of the test program. The accelerometer was positioned as close as possible to the aircraft center of gravity to obtain an adequate measurement of the acceleration of the vehicle. The small baggage compartment behind the pilot's seat served as an appropriate location. In addition, it had to be positioned in a way such that its sensitive axes were aligned with the body-fixed axes system. This was accomplished by mounting it on a "reference platform" that was properly aligned with the body fixed axes. The rotation sensor was also mounted on this platform.

The reference platform consisted of two parallel plates separated by regulating screws. The bottom plate was fixed to the baggage compartment surface; the top plate (where the sensors were mounted) orientation was adjustable. The alignment of the top plate with the body axes was done prior to the mounting of the sensors on it. This was accomplished by means of comparing the adequate reference surface (in this case the bottom surface of the rear fuselage) and the top plate surface with an "spirit level" instrument and then adjusting the plate orientation to match the reference.

The data acquisition package (including its battery pack) was mounted on the same location as the inertial sensors. The force-measuring device was installed on the control handle after removing its plastic grip. The draw wire position transducer with its correspondent amplifier was installed on the left arm rest, while the power switch that controlled the start/stop of the measurements was installed on the right arm rest. The air pressure sensors were installed behind the instrument panel and connected in parallel to the aircraft's instruments by means of additional plastic hoses. Finally, the temperature sensor was mounted on the nose, next to the pitot tube. Figure 4-1 shows the general layout of the instrumentation.

The instrumentation was appropriate and functioned properly. Particularly important were its portable characteristics: the whole instrumentation package was designed to be removable in a relative short time, in order for the aircraft to be usable for normal flight operations. The total average time required to install it on the sailplane was

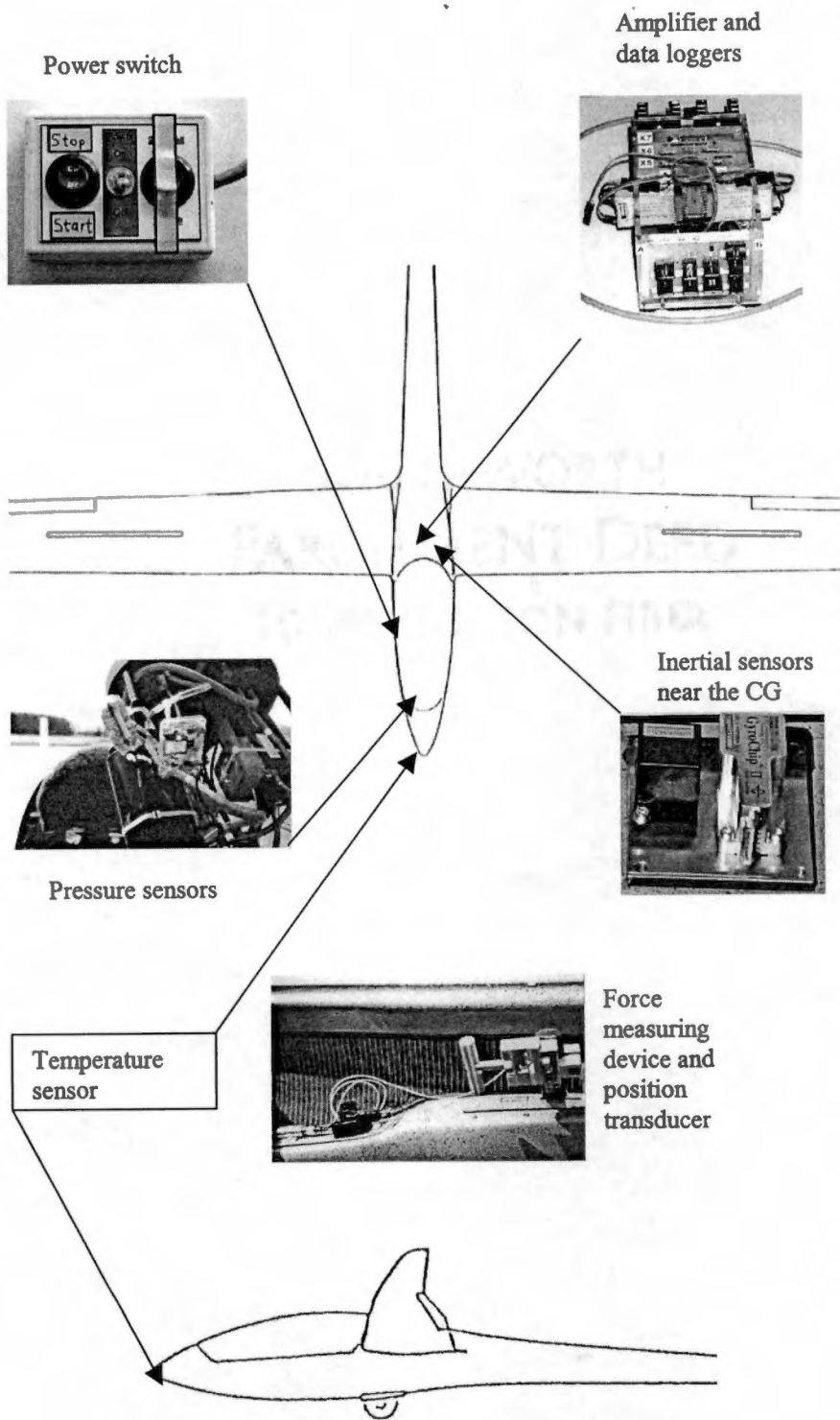


Figure 4-1
Instrumentation layout

about 90 minutes. This time included the alignment of the reference platform with the respective longitudinal and vertical axes and the mounting of all the sensors.

AIRSPEED CALIBRATION

An airspeed calibration was performed in order to correct the indicated airspeed for position errors. This calibration was accomplished using the trailing bomb method with a precision airspeed indicator (Thommen) with minimum instrument error. To avoid atmospheric disturbances the calibration was done early in the morning (6:30 am). The results are presented in figure 4-2.

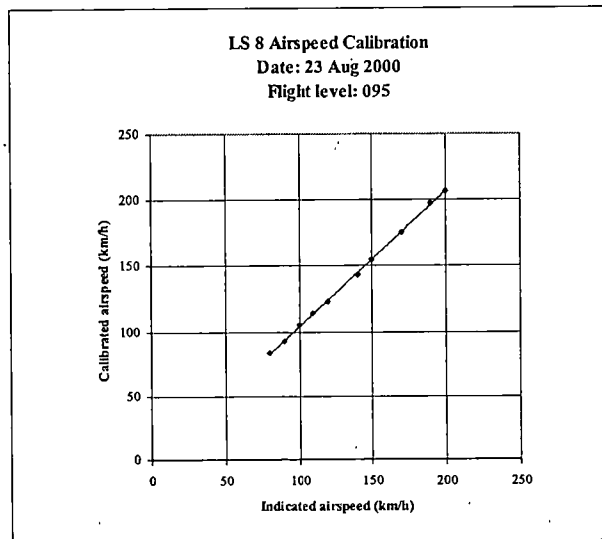


Figure 4-2

LS 8 airspeed calibration

FLIGHT TEST PLAN

The flight test plan was designed to provide experimental data on the effects of the airbrakes operation for both control forces and accelerations, with special emphasis on the safety considerations. In order to meet these objectives the following plan was prepared and executed:

- 1) The sailplane was towed up to the test altitude. The actual release altitude was determined based on the target airspeeds and on the number of experiments planned for that flight. It ranged between 1500 m and 2500 m AGL.
- 2) Once the airspace was cleared and with the sailplane flying at a relatively low airspeed (between 100 and 120 km/h), the airbrakes mechanism was unlocked.
- 3) The airbrakes were closed completely, but without locking the system. The flight test engineer performing the maneuver checked that the airbrakes were completely retracted by looking over the wings.
- 4) The sailplane was then trimmed at the highest target airspeed. Tolerance: +/- 5% .
- 5) When the pilot called out a stabilized condition ("trim"), the data loggers were started by means of the power switch.

- 6) The airbrakes were deployed using a "slow" operating speed (about 4 seconds for the total travel of the handle).
- 7) The airbrakes were hold in the open position for between 3 to 6 seconds.
- 8) The airbrakes were closed using a "slow" operating speed.
- 9) The data recording was stopped.
- 10) Steps 2 to 7 above were repeated for all the target airspeeds to be tested on the flight.
- 11) Steps 1 to 7 above were performed for a "fast" operating speed (operating the airbrakes handle as fast as possible).
- 12) The center of gravity was changed and the above procedure was repeated for some selected airspeeds.

The test maneuver was performed holding the control stick in a fixed position, since measuring only the airbrakes effects was the objective of the present investigation.

SAFETY CONSIDERATIONS AND TEST APPROACH

For the specific airspeeds to be tested on each flight a speed build-up method was used, as follows:

- a) On the first flight a moderate maximum airspeed (170 km/h) was chosen. This airspeed was tested first, immediately after releasing, since the available altitude was the highest (no “thermaling” was used to gain altitude throughout the test program). The target airspeeds were then progressively decreased by 20 km/h until the minimum test speed or the minimum safety altitude (determined by the pilot, about 500 m AGL) was reached.
- b) For the subsequent flights, the maximum target airspeed (and the first to be tested) was increased about 20 km/h with respect to the previous flight, and the other speeds were progressively decreased as in a).
- c) Six or seven airspeeds were tested on each flight

This approach ensured having a safe altitude for the high speed testing, a progressive increase of the maximum airspeed and a way to back-up several measurement points. The pilot used a parachute on all the flights.

TEST CONDUCT

A total of ten flight tests were conducted with the LS 8 at the Aalen/Elchingen location during the annual Idaflieg (Association of the Akafliegs) Summer Meeting. The flight tests with the LS 8 were performed on August 16-18, 2000 following the plan detailed in the preceding section. The weather conditions were optimum during the majority of the flights, with good visibility and no significant turbulence encountered.

The test pilots were Mr. Ralf Schneider and Mr. Jens Kämmer, both from the Akaflieg Aachen. The weight and balance information is shown in table 4-2. The CG location, pilot arm and rear ballast arm are specified in mm behind the leading edge of the wing at the wing and fuselage junction.

Table 4-2
Weight and balance information

PILOT WEIGHTS (W/ PARACHUTE)	Schneider : 82 kg Kämmer: 90 kg
AIRCRAFT EMPTY WEIGHT	263 kg
EMPTY CG LOCATION	623 mm
PERMISSIBLE CG TRAVEL	280 - 400 mm
ARM PILOT	430 mm
ARM REAR BALLAST	4300 mm

The author together with Mr. Kirschstein supervised the flight tests and controlled the aircraft loading and the airspeeds to be tested. The pilot was briefed before each flight and the target airspeeds were provided in a table carried on board. After the flight, the recorded data was inspected, the pilots were interviewed and the relevant comments recorded.

Flights 1-6 were performed with a typical CG location (pilot without any ballast), while flights 7-8 were performed with a forward CG location and flights 9-10 with a rear CG location. Flights 1,2 and 3 tested "slow" airbrakes operating speeds. The other flights, 4-10, tested "fast" operating speeds. The flight test log is shown on table 4-3. Specific comments were also recorded on the log.

Table 4-3

Flight test log

FLIGHT #	PILOT	CG LOCATION	TAKE-OFF/LANDING TIMES
1	Schneider	373 (typ.)	07:25/07:45
2	Schneider	373 (typ.)	08:07/08:30
3	Schneider	373 (typ.)	09:30/09:56
4	Schneider	373 (typ.)	11:51/12:13
5	Kämmer	362 (typ.)	08:33/09:05
6	Kämmer	362 (typ.)	09:50/10:17
7	Kämmer	312 (fwd.)	11:40/12:10
8	Kämmer	312 (fwd.)	12:55/13:28
9	Kämmer	399 (aft)	11:27/11:54
10	Kämmer	399 (aft)	12:02/12:26

CHAPTER 5

FLIGHT TEST RESULTS

The results of the flight test experiments for both control forces and accelerations generated after the airbrakes operation are presented in this chapter. The data reduction and analysis methods are also discussed.

Regarding the operating speeds, it has to be noted that "slow" operating speed refers to an opening maneuver involving between 2 to 4 seconds to complete the total deployment; this can be considered a ramp input, since the deployment rate was nearly constant. In the other hand, "fast" operating speeds can be considered step inputs; the total time for completing the opening maneuver ranged between 0.1 and 0.2 seconds.

For the operating speeds for the closing maneuver, the same previous convention applies. It must be noted, however, that the "fast" closing maneuver times were higher than those achieved in the "fast" openings. These closing times ranged between 0.2 and 0.5 seconds for the complete closing of the airbrakes. The reason for this is that the pilots exercised special caution to prevent any kind of system damage that could be induced by an abrupt maneuver. The airbrakes were only closed up to maneuvering speed, according to the sailplane operating limitations.

An example of the data collected is shown in appendix E.

CONTROL FORCES

The forces required to operate the airbrakes were measured for “slow” and “fast” operating speeds, for both the opening and closing maneuvers.

The fifth experiment of flight number three was selected to serve as a model to visualize the type of data obtained and the analysis procedure followed. Figure 5-1 shows the airbrakes height and the sailplane airspeed as a function of time for this experiment. The trim airspeed (before performing the maneuver) was 43 m/s (155 km/h). Note that at time = 138.0 seconds the airbrakes began to open and at time = 138.2 they reached their maximum height. As explained before, this is considered a “fast” opening maneuver. For the closing maneuver in this same experiment a similar operating speed was reached: about 0.2 seconds were required to fully close the airbrakes. Another fact that can be observed from figure 5-1 is a progressive decrease in airspeed following the opening of the airbrakes: the airspeed dropped from 43 m/s to 38 m/s in 3.9 seconds.

Figure 5-2 shows the force vs time data for the same experiment. The forces were measured with respect to the neutral condition (no force applied). The analysis consisted in finding the peak forces exerted by the pilot on the airbrakes control handle. A negative force indicates that the pilot exerted a “pushing” force, while a positive force indicates that he exerted a “pulling” force. For this particular experiment a maximum pulling force

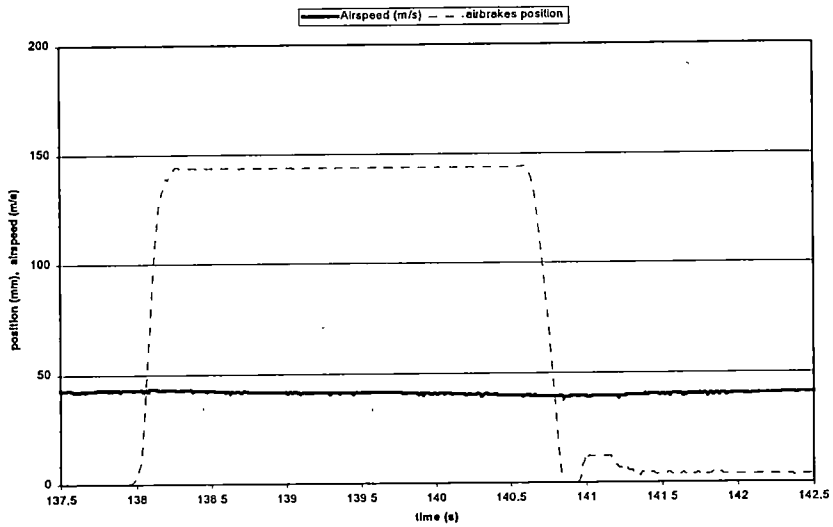


Figure 5-1 - Flight test data - LS 8 Flt # 3, exp # 5

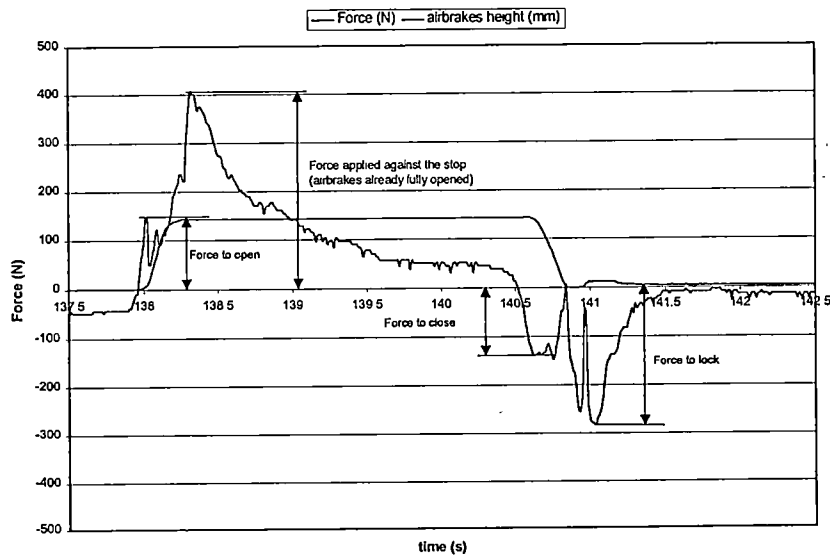


Figure 5-2 - Flight test data - LS 8 Flt # 3, exp # 5

of 400 N was measured to open the airbrakes (sudden deployment), and a 150 N pushing force to close them. The locking force was about 290 N.

Some of the inputs applied for measuring the opening control forces with “slow” operating speeds are shown in figure 5-3. It can be seen that these six inputs are very similar among them: the time required for a complete opening is about four seconds for every case. They represent a typical “slow” opening maneuver. The forces measured with these operating speeds are representative of the real operating forces required. If the maneuver is performed with “fast” operating speeds the inertia effects can lead to incorrect force measurements.

Figure 5-4 is a plot of handle forces vs airbrakes position (height over the wing surface, in %) that corresponds to the inputs of figure 5-3. The six sailplane airspeeds cover the entire flight envelope. It can be seen that, once the airbrakes were unlocked, almost no force was required to open them; the airflow tended to “pop” them open, so a pushing force was required to prevent them from fully opening. This holding force gradually decreased and disappeared at about 20% height. Then the sense of the operating force reversed. After this, a slight and nearly constant force was required to continue with the opening process up to about 55% height. This pulling force increased with increasing airspeed. Finally, a pulling force was required to fully extend the airbrakes. The experiments show that this force gradually increased with increasing airspeed.

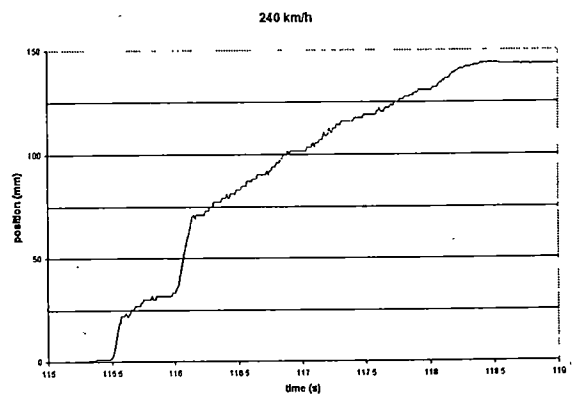
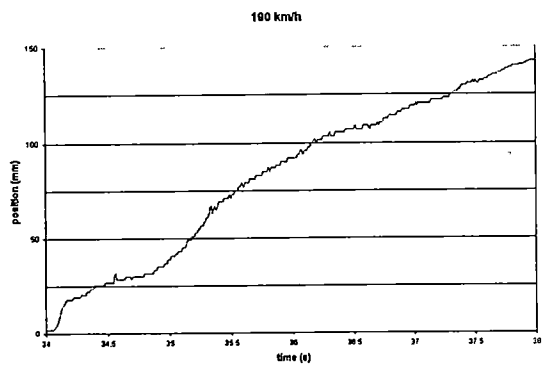
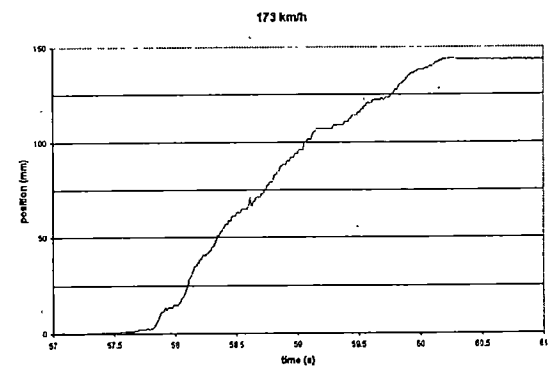
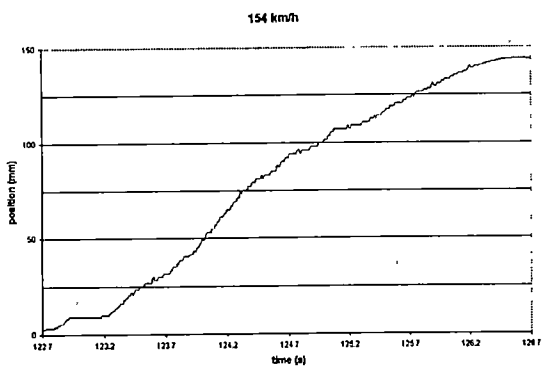
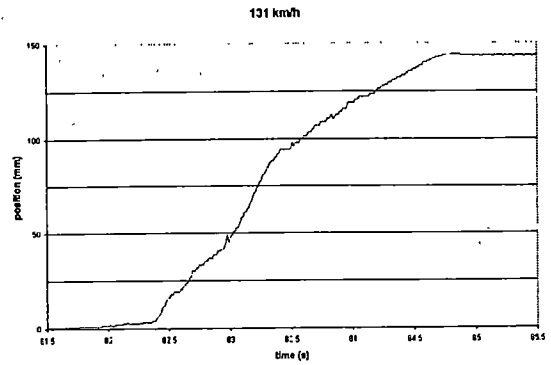
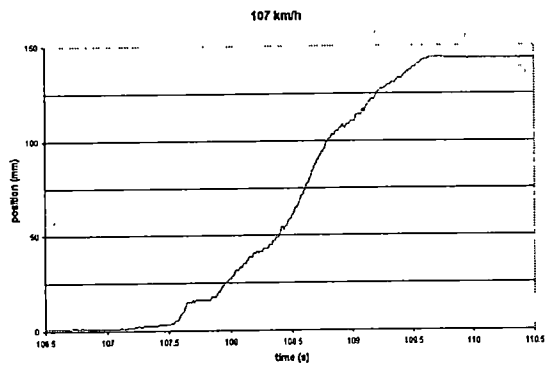
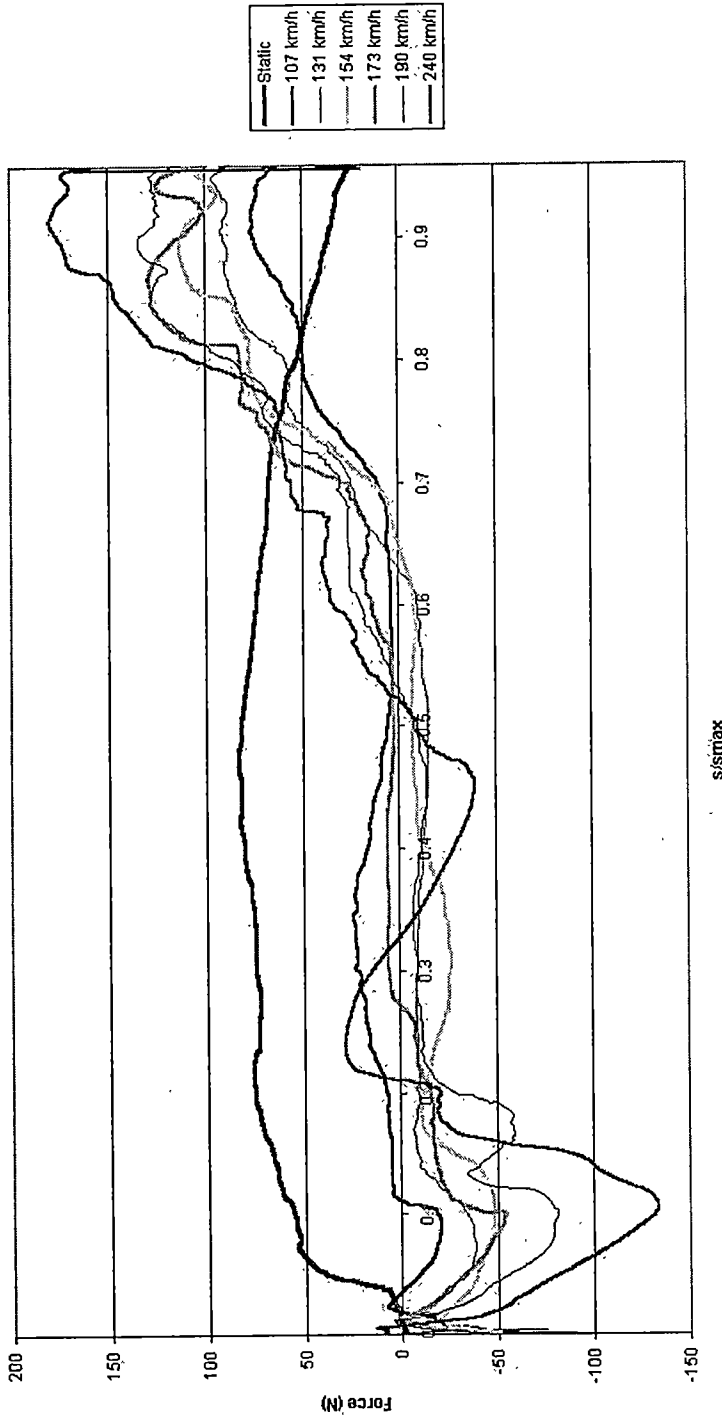


Figure 5-3

Time histories for the airbrakes slow deployment at 6 different airspeeds increased with increasing airspeed. At about 10% of deployment height the holding force



s/s/riax

Figure 5-4

Force required (N) vs airbrakes height (%) at 6 different airspeeds and on the ground

A static measurement (on the ground) was performed and is also shown in figure 5-4. It can be noticed that, in the absence of dynamic effects, a nearly constant pulling force (to overcome the airbrake system weight) is required in order to progressively open the airbrakes from the closed position up to their maximum height over the wing.

The results for the operating forces are presented as a plot force vs airspeed in figure 5-5. The forces shown refer to the maximum forces exerted by the pilot on the airbrakes control handle after unlocking the system and performing the maneuver. It was determined not to include the unlocking/locking operations as part of the experiments. This was decided because the locking mechanism can be adjusted on the ground and the present investigation focuses on dynamic effects. However, it is important to mention here that the wing bending can affect substantially these locking/unlocking forces. As a reference, the average in-flight measured force required to unlock the airbrakes was 208 N. For locking them back, the average force was 235 N.

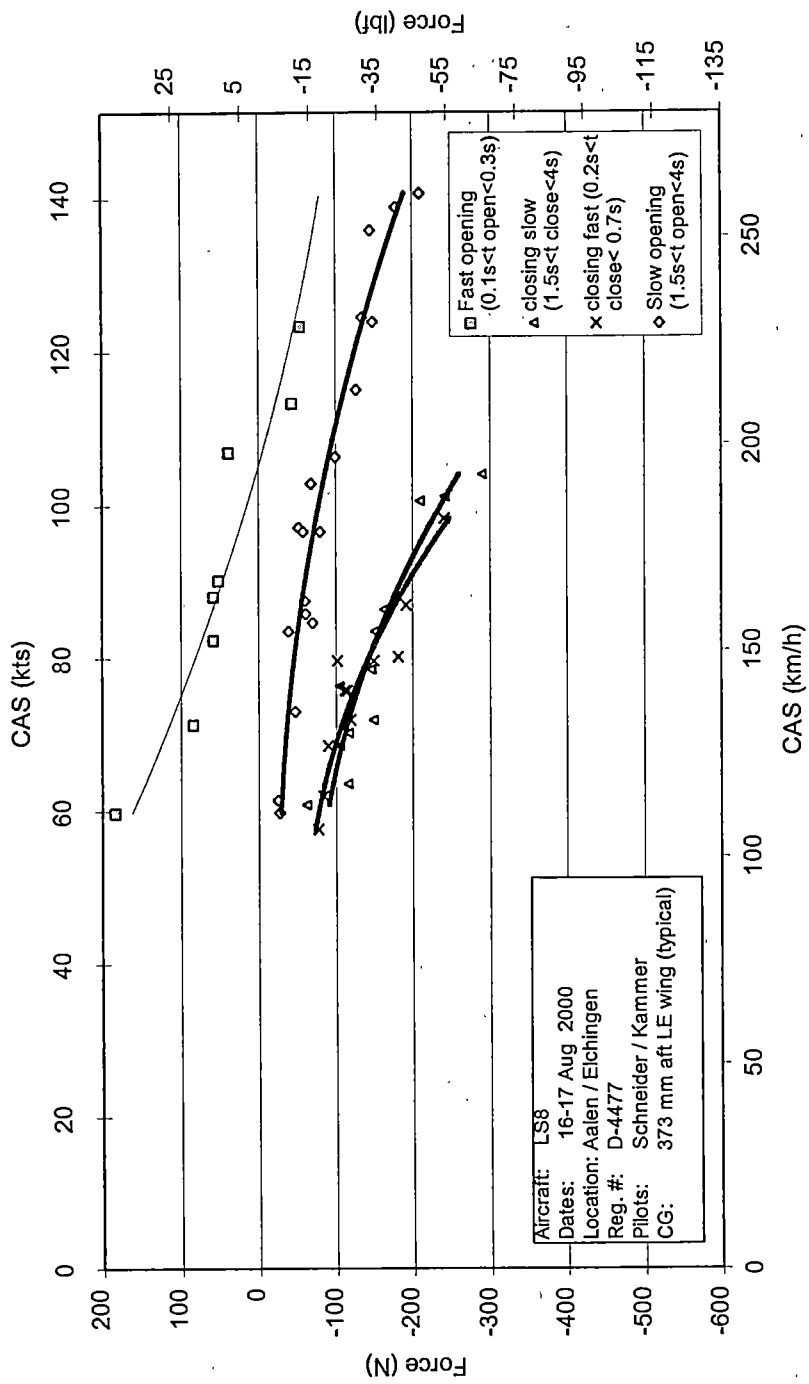
A second order curve-fitting was used to connect the data points. The assumption behind this is that the required force is a function of dynamic pressure (which depends on the square of the airspeed). For the ease of interpretation, the results are presented in both SI and US customary units. Figure 5-5 results lead to the following conclusions:

- The airflow over the wings tends to open the airbrakes without any input required from the pilot. This can be seen on the “slow opening” curve: the

opening force is always negative which means that the pilot has to constantly hold a pushing force to prevent the airbrakes from fully opening.

- This holding force increases as the airspeed increases. Close to the maximum permissible flying speeds its value is about 200 N
- For the fast operating speeds, an initial pulling force is required to get the opening process started, up to an airspeed of about 200 km/h. After this, almost no force is required to complete the total opening. Above 200 km/h, a very small pushing force was sensed. This force prevents the system from “banging” against the stop at the end of a rapid opening.
- The closing forces required are higher than the opening forces: they reach values of about 300 N at an airspeed of 200 km/h. These values are higher than the current regulations permit. For instance, as pointed in Chapter 2, JAR 22.143 states that the maximum force allowed on the airbrakes handle for a temporary application is 200 N.
- Both the slow and fast closing maneuvers required similar amounts of force to get the closing process started. Once the airbrakes begin to retract this force diminished quickly.

pull



push

Figure 5-5

Forces vs calibrated airspeed - CG location: typical (373 mm aft datum)

ACCELERATIONS

The objective was to obtain values for the peak aircraft accelerations generated after the opening and closing of the airbrakes. The accelerations in the x-axis and in the z-axis (body fixed) were measured, like for the handle forces, for both "slow" and "fast" operating speeds. As expected, the critical case for the peak accelerations was the second one. With the "slow" operating speeds the deployment action was obviously slow and the generated accelerations were small when compared to those generated with the "fast" maneuvers.

Theoretically, in a trimmed condition the x and z accelerations (longitudinal and vertical respectively) should only be functions of the acceleration of gravity and of the pitch angle θ . See figure 5-6. The x acceleration should be $g \sin \theta$, while the z acceleration should be $g \cos \theta$.

The flight test data, however, showed some oscillations in the acceleration and pitch rate traces before the opening and closing maneuvers. As an example, let us consider the data obtained on the sixth experiment of flight number three. Figure 5-7 shows a complete maneuver, from time = 145.0 to time = 160.0 seconds. At time = 147.0 the unlocking maneuver occurs. The data shows a disturbance in the longitudinal acceleration (a_x), vertical acceleration (a_z) and pitch rate (q) signals. The opening of

the airbrakes occurs at time = 154.4. Note that the opening and the closing maneuvers are very close to a step input.

The problem here is the reference trim signals used to measure the peak values generated by the airbrakes operation. The longitudinal acceleration signal shows a good trim condition before the opening. However, the vertical acceleration and pitch rate signals seem to be "not in trim". Figure 5-8 shows these signals on the trim condition, from time = 147.5 to time = 154.4 (just before the opening of the airbrakes). The airspeed signal is also shown.

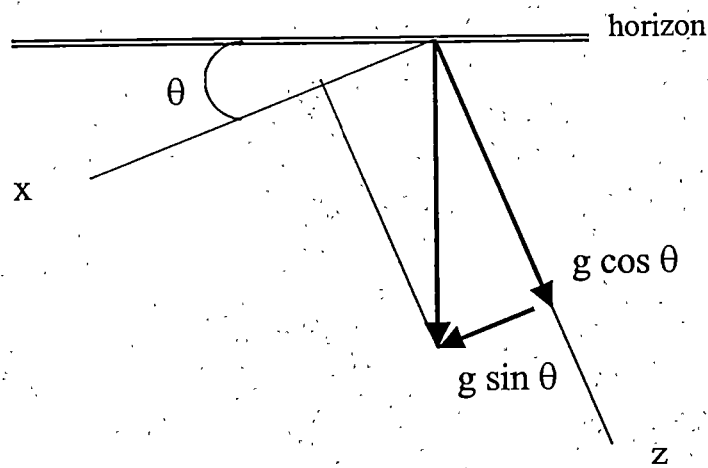


Figure 5-6

Gravity force in trim condition

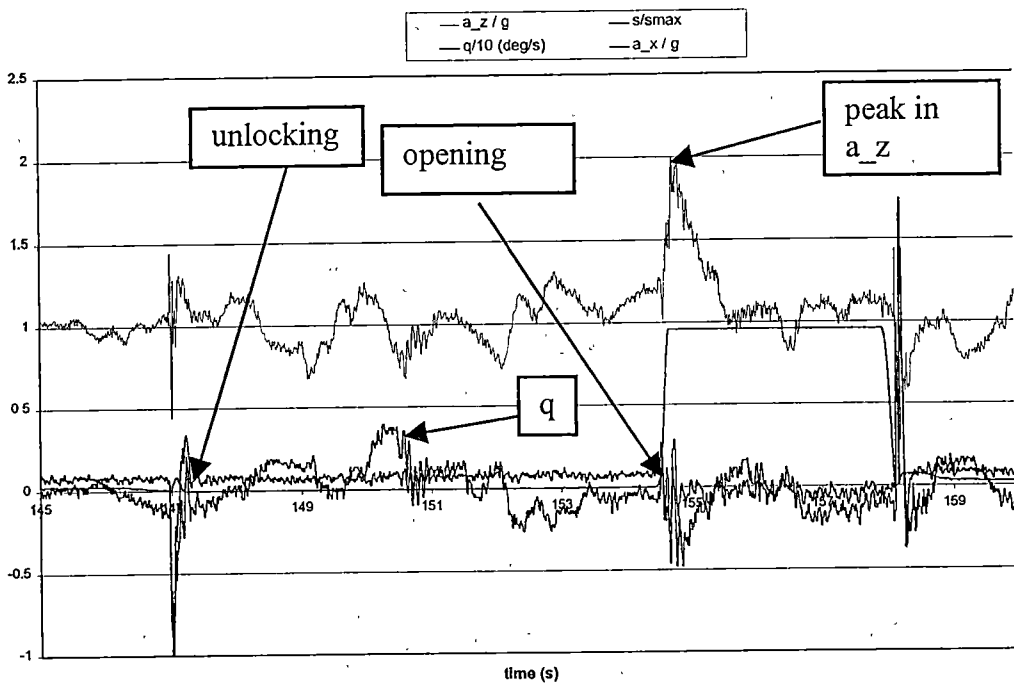


Figure 5-7

Flight #3, experiment # 6 flight test data

In an attempt to identify these oscillations and to describe the frequency content of these signals, an spectral analysis was accomplished using the Matlab Signal Processing Toolbox. The `psd` command applied to the vertical acceleration and pitch rate signals returned the power content of the frequencies from zero to the Nyquist frequency (half of the sampling frequency = $92/2$). Figure 5-9 was obtained.

It can be seen that the oscillations occur at two frequencies: At about 0.8 and 12 Hz. The 0.8 Hz oscillation translates into a period of 1.2 seconds. This oscillation could be identified as the short period mode of the sailplane, excited by some kind of turbulence or by the pilot's inadvertent operation of the control stick. The 12 Hz oscillation frequency could be identified as some structural vibration mode. Electronic noise is also a possibility for this "high-frequency" oscillation.

In any case, for the objectives of this project the trim condition was satisfactory and consistent values for the peak accelerations generated by the airbrakes deployment were obtained. In order not to ignore any of the flight test data, the peak accelerations were measured taking into account these "trim oscillations". Figure 5-10 shows the procedure used to analyze the vertical acceleration flight test data: the peaks in the acceleration were measured from the mid-point of the "trim oscillations" to the maximum value of the acceleration signal.

A similar approach was used to measure the peak longitudinal accelerations and

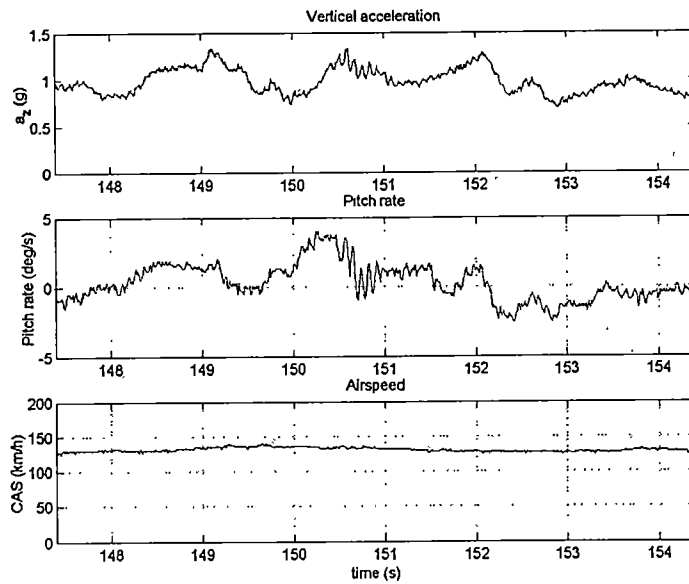


Figure 5-8
Signals in the trim condition

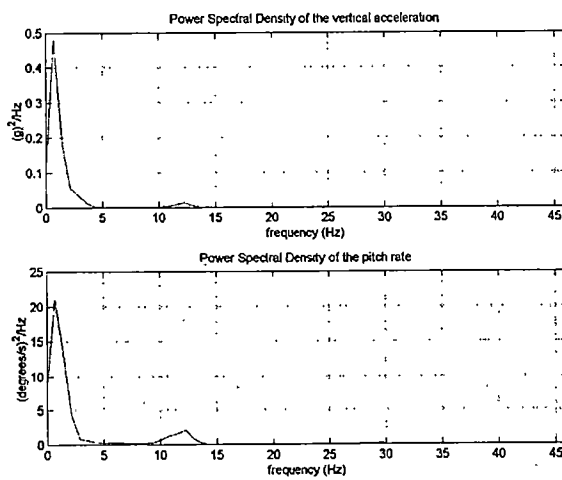


Figure 5-9
Frequency content of the vertical acceleration and the pitch rate signals

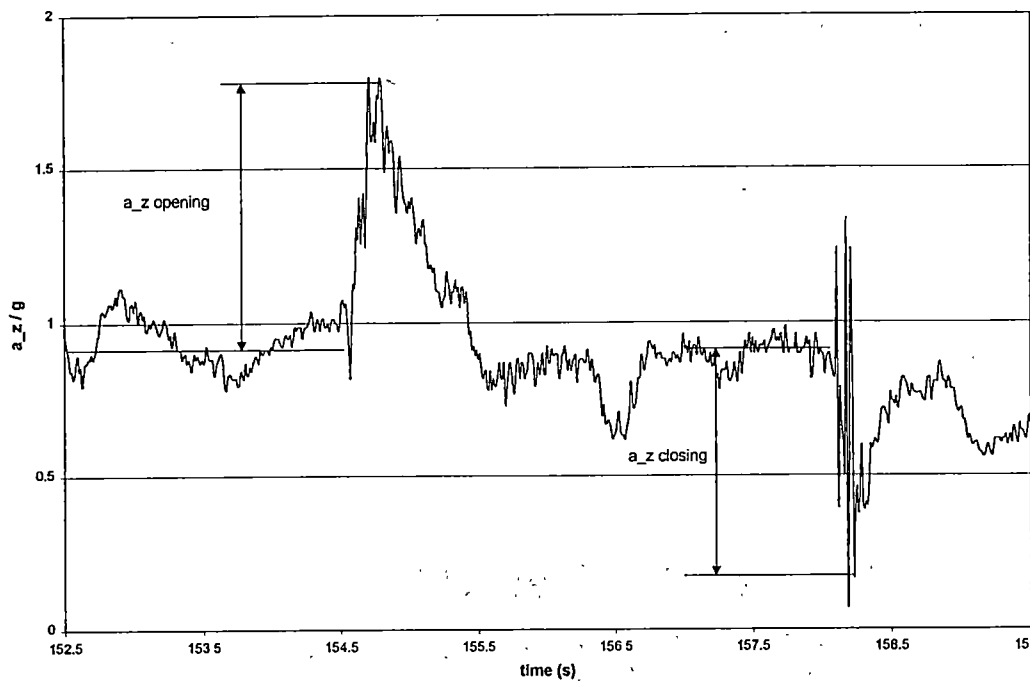


Figure 5-10

Definition of a_z after the opening and closing maneuvers

pitch rates generated. It was concluded that the change in longitudinal acceleration is mainly produced by an increment in the drag force, while the change in vertical acceleration is mainly produced by a loss in the lift force.

Five typical inputs used to generate maximum accelerations (the ones that lead to a sudden deployment or "fast" operating speeds) are shown in figure 5-11. In all of the five cases presented the maneuver approximated a theoretical step input; the time required for the total deployment was about 0.2 seconds.

In some experiments the pilot performed a partial deployment of the airbrakes, approximating a step input of partial height. These steps ranged from 5 to 25% of the maximum height of the airbrake. It was observed that the first few cm of deployment were very influential for the z-accelerations: high g-values were attained with only about 10% deployment. These values were close to the ones obtained with full airbrakes deployment. For the case of the x-accelerations, 25% deployments approximated the maximum decelerations obtained with full deployments.

The results for the LS8 airbrakes-induced accelerations are presented in figures 5-12 to 5-15 in terms of plots airspeed vs accelerations. As for the control forces, a second-order curve fit was selected to connect the data points. The plots show the maximum acceleration generated on the sailplane after the deployment or retracting maneuver. From figures 5-12 to 5-15 it can be concluded:

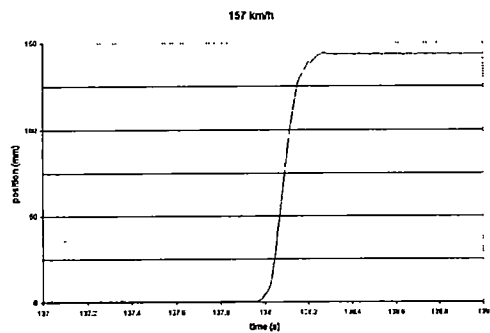
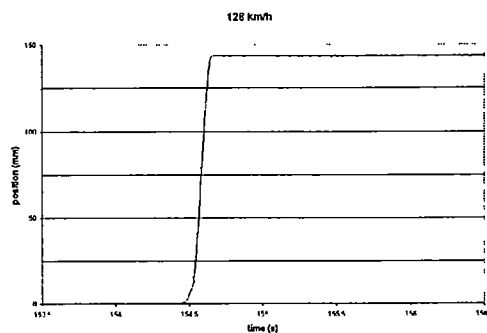
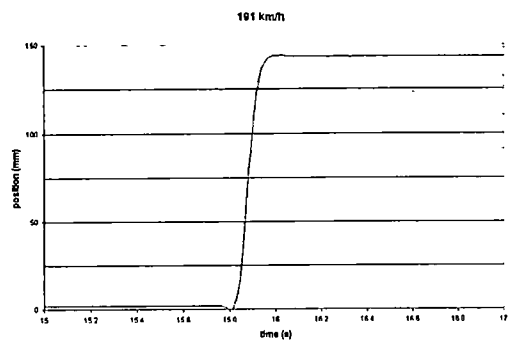
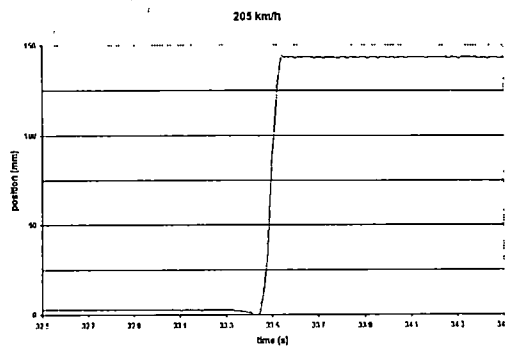
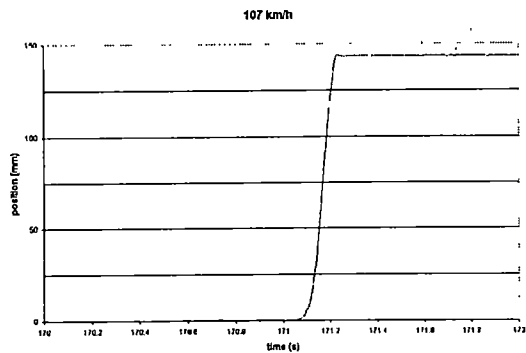


Figure 5-11

Time histories for the airbrakes fast deployment at 6 different airspeeds

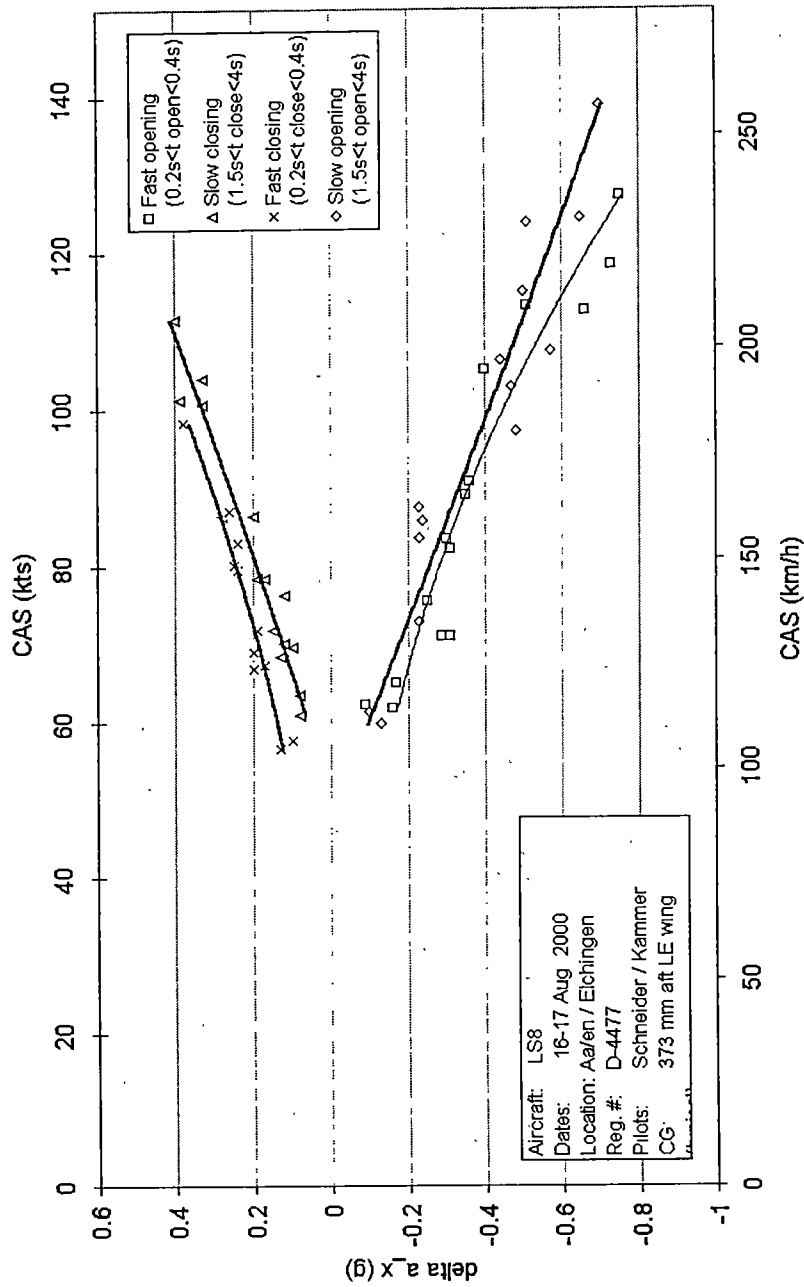


Figure 5-12

X-acceleration vs calibrated airspeed – CG location: typical (373 mm aft datum)

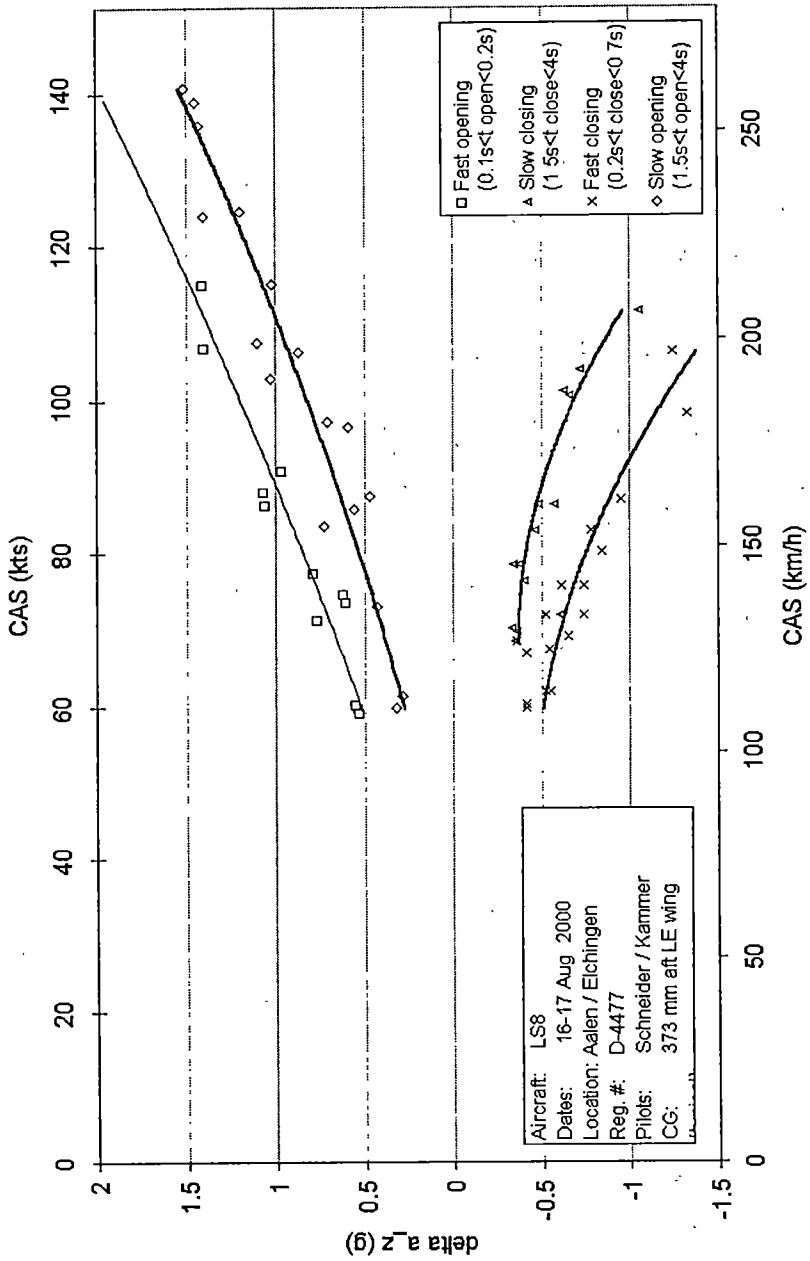


Figure 5-13

Z-acceleration vs calibrated airspeed – CG location: typical (373 mm aft datum)

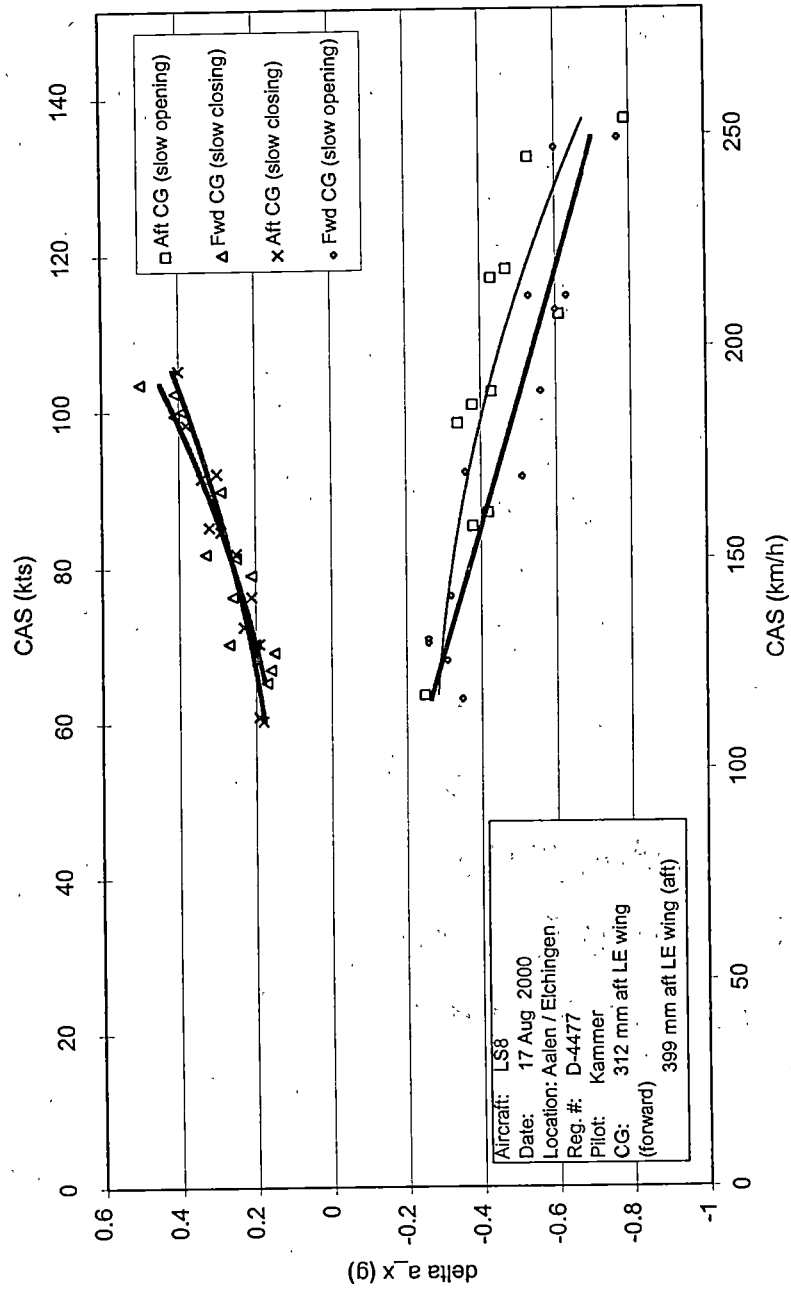
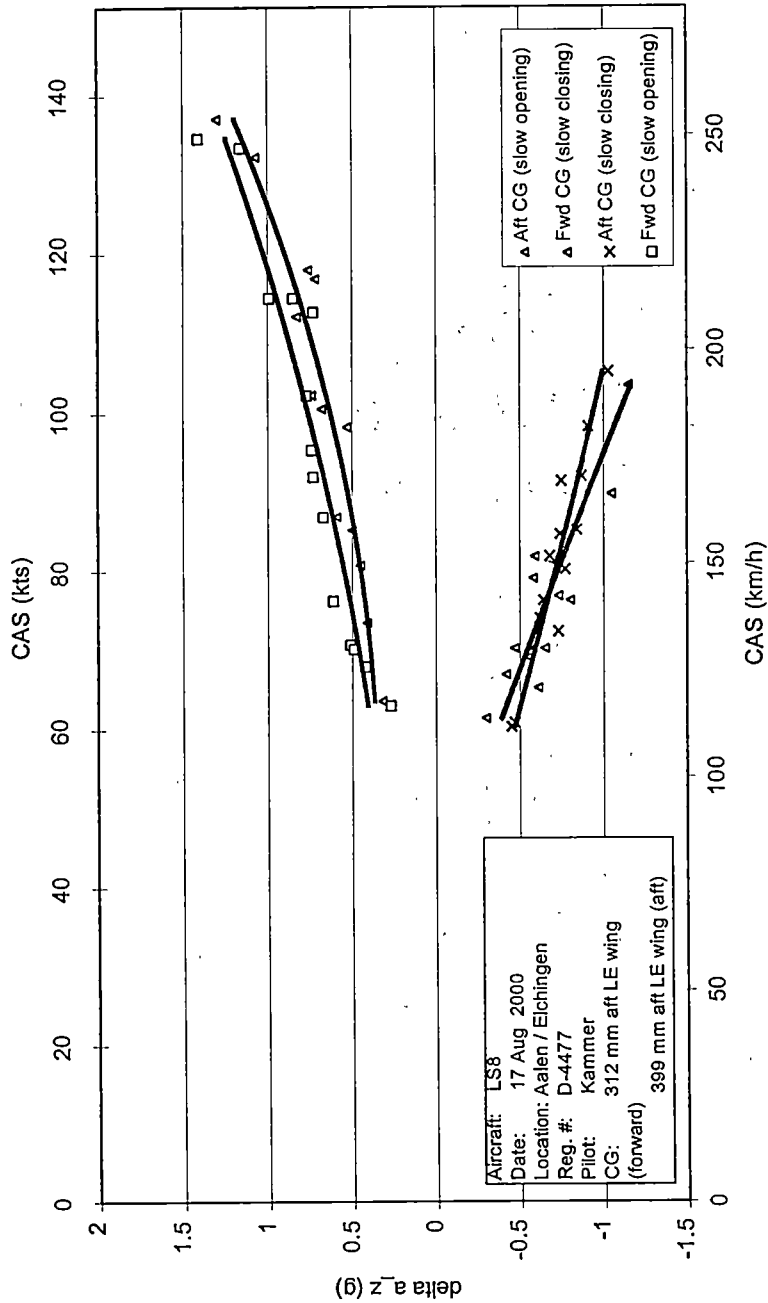


Figure 5-14

X-acceleration vs calibrated airspeed – CG location: aft & fwd (see legend)



Aircraft: LS8
 Date: 17 Aug 2000
 Location: Aalen / Eichingen
 Reg. #: D-4477
 Pilot: Kammer
 CG: 312 mm aft LE wing
 (forward)
 399 mm aft LE wing (aft)

▲ Aft CG (slow opening)
 △ Fwd CG (slow closing)
 × Aft CG (slow closing)
 □ Fwd CG (slow opening)

Figure 5-15

Z-acceleration vs calibrated airspeed – CG location: aft & fwd (see legend)

- The change in longitudinal acceleration generated by the airbrakes operation is small when compared to the change in vertical acceleration.
- At low speeds the longitudinal acceleration produced when opening the airbrakes slowly is similar to the one produced with a fast deployment. However, at high speeds the fast operation of the airbrakes produces a larger change in this acceleration when compared to the slow operation. The maximum longitudinal acceleration measured with a fast opening speed is -0.8 g at 250 km/h. A small difference appears when closing the airbrakes with fast or slow speeds. The maximum longitudinal acceleration generated is small, about 0.4 g for the fast case at 200 km/h.
- The vertical accelerations produced seem to be more dependent on the operating speeds. For a fast opening speed a value of 1.9 g is reached at 250 km/h. For a slow opening speed this value is 1.5 g at the same airspeed. For the closing case and for a fast operation, a value of -1.5 g is obtained at an airspeed of 200 km/h; and -1.0 g is obtained for the slow operation at the same airspeed.
- The influence of the center of gravity variation seems to be very small on the accelerations obtained after deploying the airbrakes.

The angular accelerations generated after the airbrakes application were negligible. The first few centimeters of the deployed airbrakes seemed to produce, initially, an instant pitch up acceleration that died out rapidly. Ultimately, these angular accelerations generated a slow pitch down motion: About -1 degrees/second for the slow speeds and about -8 degrees/second for the high speeds. If no corrective action was taken, the pitch down motion developed and the sailplane airspeed increased progressively. However, these induced pitch rates were easily controllable by the pilot. No apparent difference was sensed with different CG locations.

A qualitative evaluation of the test pilots led to the same results: small angular accelerations generated. An important factor affecting the pitch rate measurements was the fact that the control stick was held at the fixed position only by means of the pilot hand and legs. With such a violent maneuver while flying at high speeds it was very difficult to assure a good "fixing" of the control stick: Small inputs to the elevator produced large moments that could substantially affect the rotational motion of the sailplane. Future investigations of angular accelerations should consider fixing the stick position with a physical stop carefully designed considering safety issues.

CHAPTER 6

SIMULATION OF THE LONGITUDINAL MOTION OF THE LS 8

OBJECTIVES OF THE SIMULATION

A computer simulation for the longitudinal motion of the LS 8 is presented in this chapter. The simulation helps to analyze the behavior of the sailplane when different airbrake control inputs are applied to it. For example, it can predict the response of the sailplane to partial airbrakes deployments. It also provides a way to extrapolate results to conditions not tested (like speeds greater than V_{NE}).

In the context of the objectives of the present study, the simulation is able to predict the vertical and longitudinal accelerations that follow a deployment or retraction of the airbrakes, as well as all of the other dynamic parameters of the longitudinal motion of the sailplane. It is not able to predict the control forces that the pilot must apply to the airbrakes handle.

The simulation is constructed for one CG location (2236 mm from the nose of the sailplane or 373 mm behind the leading edge of the wing at the wing and fuselage junction-see figure 6-1). For the nomenclature used, refer to pages xiv – xvii.

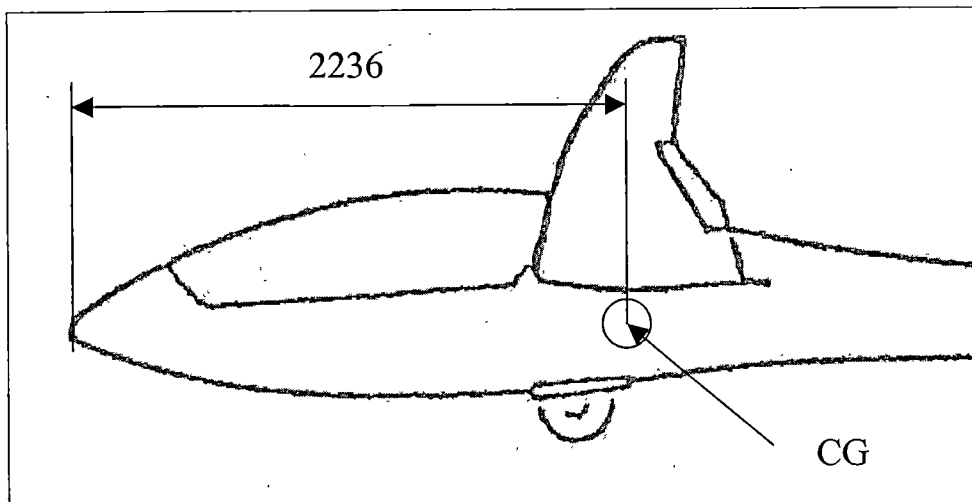


Figure 6-1

Longitudinal CG location for the simulation

STRUCTURE OF THE SIMULATION

The simulation of the longitudinal motion of the LS 8 was developed using the software MATLAB© and its dynamic system modeling package SIMULINK©. Its three principal elements are:

- The look-up tables, which provide the aerodynamic characteristics of the sailplane.
- A trim program, which provides the inputs.
- The SIMULINK blocks, which constitute the essence of the simulation.

The simulation structure is shown on figure 6-2.

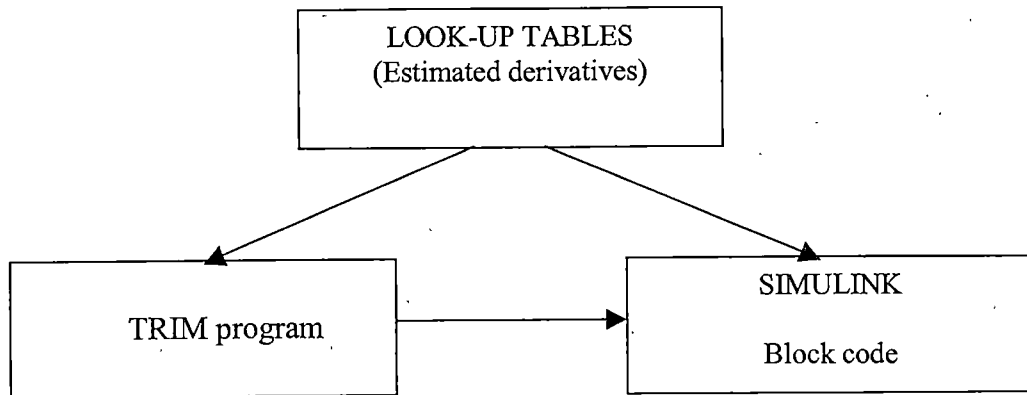


Figure 6-2

Simulation structure

DERIVATIVES ESTIMATION

The stability and control parameters (derivatives) required for the simulation were obtained from three different sources: The software “Digital Datcom”, the measured polars of the aircraft and the results of wind tunnel experiments. Table 6-1 summarizes the sources for the different derivatives.

The derivatives were compiled in an m-file (“tables_ls8”) in the form of look-up tables and are presented in appendix NN. For instance, “table_Cl_alpha1” is a vector that gives the values of the lift coefficient (C_L) for different values of the angle of attack (α_1). For the airbrake-derivatives, the matrix “table_Cl_s” gives the values of the lift

coefficient for a given angle of attack (row) and airbrakes height (column). The same logic applies for the drag and pitching moment coefficients.

The software "Digital Datcom" was the principal source of derivatives for this study. This is a USAF compilation of methods widely used in the aviation industry to estimate aircraft stability derivatives.

The wing-body-vertical tail-horizontal tail DATCOM configuration was selected for the derivatives estimation. Other parameters required were the sailplane dimensions, weight, CG location, airspeed and altitude. An airspeed of 50 m/s and an altitude of 1000 m were selected for being representative of the flight tests conditions.

Table 6-1
Stability Derivatives

Measured polars	"Digital Datcom":	Wind tunnel exper.
$C_L(\alpha)$	$C_M(\alpha), C_{M_q}, C_{L_q}, \Delta C_L(\eta), \Delta C_D(\eta, \alpha),$	$\Delta C_L(s), \Delta C_D(s),$
$C_D(\alpha)$	$\Delta C_M(\eta), C_{L\dot{\alpha}}(\alpha), C_{M\dot{\alpha}}(\alpha)$	$\Delta C_M(s)$

It was found, however, that the C_L and C_D values estimated using this source were inadequate for a sailplane. Particularly, the values for the drag coefficient were too high for the LS 8. Instead, the polars for the LS8 were used for these estimations. The $C_{L\alpha}$ and $C_{D\alpha}$ DATCOM derivatives are presented (preceded by a “%” symbol) for comparison purposes in the same “tables_ls8” m-file.

The polars for the LS 8 standard class sailplane (15 m span with winglets, same model as the one used for the flight tests) were measured by Idaflieg and DLR in 1995 and provided by the Akaflieg Aachen. They are presented in appendix C. Note that the angle of attack in the $C_L - \alpha$ diagram is measured with respect to the longitudinal axis of the sailplane. For that reason in order to obtain the $C_L - \alpha$ characteristics based on the wing angle of attack (standard practice), the wing incidence angle (2°) was added.

The airbrakes related derivatives were obtained from wind tunnel experiments performed at the ILR of the Technical University of Aachen.

WIND TUNNEL DERIVATIVES SCALING

The wind tunnel model used in these experiments had a similar airfoil to the one in the LS 8, but the airbrakes dimensions were slightly different. For this reason a semi-

empirical scaling of the airbrake derivatives was necessary. The factors N_1 , N_2 and N_3 were introduced to modify the wind tunnel airbrakes-related derivatives. The factor 2 was also introduced in order to account for both the right and left wing airbrakes.

The wind tunnel model airfoil had the following dimensions: Length (span) = 0.54 m, chord = 0.14 m, airbrake length = 0.37 m, airbrake height = 0.031 m. The ratio of the chord of the LS 8 at the airbrake location to the chord of the model ($0.75/0.14=5.357$) was used to “up-scale” the model. For the area “up-scale” the square of the ratio was used. Table 6-2 summarizes this procedure.

The airbrakes-related derivatives and their corresponding scaling factors are presented in the “tables_ls8” m-file in appendix B.

Table 6-2
Scaling Factors

	Model	LS 8	Up-scale model	Scaling factors
Airbrake length	0.370 m	1.408 m	1.982	$N_1 = 0.7104$
Airbrake height	0.031 m	0.150 m	0.166	$N_2 = 0.9036$
Wing Area	0.076 m^2	10.5 m^2	2.170	$N_3 = 0.2066$

TRIM PROGRAM

The inputs for the simulation are to be proportioned by the "trim" program. A listing of "trim" is provided in appendix A. Some of these inputs are to be proportioned by the user and others are calculated by TRIM. The user-defined parameters are:

- the sailplane total velocity
- the altitude
- the mass, inertia and geometric characteristics (wing area and mean aerodynamic chord) of the sailplane
- the value of the acceleration of gravity at sea level, the air density at sea level and the speed of sound at sea level
- the aerodynamic derivatives. These are proportioned as a separate m-file.

The moment of inertia (I_{yy}) was estimated using theoretical data provided by the DLR (German Agency for Space and Aeronautics). According to DLR, for this type of sailplane a typical value for the ratio of the radius of gyration and the length of the sailplane (r/l) is given as 0.169. Then, with the mass being 345 kg and the length 6.74 m and using the equation $r = \sqrt{I_{yy}/m}$, the moment of inertia was calculated to be 447.6 kg/m².

The TRIM program calculates the following parameters:

- the elevator angle required to trim
- the lift and drag coefficients at the trim condition
- the angle of attack (alpha), the pitch angle (theta) and the flight path angle (gamma)

It is convenient here to define the trim condition. An aircraft is said to be in trim, steady level flight or equilibrium when the lift and drag forces acting on it exactly balance the components of weight and thrust (in the case of a sailplane thrust equals zero), and the total moment about its center of gravity is zero. These conditions are used in the TRIM program to find the equilibrium operating point.

If x and z are considered to be stability axes (thus, the relative wind acting parallel to the longitudinal axis of the sailplane – see figure 6-3) the equilibrium equations in the lift and drag directions can be written as:

$$\Sigma F_L = 0$$

$$L - W \cos(\gamma) = 0$$

$$L - mg \cos(\gamma) = 0$$

$$C_L \frac{1}{2} \rho v^2 S = mg \cos(\gamma)$$

$$v^2 - 2 mg \cos(\gamma) / C_L \rho S = 0 \tag{1}$$

$$\Sigma F_D = 0$$

$$D + W \sin(\gamma) = 0$$

$$D + mg \sin(\gamma) = 0$$

$$C_D \frac{1}{2} \rho v^2 S = -mg \sin(\gamma)$$

$$v^2 + 2 mg \sin(\gamma) / C_D \rho S = 0 \quad (2)$$

The TRIM program uses these two conditions together with $\Sigma M_{CG} = 0$ to find the equilibrium point. This is accomplished using a “while condition” and the look-up tables from the tables_LS8 m-file.

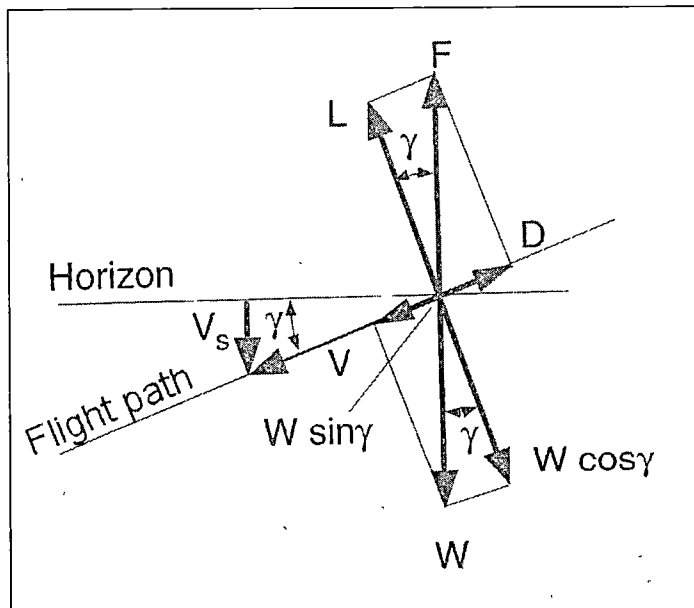


Figure 6-3

Balance of forces (from ref. 29)

The program evaluates conditions (1) and (2) until the error becomes lower than the specified one. Every time the program goes inside this "loop" the flight path angle is recalculated. To do this, the program goes through the following sequence:

- 1) For the current angle of attack (α), the program finds the correspondent pitching moment depending on α , $C_M(\alpha)$.
- 2) The program finds then the elevator angle (η) required to produce a pitching moment depending on η , $C_M(\eta)$ of the same magnitude and opposite sign as the one found in step (1).
- 3) The lift and drag coefficients are calculated from the look-up tables with the angle of attack and the elevator angle:

$$C_L = C_L(\alpha) + \text{delta } C_L(\eta)$$

$$C_D = C_D(\alpha) + \text{delta } C_D(\eta)$$

- 4) The flight path angle is calculated using:

$$\gamma = \arctan\left(-\frac{C_D}{C_L}\right)$$

5) When both conditions in the while loop are satisfied, the program calculates the pitch angle (theta) using:

$$\theta = \alpha + \gamma$$

The user can specify in this TRIM program the “shape” of the airbrakes input. This is accomplished by creating two vectors, named “tsim” and “usim”. The first one specifies the simulation time, while the second one specifies the simulation inputs “eta” (elevator angle to trim) and “s” (airbrakes height in percentage).

The simulation inputs are called “control surfaces”. Figure 6-4 is an example of the CONTROL SURFACES SCOPE for the trim airspeed = 50 m/s.

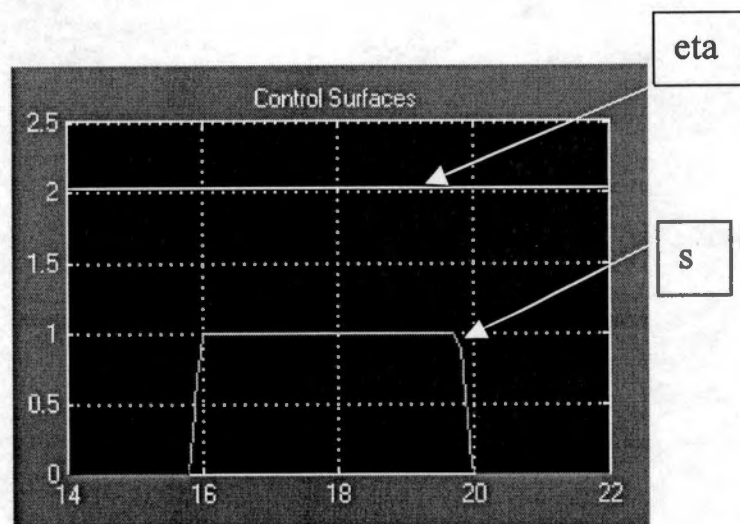


Figure 6-4
Control surfaces scope

SIMULINK MODEL

The SIMULINK model is structured as a graphical representation of the equations of motion, and built using blocks that represent functions or sub-systems. Figure 6-5 is a tree-diagram showing the hierarchy of the different elements that constitute the simulation model.

The main screen of the model is showed on figure 6-5. Note that the model has two input variables (eta and spoilers), two main blocks (AERODYNAMIC and SAILPLANE DYNAMICS) and an OUTPUTS block.

The OUTPUTS block is set to provide the following parameters: C_l , C_d , C_m , alpha, v_t , $v_t \dot$, s, u_{\dot} , w_{\dot} , rho, a_x , a_z , time, theta, and q.

In the following sections the main blocks are presented and explained.

AERODYNAMIC BLOCK (figure 6-7)

This sub-system receives three inputs: Control surfaces, parameters and states.

- The control surfaces are the airbrakes height (in %) and the elevator angle (eta).

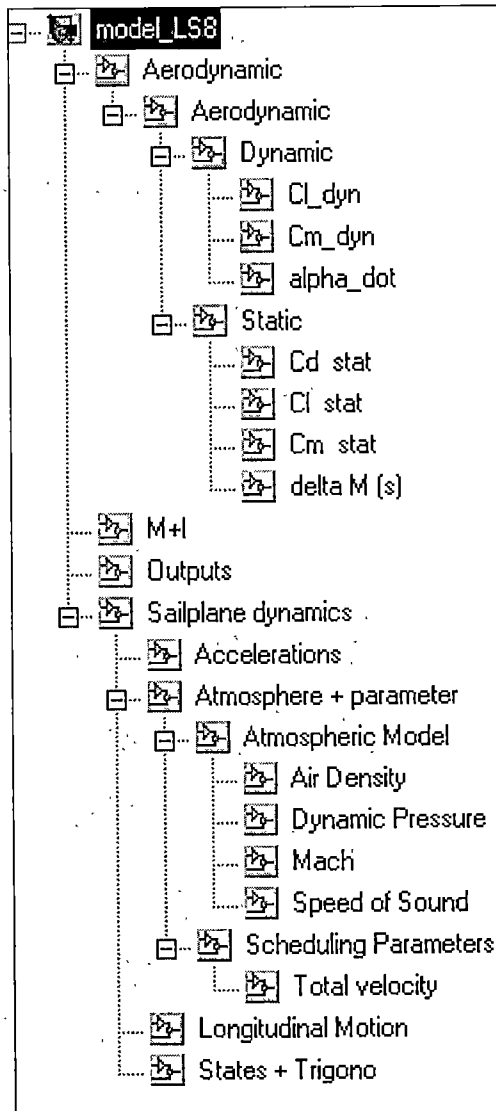


Figure 6-5

Simulink Model Structure

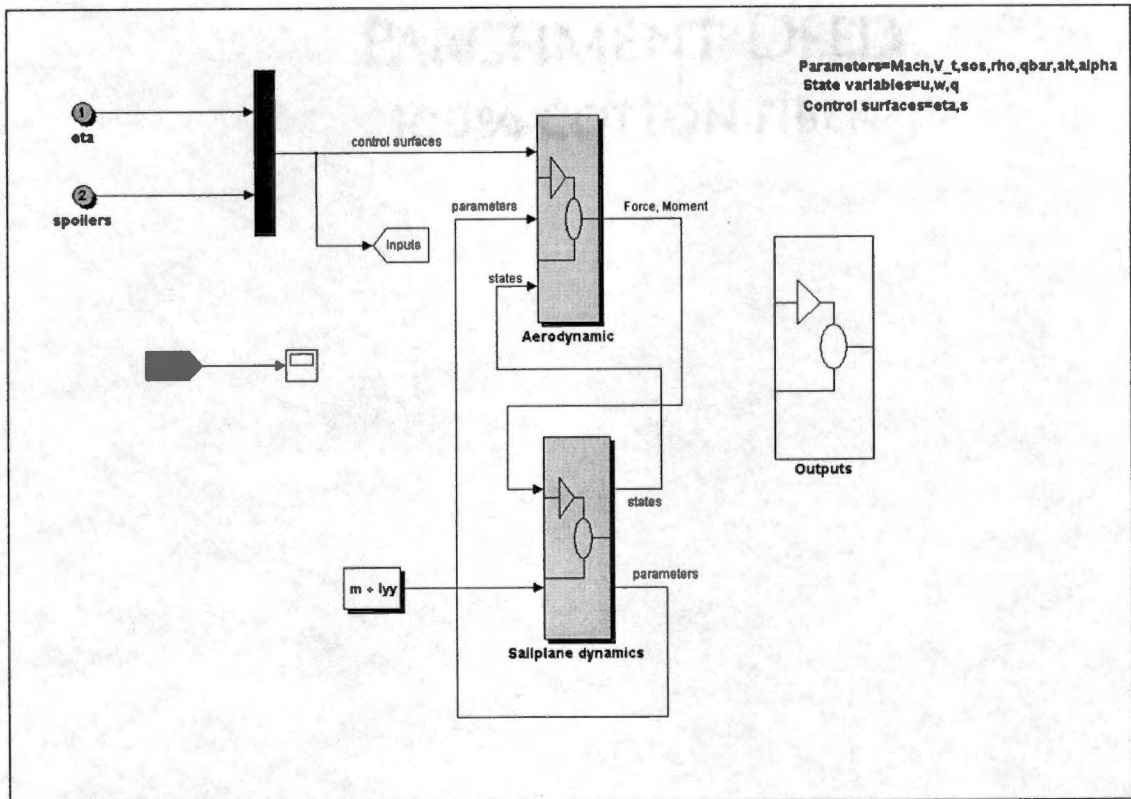


Figure 6-6
Model Main Screen

- The parameters are: Mach number (Mach), total velocity (v_t), speed of sound (sos), density (rho), dynamic pressure (qbar), altitude (alt), angle of attack (alpha).
- The states are forward velocity (u), vertical velocity (w) and pitch rate (q).

The outputs of the AERODYNAMIC sub-system are the longitudinal force (X), normal force (Z) and pitching moment (M).

The AERODYNAMIC sub-system calculates the lift, drag and pitching moment coefficients as the sum of “static” and “dynamic” components (i.e. $C_L = C_{L_{stat}} + C_{L_{dyn}}$). For this reason it is further divided into two sub-systems: STATIC and DYNAMIC.

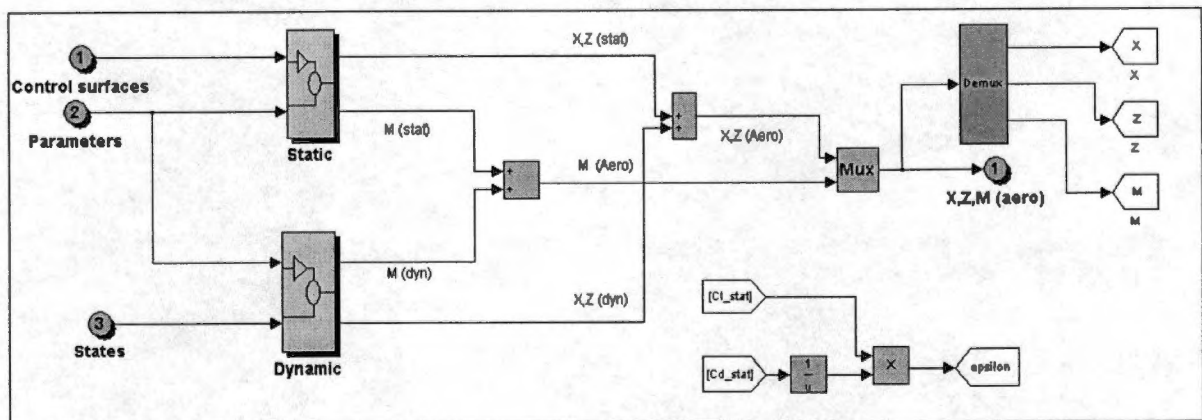


Figure 6-7
Aerodynamic Block

STATIC BLOCK (Figure 6-8)

In this sub-system the lift, drag and moment coefficients depending on alpha, eta and s (airbrakes height) are calculated using the look-up tables.

Note that the force calculations are made using aerodynamic axes (parallel to the lift and drag forces). Therefore, an angular transformation is required in order to obtain the longitudinal and normal forces in the body-fixed axes system.

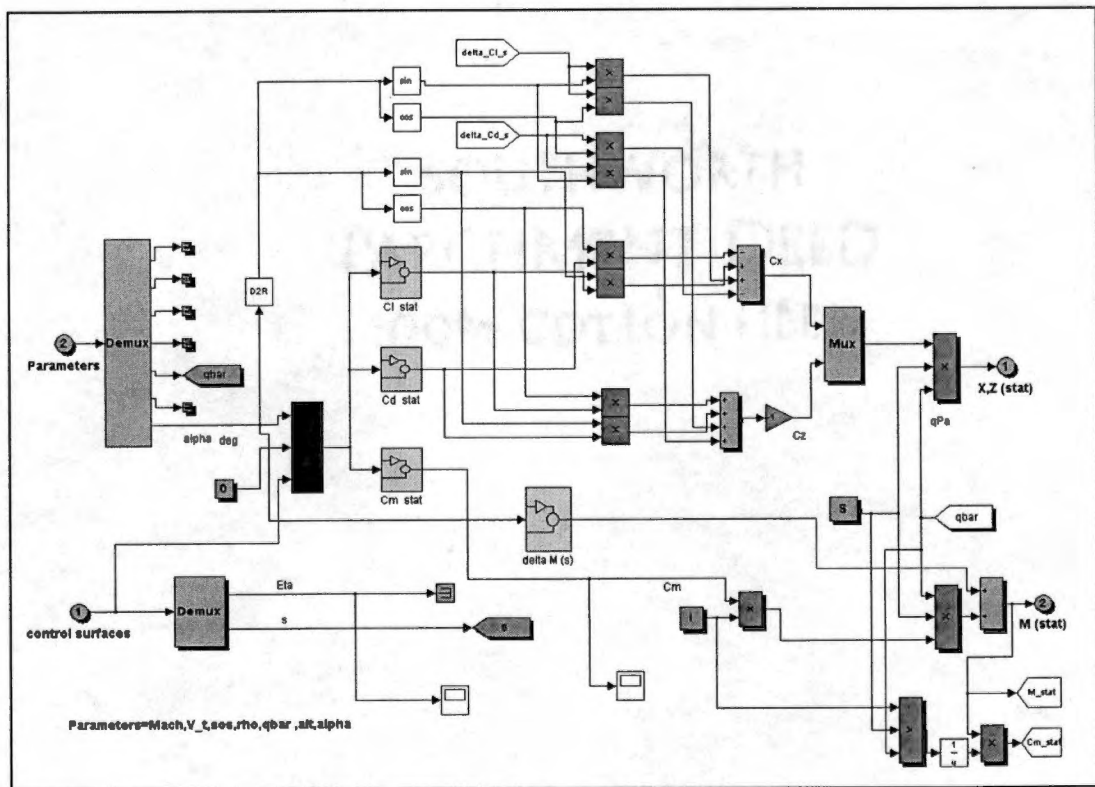


Figure 6-8

Static Block

The following equations apply:

$$X_{stat} = qbar.S.C_{Xstat}$$

(See figure 6-9)

$$Z_{stat} = qbar.S.C_{Zstat}$$

$$M_{stat} = qbar.l.S.C_{Mstat} + DeltaM(s)$$

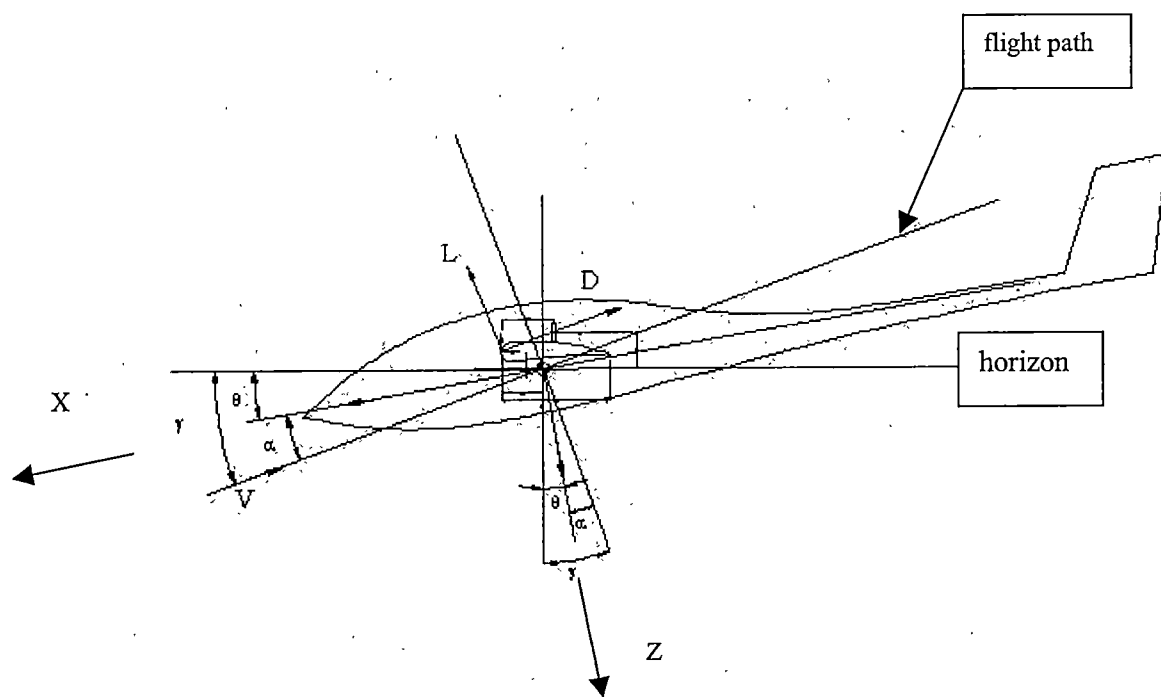


Figure 6-9
Axes and angles

$$C_{L\text{ stat}} = C_L(\alpha) + \Delta C_L(\eta) \quad (\text{See figure 6-10})$$

$$C_{D\text{ stat}} = C_D(\alpha) + \Delta C_D(\eta, \alpha) \quad (\text{See figure 6-11})$$

$$C_{M\text{ stat}} = C_M(\alpha) + \Delta C_M(\eta) + \Delta C_M(s, \alpha) \quad (\text{See figure 6-12})$$

$$C_{X\text{ stat}} = C_{L\text{ stat}} \sin(\alpha) - C_{D\text{ stat}} \cos(\alpha) + \Delta C_L(s, \alpha) \sin(\alpha) - \Delta C_D(s, \alpha) \cos(\alpha)$$

$$C_{Z\text{ stat}} = -(C_{L\text{ stat}} \cos(\alpha) + C_{D\text{ stat}} \sin(\alpha) + \Delta C_L(s, \alpha) \cos(\alpha) + \Delta C_D(s, \alpha) \sin(\alpha))$$

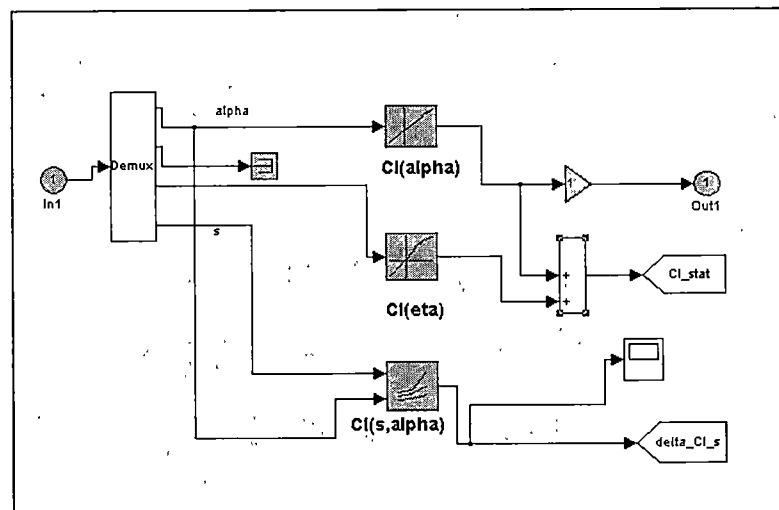


Figure 6-10

$C_{L\text{ stat}}$ Block

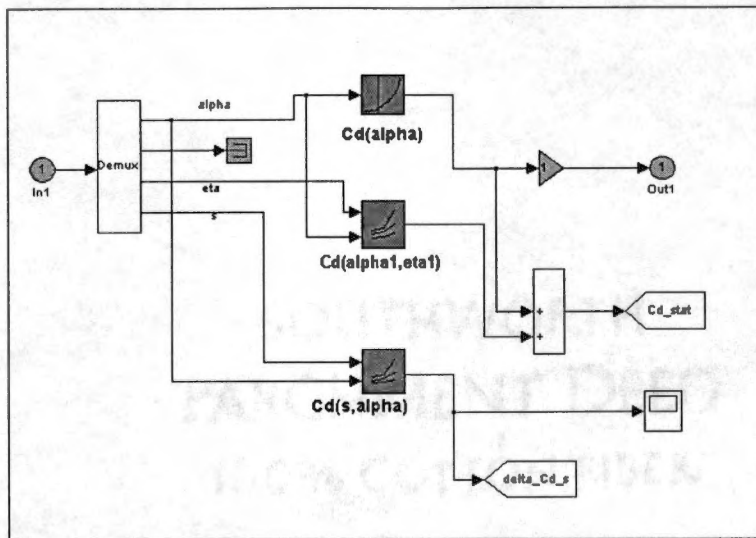


Figure 6-11
 C_D stat Block

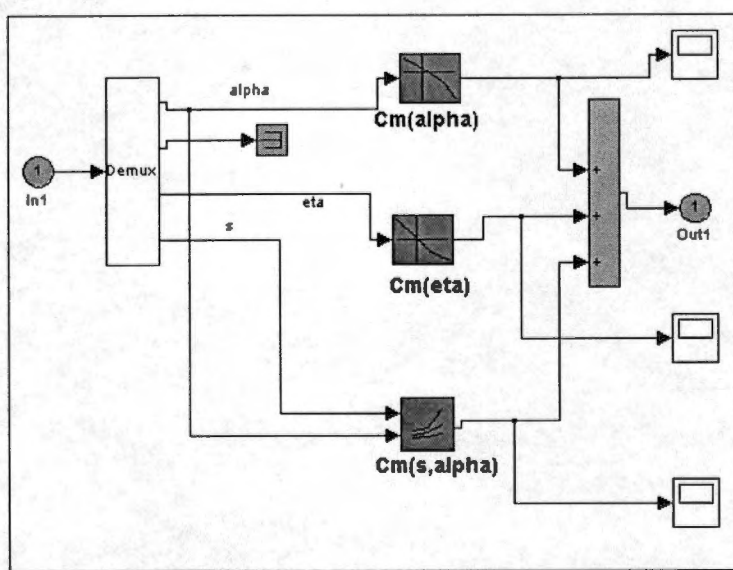


Figure 6-12
 C_M stat Block

A block named DELTA M(s) is also included here to correct the forces generated by the airbrakes. When estimating the airbrakes-related derivatives the reference point used was not the aircraft CG but to the quarter-chord point of the wing. See figure 6-13.

Finally, these coefficients are multiplied by the dynamic pressure and by the reference area in order to get the longitudinal and normal forces and the pitching moment. See figure 6-14.

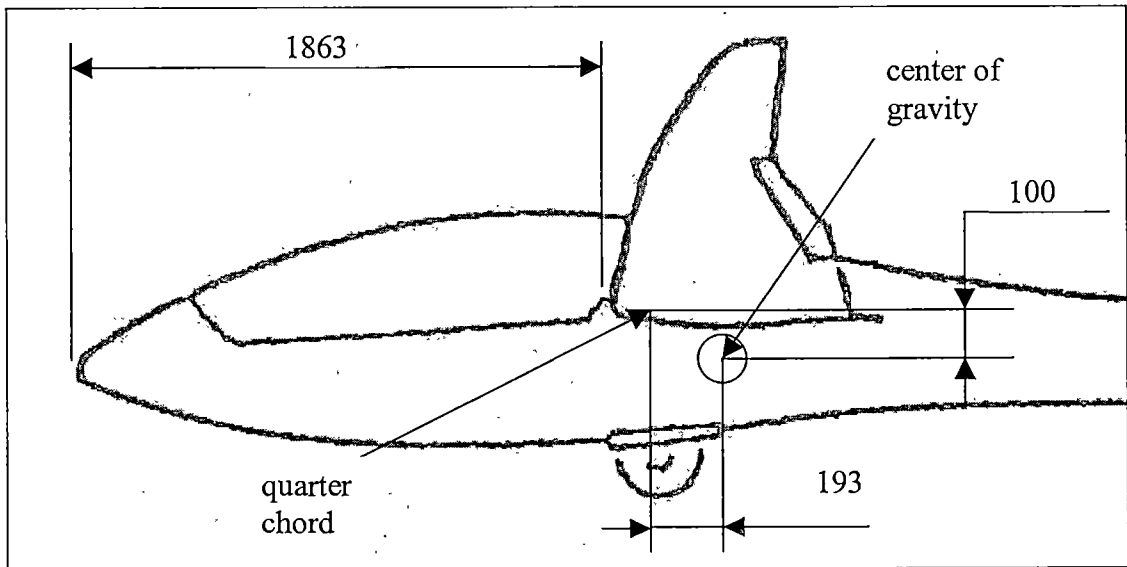


Figure 6-13

CG location for the simulation

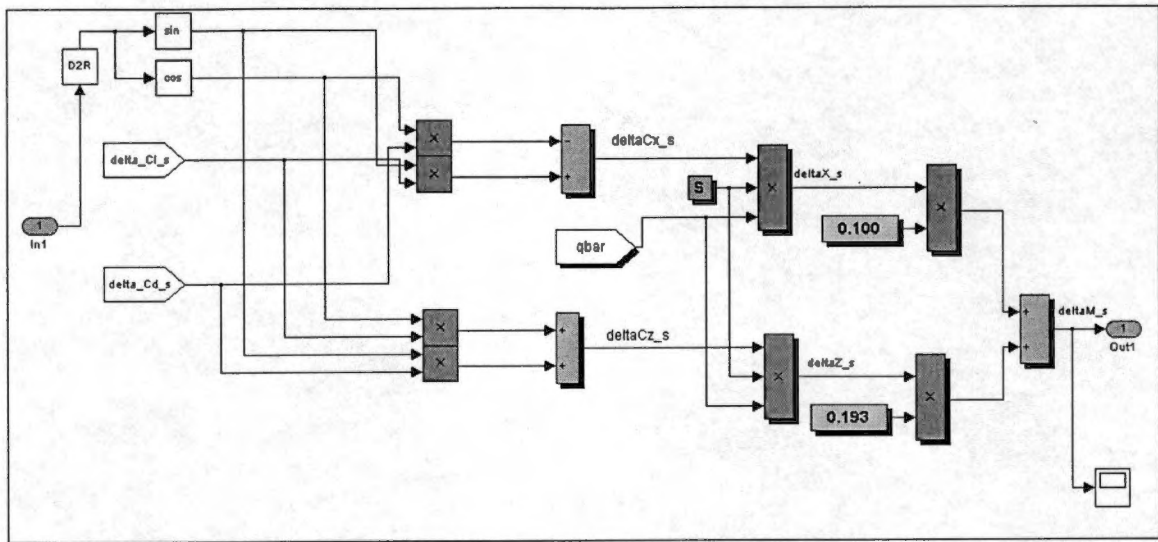


Figure 6-14

Delta M(s) Block

DYNAMIC BLOCK (figure 6-15)

In this sub-system the lift and moment coefficients depending on the dynamic parameters (alpha dot, pitch rate) are calculated using:

$$C_{L_{dyn}} = C_{L(\dot{\alpha})}\dot{\alpha}^* + C_{Lq}q^* \quad \text{(See figure 6-16)}$$

$$C_{M_{dyn}} = C_{M(\dot{\alpha})}\dot{\alpha}^* + C_{Mq}q^* \quad \text{(See figure 6-17)}$$

$$X_{dyn} = (qbar.S.C_{Ldyn}) \sin \alpha$$

$$Z_{dyn} = (qbar.S.C_{Ldyn}) \cos \alpha$$

$$M_{dyn} = (qbar.l.S.C_{Mdyn})$$

Where $\alpha \dot{^*}$ and q^* are non-dimensional and defined as:

$$\dot{\alpha}^* = \frac{(l.\dot{\alpha})}{(2.V)}$$

$$q^* = \frac{(l.q)}{(2.V)}$$

($\alpha \dot{}$ and q are given in radians)

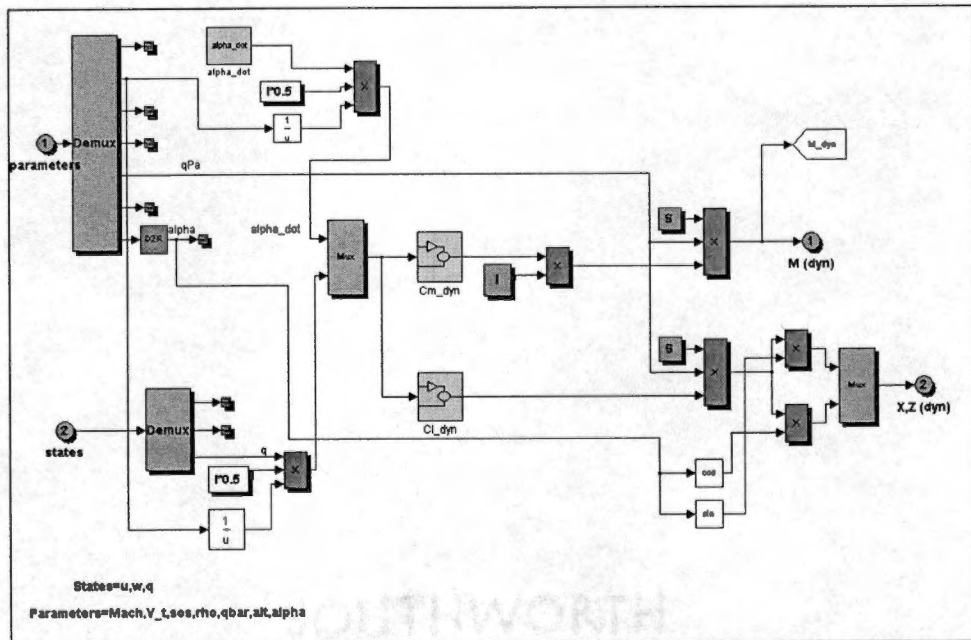


Figure 6-15

Dynamic Block

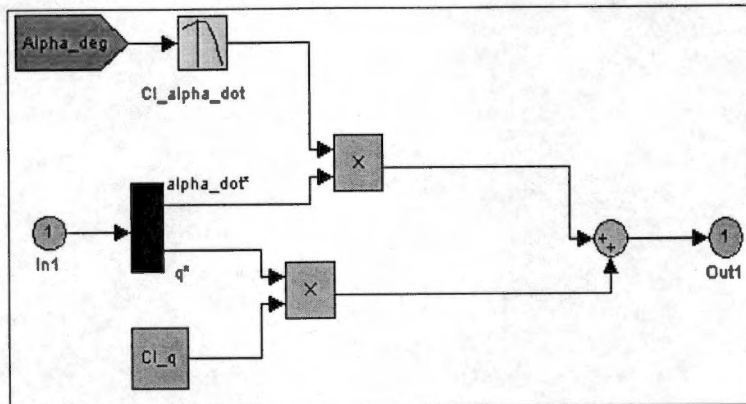


Figure 6-16

$C_{L,dyn}$ Block

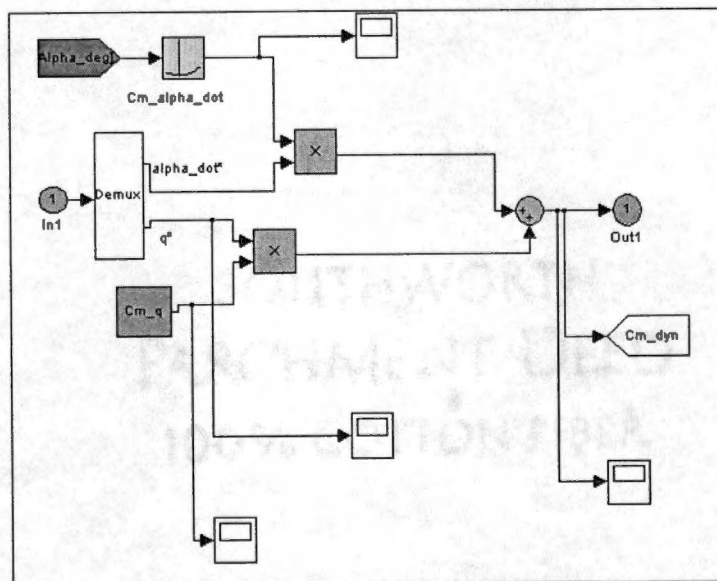


Figure 6-17

$C_{M,dyn}$ Block

SAILPLANE DYNAMICS BLOCK (figure 6-18)

Inputs Forces and moment calculated above
 Mass and moment of inertia

Outputs States
 Parameters

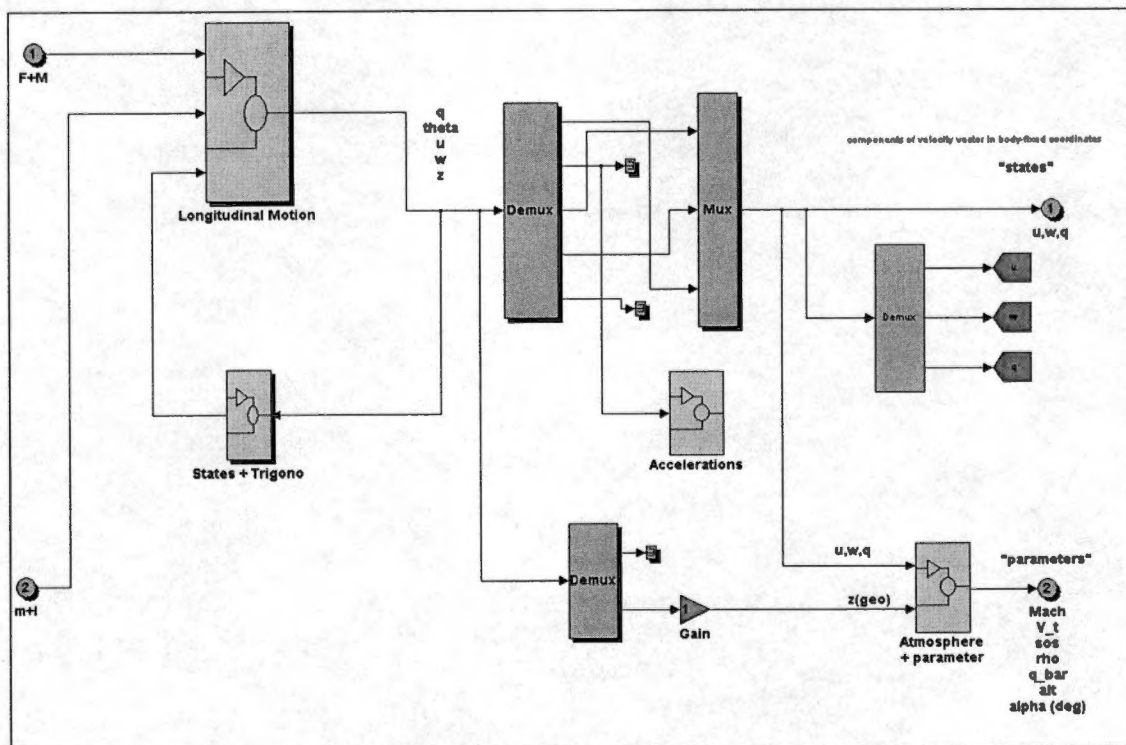


Figure 6-18
 Sailplane Dynamics Block

Inside the SAILPLANE DYNAMICS sub-system there are the following blocks:

LONGITUDINAL MOTION (figure 6-19)

This sub-system calculates \dot{q} , \dot{u} , \dot{w} and w_s using:

$$\dot{q} = \frac{M}{I_{yy}}$$

$$\dot{u} = \frac{1}{mX} - g \sin \theta - qw$$

$$\dot{w} = \frac{1}{mZ} + g \cos \theta + qu$$

$$w_s = w \cos \theta - u \sin \theta$$

The values for q , θ , u , and w are obtained after integrating the respective parameters.

STATES + TRIGONO (figure 6-20)

This subsystem calculates $\sin(\theta)$, $\cos(\theta)$ and γ as:

$$\gamma = \theta - \alpha$$

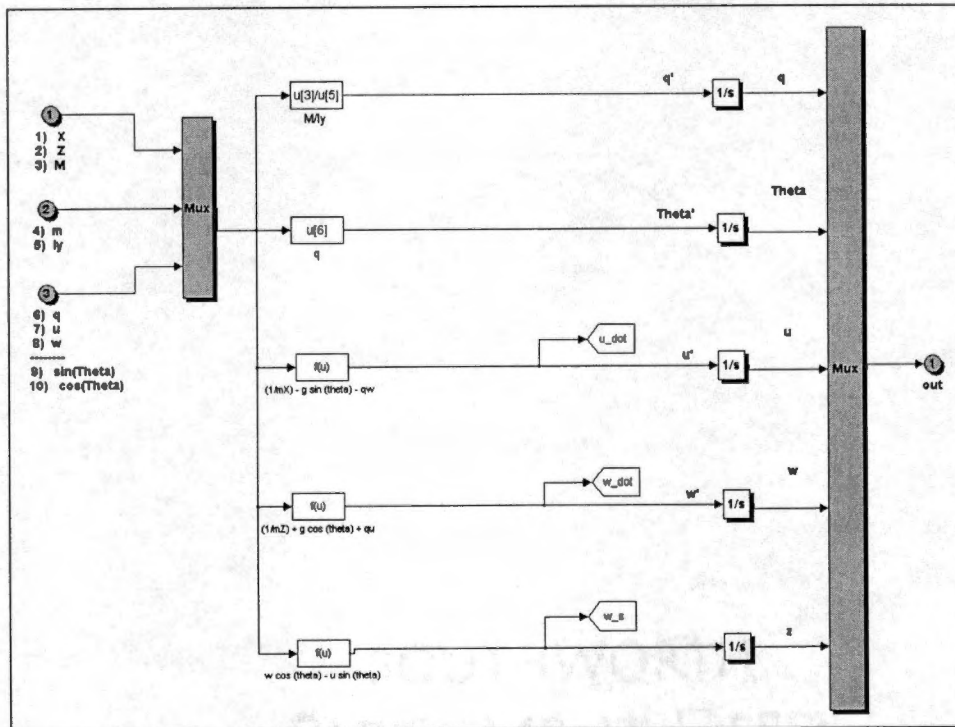


Figure 6-19
Longitudinal Motion Block

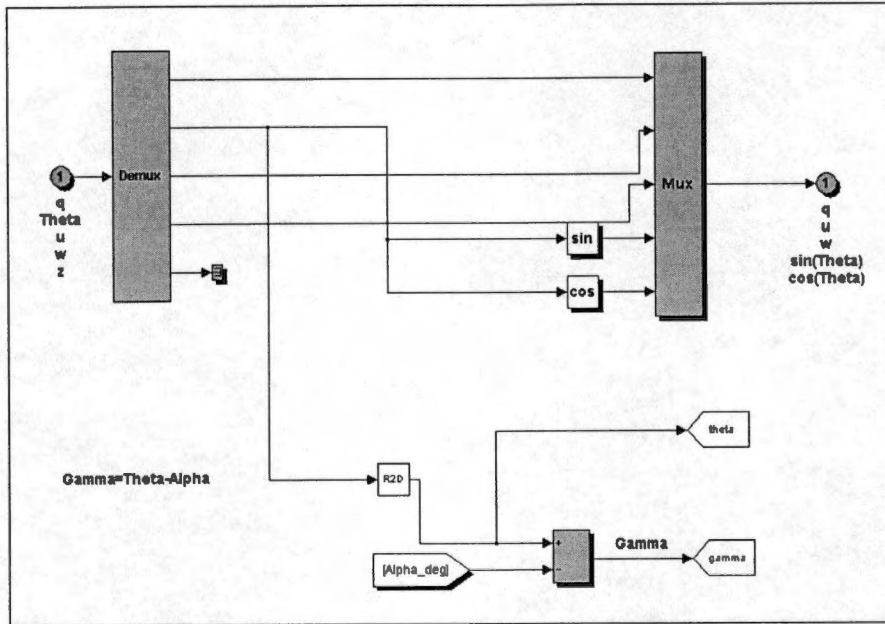


Figure 6-20
States + Trigonon Block

ACCELERATIONS (figure 6-21)

This sub-system calculates a_x and a_z using:

$$a_x = \frac{(g \sin \theta) + \dot{u}}{g}$$

$$a_z = \frac{(g \cos \theta) + \dot{w}}{g}$$

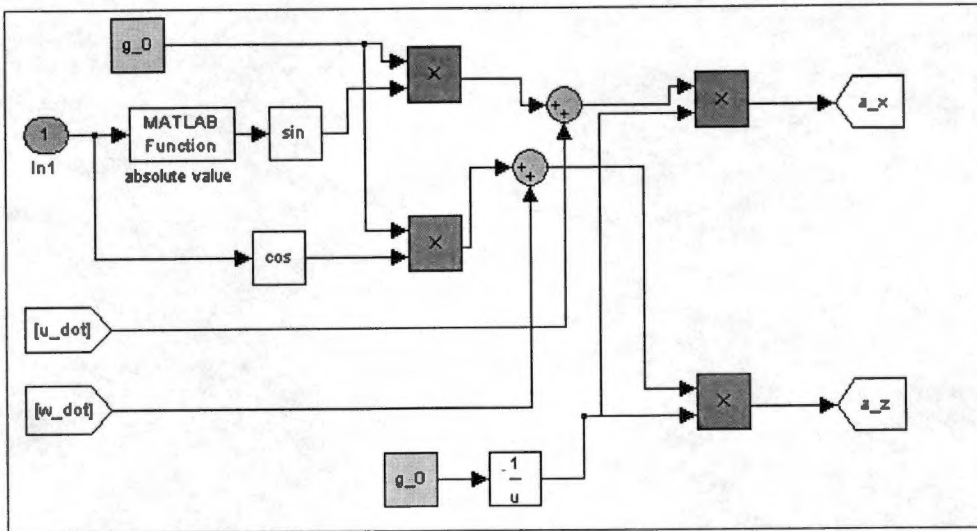


Figure 6-21
Accelerations Block

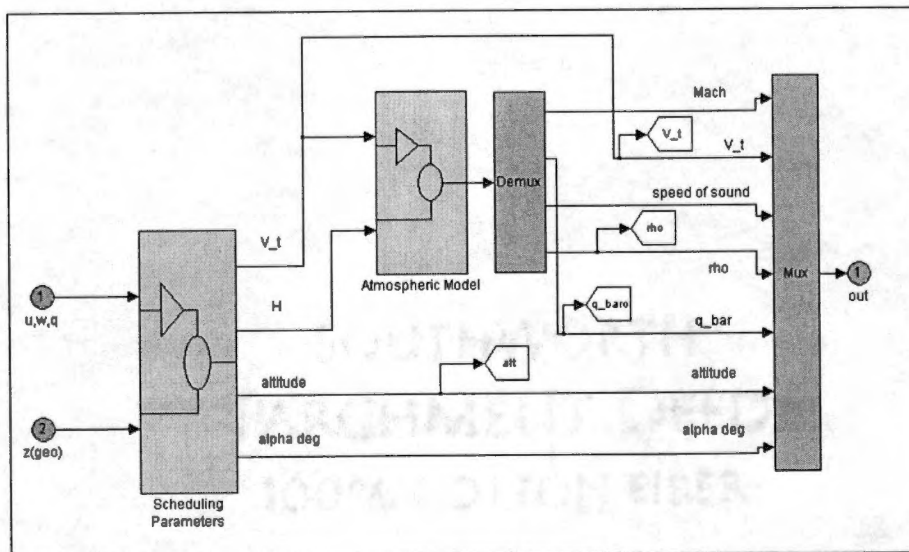


Figure 6-22
Atmosphere + Parameter Block

ATMOSPHERE + PARAMETER (figure 6-22)

This sub-system consists of the ATMOSPHERIC MODEL and the SCHEDULING PARAMETERS blocks.

ATMOSPHERIC MODEL (figure 6-23)

This sub-system calculates Mach number, dynamic pressure, speed of sound and air density using:

$$Mach = \frac{Vt}{sos}$$

$$qbar = \frac{1}{2} \cdot \rho \cdot Vt^2 \quad (N/m^2)$$

$$sos = sos_sea_level - 0.004 \cdot height \quad (m/s)$$

$$\rho = \rho_sea_level - 0.000094 \cdot height \quad (kg/m^3)$$

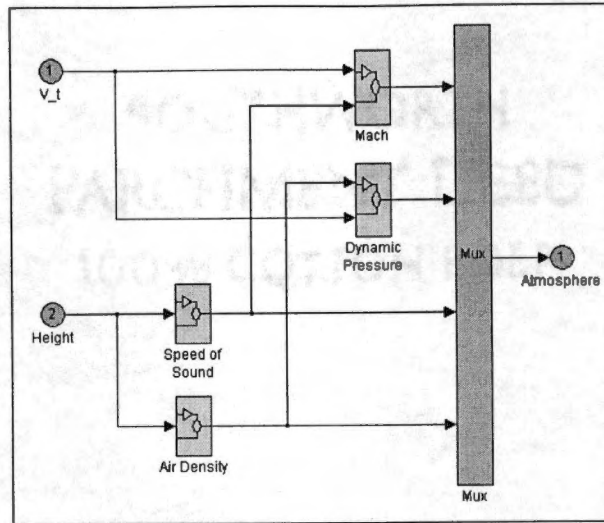


Figure 6-23
Atmospheric Model

SCHEDULING PARAMETERS block (figure 6-24)

This sub-system calculates total velocity, altitude and angle of attack using:

$$V_t = (u^2 + w^2)^{1/2} \quad (\text{m/s})$$

$$\text{height} = z \quad (\text{m})$$

$$\text{alt} = 0.001 * z \quad (\text{km})$$

$$\alpha = \arctan\left(\frac{w}{u}\right) \quad (\text{deg})$$

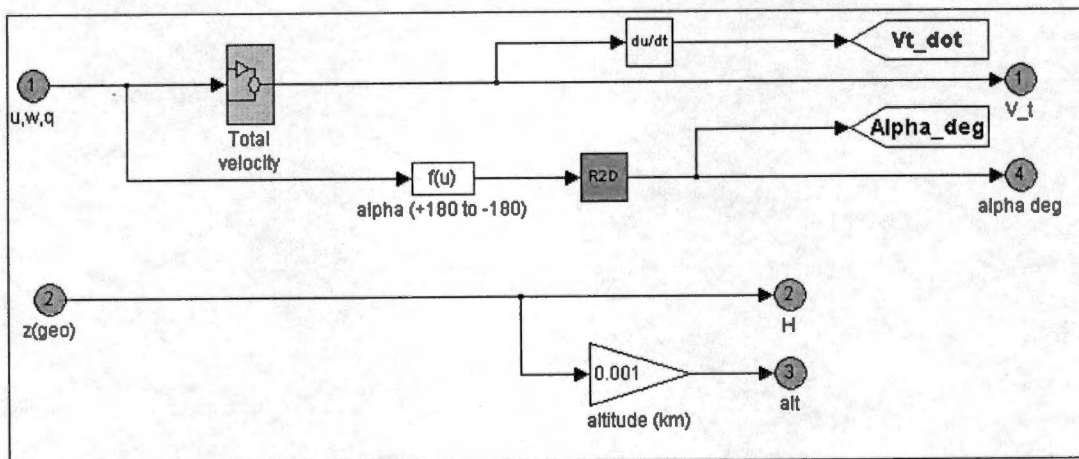


Figure 6-24
Scheduling Parameters Block

CHAPTER 7

SIMULATION RESULTS

The SIMULINK model presents the results by means of "scope windows". Examples of these scopes for six different parameters (control surfaces, pitch rate, angle of attack, total velocity, longitudinal acceleration and vertical acceleration) are shown in figures 7-1 and 7-2.

In this chapter the simulation results are presented for four different trim airspeeds: 129 km/h (36 m/s), 155 km/h (43 m/s), 190 km/h (53 m/s) and 207 km/h (57.5 m/s). Besides changing the trim airspeed, since the simulation also allows the user to change the "shape" of the input (airbrakes position), different operating speeds can be simulated. The results presented in this chapter correspond to sudden deployment and retraction maneuvers (fast operating speeds).

TIME HISTORIES FROM SIMULATION AND FLIGHT TESTS

The simulation time histories for airbrakes position, longitudinal acceleration and vertical acceleration are presented in figures 7-3 to 7-6 and compared to those obtained from the flight tests. A good correspondence between both can be observed. This comparison provides a means to analyze the validity of the simulation and, specifically, of the airbrake-related derivatives obtained from the wind tunnel experiments.

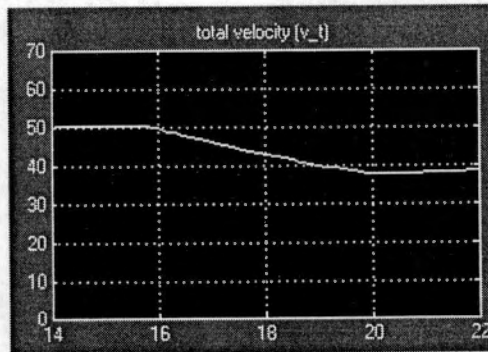
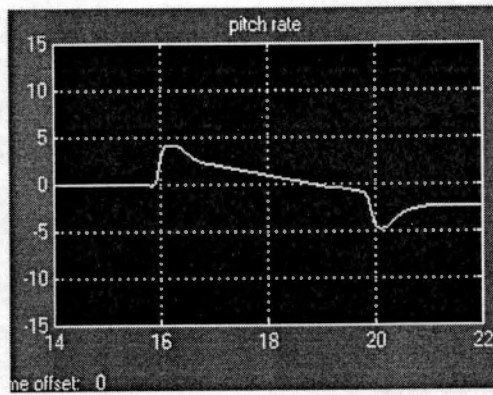
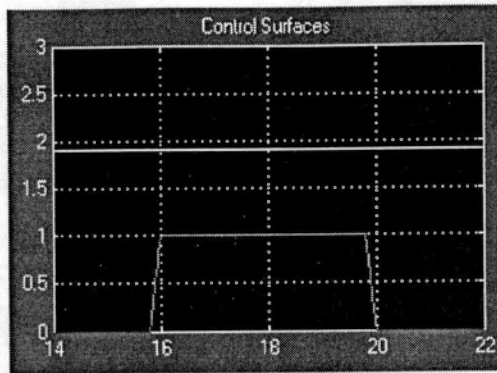


Figure 7-1

Simulation scope windows. The trim airspeed is 50 m/s (180 km/h)

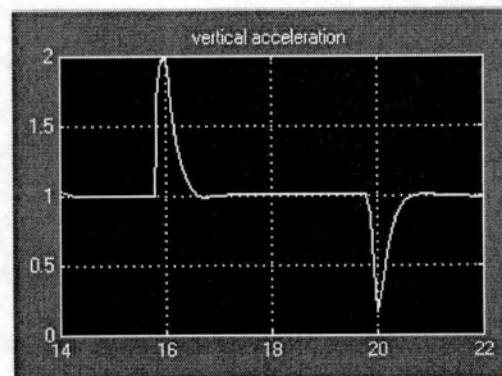
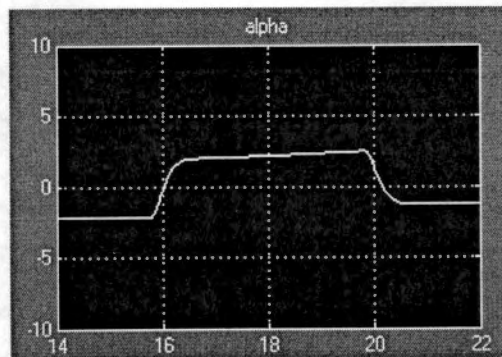
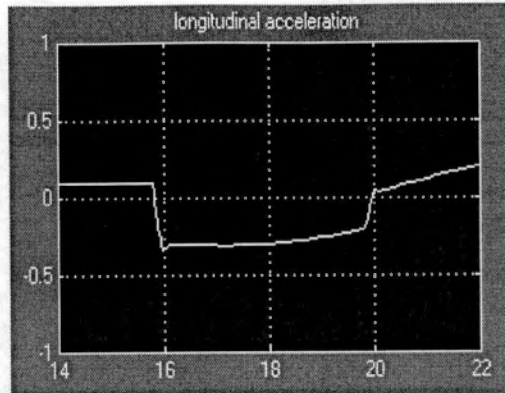


Figure 7-2

Simulation scope windows. The trim airspeed is 50 m/s (180 km/h)

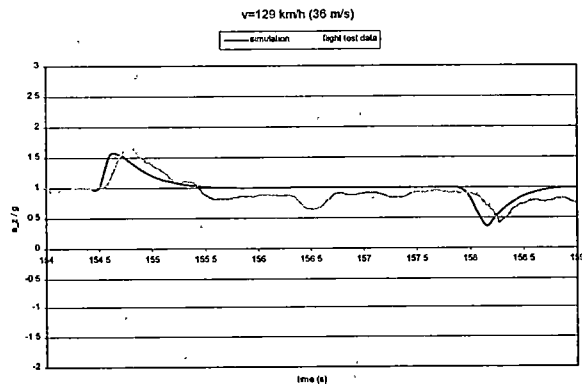
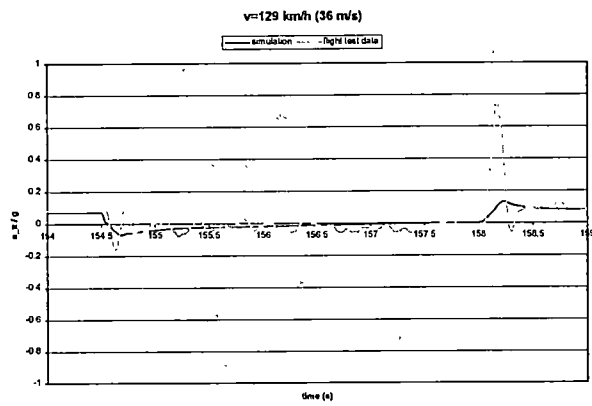
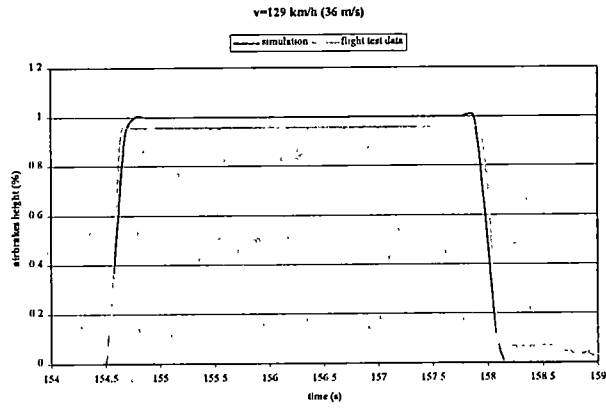


Figure 7-3
Simulation-Flight test results

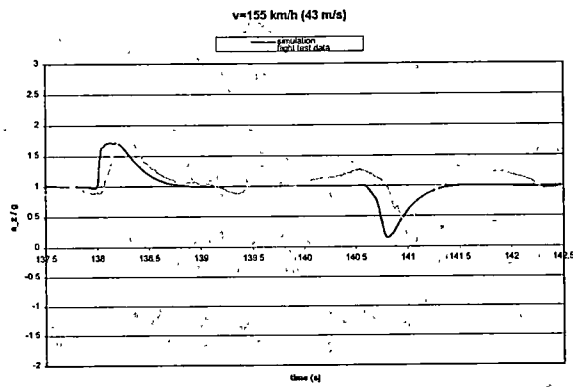
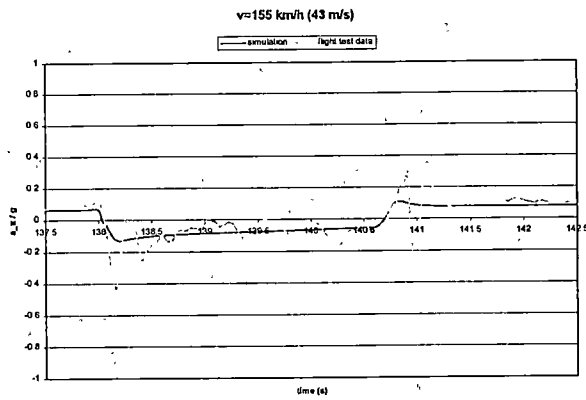
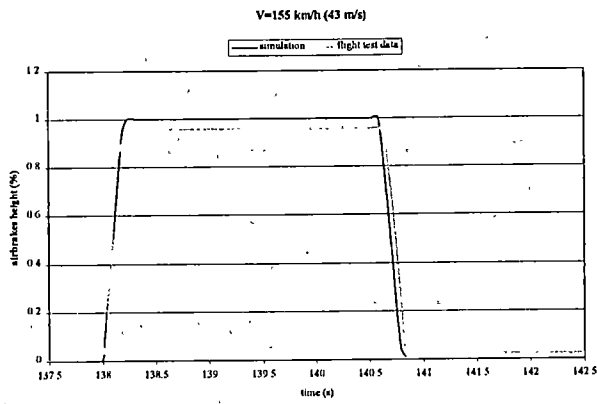


Figure 7-4
Simulation-Flight test results

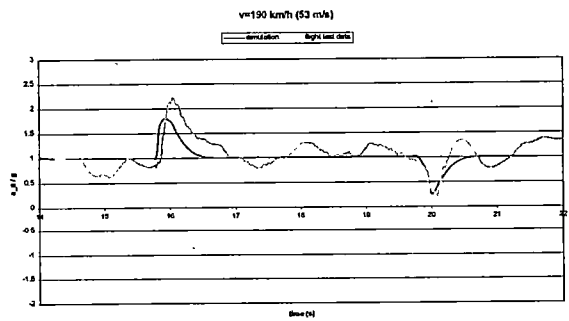
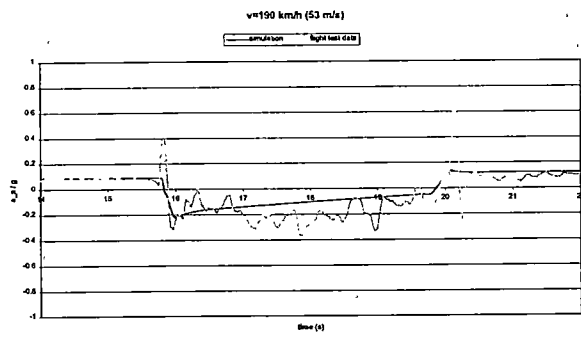
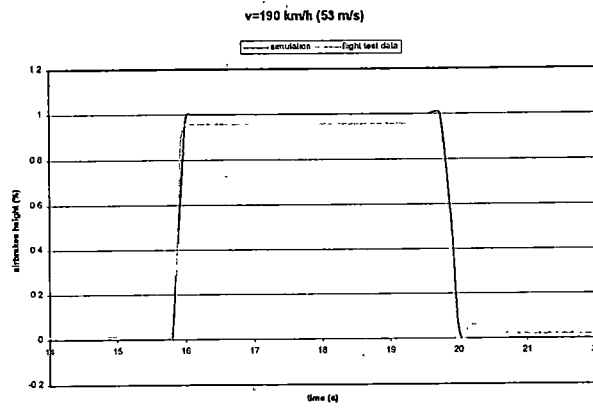


Figure 7-5

Simulation-Flight test results

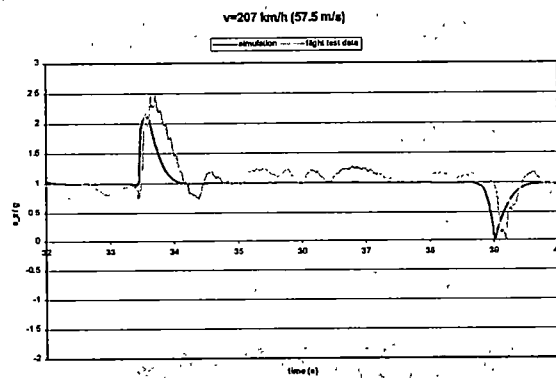
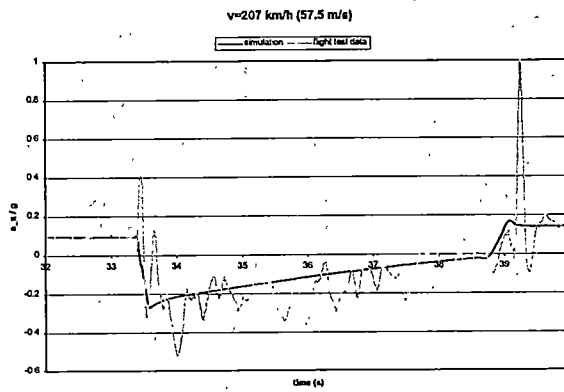
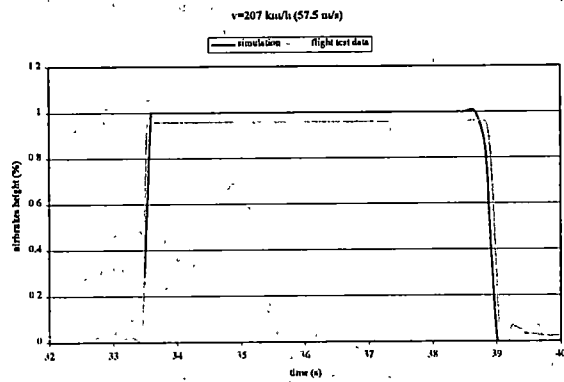


Figure 7-6

Simulation-Flight test results

RESULTS FROM SIMULATION AND FLIGHT TESTS

The longitudinal and vertical accelerations generated after the airbrakes operation are summarized in figures 7-7 and 7-8. A good correlation between the simulation and the flight test results is observed. See also figures 5-12 and 5-13.

Regarding the pitching motion, the simulation shows that at high airspeeds (above approximately 190 km/h) an abrupt full deployment of the airbrakes leads to an initial pitch up motion, and then a slight pitch down motion develops. At low airspeeds the initial tendency is to pitch down and the nose-down motion develops faster than in the high airspeed cases.

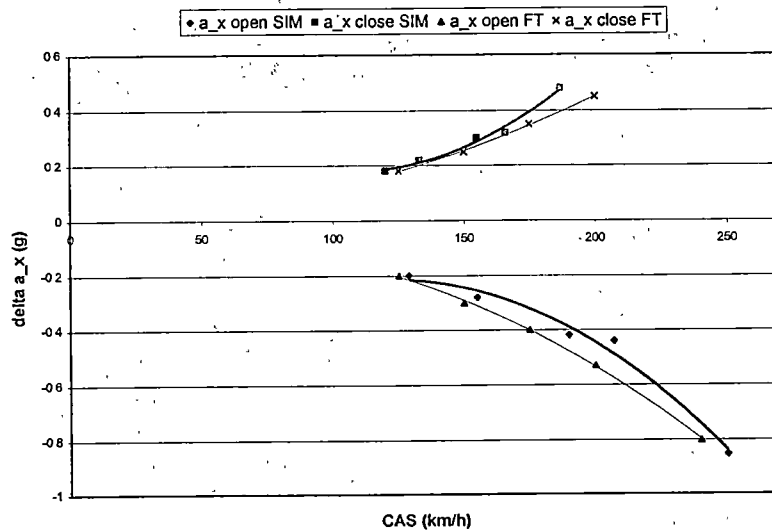


Figure 7-7

Simulation and flight test results - Longitudinal acceleration generated after a sudden deployment and retraction of the airbrakes

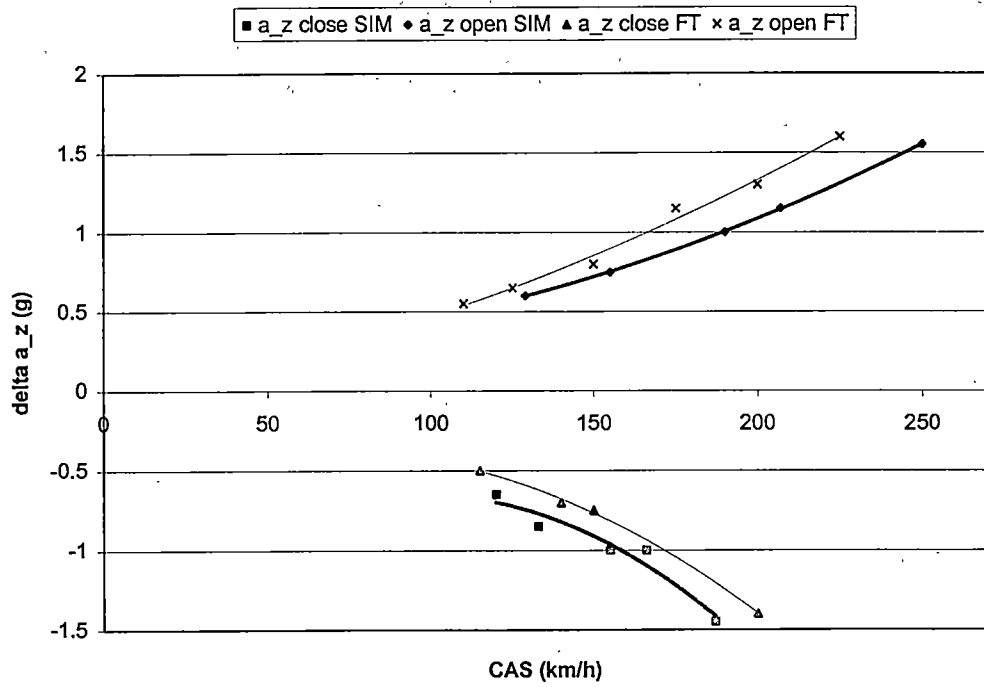


Figure 7-8

Simulation and flight test results - Vertical acceleration generated after a sudden deployment and retraction of the airbrakes

Partial deployments were also investigated using the simulation. The following partial heights were used as airbrake control inputs: 10%, 25%, 50%, 75% and 100%. The results for an airspeed of 53 m/s (190 km/h) are shown in figures 7-9 and 7-10.

Figure 7-9 is a plot airspeed vs % of deployment for an example trim airspeed. It indicates how much the sailplane airspeed will decrease after a partial deployment of the airbrakes in a given time span (4 seconds in this case). Figure 7-10 shows, for the same trim airspeed, the longitudinal and vertical accelerations generated after the airbrakes operation. The airspeed when closing is assumed the same as the airspeed when opening.

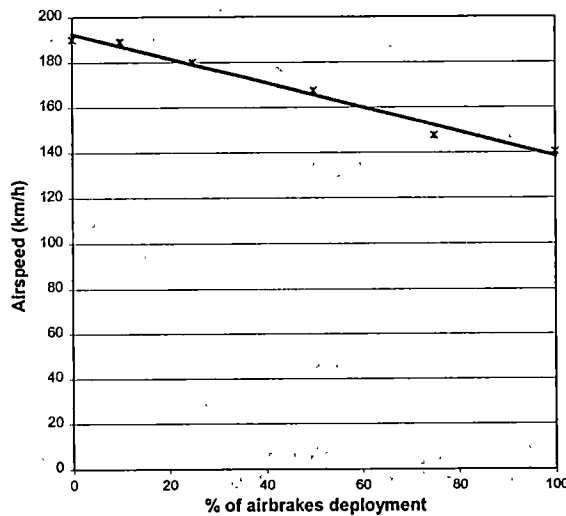


Figure 7-9

Partial deployments at 53 m/s
Airspeed after 4 seconds vs % of airbrakes deployment

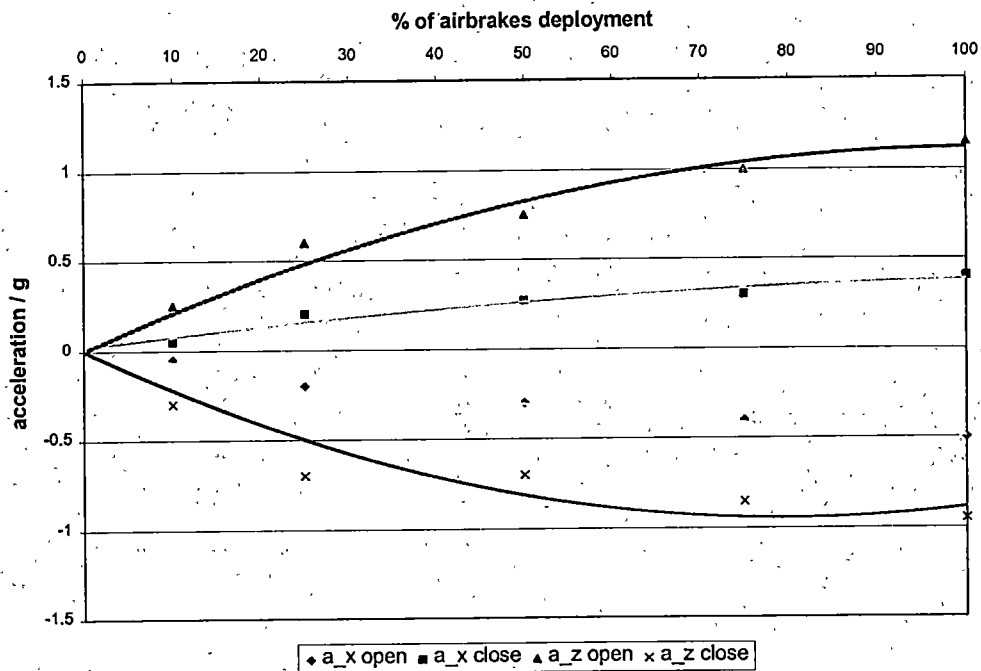


Figure 7-10
 Partial deployments at 53 m/s
 Longitudinal and vertical accelerations vs % of airbrakes deployment

It can be concluded from figure 7-10 that the vertical acceleration is more sensitive to partial airbrakes deployments than the longitudinal acceleration; i.e., for a 25% deployment the delta in vertical acceleration is about 50% of its maximum delta, while the delta in longitudinal acceleration is only about 30% of its maximum delta.

Regarding the pitching motion generated after partial deployments of the airbrakes, the simulation shows (always considering abrupt -step inputs- deployments and retractions) that the initial pitch up tendency of the aircraft at high speeds disappears for

partial deployments of 50% or less; the induced pitching motion is nose down since the beginning of the opening maneuver for these partial deployments.

A simplified explanation of this phenomenon is given in figure 7-11. Observe that the deployed airbrakes generate a reduction in the lift force (which translates in this case to a delta in the vertical force, ΔZ) and an increase in the drag force (which translates in this case to a delta in the longitudinal force, ΔX). The resultant moment will depend on the sailplane dimensions and on the magnitude of these airbrakes-induced forces. This simplified explanation does not consider the change in pitching moment coefficient.

In any case (full or partial deployments) the maximum airbrakes-induced pitch rates are small (about $-3 \text{ }^\circ/\text{s}$).

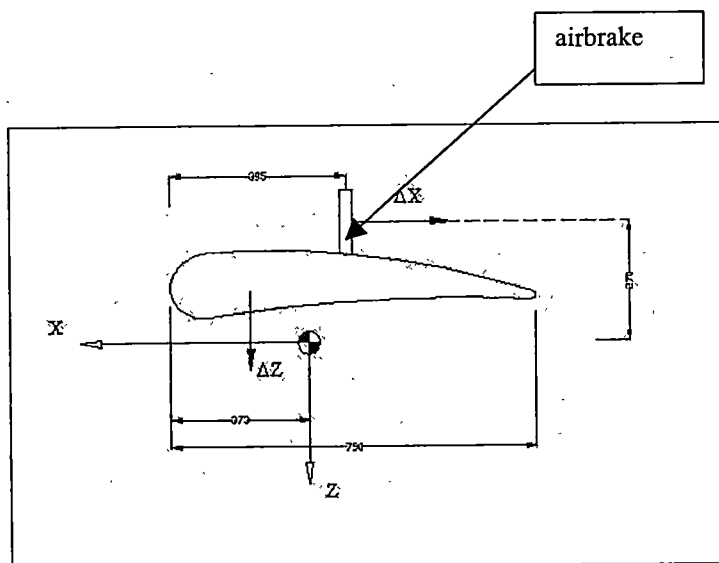


Figure 7-11

Simplified airbrake over the wing surface

CHAPTER 8

CONCLUSIONS AND RECOMMENDATIONS

General conclusions and recommendations are presented in this chapter. For convenience, several specific conclusions and observations were discussed while presenting the results for both flight tests and simulation. The reader should refer to Chapters 5 and 7 for these specific conclusions.

The flight test program proved to be adequate in order to meet the project objectives; it provided valuable information to investigate the effects of the operation of the airbrakes, in terms of handle forces and accelerations generated. A good correlation between these parameters and the sailplane airspeed was obtained. The investigation also considered different operating speeds over the entire airspeed range.

An analysis of the results of the flight tests regarding forces suggests a revision and possible modification of present airworthiness requirements concerning the airbrake system operating characteristics. The flight test results showed that the current regulations are not satisfied in terms of operating forces. The forces required to close the airbrakes in the LS 8 at high airspeeds were above the limits stated in JAR 22. Also, it was found that at high speeds the sucking forces over the wing were considerably high and will tend to open the airbrakes with no force applied on the handle. The locking mechanism should be properly designed considering these forces.

Regarding the accelerations, it was found that both vertical and longitudinal accelerations generated after the airbrakes operation were small and presented no difficulties to the pilot. The angular accelerations were also small and no dangerous situation (like a sudden pitch-up) occurred. Following the airbrakes deployment, the tendency of the aircraft was to slowly begin a pitch down motion. The accelerations data could be used for structural design purposes.

In order to isolate the airbrakes, the control stick was held in a fixed position during the maneuver. A recommendation for future testing would be to consider a fixture or gadget to prevent inadvertent operation, especially when testing at high speeds.

The theoretical analysis of the simulation helped to understand the airbrakes effects and provided with a way to extrapolate results to conditions not tested (like V_{NE}) and to simulate the effects of partial deployments. Good comparisons were obtained between flight tests and simulation results.

The good coordination among the test team members, and their different and complementary backgrounds were determinant for the project success. The author considers very important the fact of participating in the testing as an on-board flight test engineer.

Finally, the author strongly recommends continuing and enhancing the partnership

agreement between the University of Tennessee Space Institute and the Institute of Aeronautics and Astronautics of the Technical University of Aachen.

REFERENCES

REFERENCES

1. Bernier, R., Parkinson, G.V., "Oscillatory Aerodynamics and Stability Derivatives for Airfoil Spoiler Motions", AGARD CP-235
2. Brown, S.C., Hardy, G.H., Hindson, W.S., "A Flight-Test and Simulation Evaluation of the Longitudinal Final Approach and Landing Performance of an Automatic System for a Light Wing Loading STOL Aircraft Equipped with wing spoilers". NASA-TM-85873, 1984.
3. Cook, M.V., "Flight Dynamics Principles, New York. John Wiley & Sons, Inc., 1997.
4. DLR & Idaflieg, LS 8 Measured Polars, Idaflieg Summer Meeting, 1995 .
5. Etkin, B., "Dynamics of Flight". John Wiley & Sons, Inc., 1982.
6. FAA Human Factors Design Guide, 1996. DOT/FAA/CT-96/1, FAA Technical Center, Atlantic City International Airport, NJ 08405
7. Gerlach, O.H., "Determination of Performance and Stability Parameters From Nonsteady Flight Test Maneuvers, Society of Automotive Engineers, March 1970.
8. Iliff, K.W., Maine, R.E., Montgomery, T.D.. "Considerations in the analysis of flight test maneuvers", Ninth Symposium of the Society of Flight Test Engineers. Arlington, TX, October 4-7, 1978
9. JAR 22 – Sailplanes and Powered Sailplanes
10. Johnson, R.H., "Sailplane Performance Measurements", Soaring Magazine, April 1968.

11. Kimberlin, R., "Lecture Notes on Flight Testing", The University of Tennessee Space Institute.
12. Kirschstein, S., Wind Tunnel Measurements to Determine Airbrakes Characteristics, Institute for Aeronautics and Astronautics, Technical University of Aachen, Germany, 2000.
13. Klein, V., "Determination of Longitudinal Aerodynamic derivatives from steady-state measurement of an aircraft" The George Washington University JIAFS/NASA Langley Research Center, 1977.
14. Lamson, R.T., "Possible Overloading of Sailplane Wings In Bending Through Spoiler Operation At High Speed, Technical Soaring, Vol VI, NO. 3, 1981.
15. Matlab Signal Processing Toolbox User's Guide
16. Matteson, F.H., "Considerations on Dive Brakes", Aero Revue September 1968
17. Merklein, H.J., "Flight Performance Measurements On Twelve Sailplanes", Aero Revue, October 1964.
18. Milgram, J., "Flight testing Sailplanes at the Idaflieg Summer Meet", Soaring magazine, April 1999.
19. Morelli, P., "On the Dynamic Response of Sailplanes to Longitudinal Manoeuvres", Aero Revue, May 1967
20. Paiewonsky, B., "A Flight Test Program For Examining Sailplane Lateral-Directional Stability and Control", Soaring Magazine, February 1969.
21. Parkinson, G.V., Tam Doo, P., Bernier, R., "A Prediction Method for Spoiler Performance", SAE 770459

22. Perry, M.A. (Editor), "Flight Test Instrumentation", Proceedings of the Third International Symposium, 1964.
23. Reithmaier, L., "The Aviation/Space Dictionary", Aero, 1990.
24. Rolladen-Schneider Flugzeugbau GmbH, LS8 Detailed Drawing.
25. Rolladen-Schneider Flugzeugbau GmbH, LS8 Maintenance Handbook.
26. Rolladen-Schneider Flugzeugbau GmbH, LS8 Operating Handbook.
27. Rotondi, G., "Sulla Risposta Di Un Aliante Ad Una Brusca Manovra Dei Diruttori", 1964.
28. Stafiej W., "Loading Consequences Of The Wing Upper Surface Air Brake", Technical Soaring, Vol VI, NO. 3, 1981.
29. Thomas, F., "Fundamentals of Sailplane Design". College Park Press, 1999.
30. USAF, "Digital Datcom", 1976.
31. Waibel, G., "Special Problems in the Flight Testing of Sailplanes", Seventh Annual Society of Experimental Test Pilots European Section Symposium, April 1975.
32. Wolowicz, C.H., "Considerations in the Determination of Stability and Control Derivatives and Dynamic Characteristics From Flight Data", 1966, AGARD Report 549-Part I.

APPENDICES

APPENDIX A

Trim program (listing).

```
%TRIM program
```

```
clear all;  
V_t=50;  
H=1000;
```

```
m=345.0;           %Sailplane mass (kg)  
Iy=447.6;         %Moment of Inertia y-Axis (kg.m^2)  
S=10.50;         %Wing area (m^2)  
l=0.70;          %MAC  
g_0=9.81;        %Acceleration of gravity at sea level  
rho_sl=1.225;    %Air Density at sea level  
s_sl=340.0;      %Speed of Sound at sea level
```

```
rho= rho_sl - 0.094*H/1000.0;  
d2r = pi / 180;  
r2d = 180 / pi;
```

```
%Aerodynamic  
tables_LS8;  
Cl_q=4.051;  
Cm_q=-27.94;
```

```
alpha_trim=-4.0;  
gamma=-0.001;
```

```
Cl=0.0001;  
Cd=0.0001;  
Cm=0.0;
```

```
while abs(V_t^2+(2*m*g_0*sin(d2r*gamma))/(rho*S*Cd))> 0.01 | abs(V_t^2-  
(2*m*g_0*cos(d2r*gamma))/(rho*S*Cl)) > 0.01
```

```
alpha_trim=alpha_trim+abs(V_t^2+(2*m*g_0*sin(d2r*gamma))/(rho*S*Cd))/50000
```

```
var1=interp1(alpha3,table_Cm_alpha3,alpha_trim,'linear')
```

```
eta=interp1(table_Cm_eta1,eta1,-var1,'linear')
```

```
var9=interp1(eta1,table_Cm_eta1,eta,'linear')
```

```
Cm=var1+var9
```

```
var3=interp1(alpha1,table_Cl_alpha1,alpha_trim,'linear');
```

```
var4=interp1(eta1,table_Cl_eta1,eta,'linear');
```

```
Cl=var3+var4
```

```
var5=interp1(alpha2,table_Cd_alpha2,alpha_trim,'linear');
```

```
var6=interp2(eta1,alpha1,table_Cd_eta1_alpha1,eta,alpha_trim,'linear');
```

```
Cd=var5+var6
```

```
gamma=r2d*atan(-Cd/Cl)
```

```
error1=abs(V_t^2+(2*m*g_0*sin(d2r*gamma)/(rho*S*Cd)));
```

```
error2=abs(V_t^2-(2*m*g_0*cos(d2r*gamma)/(rho*S*Cl)));
```

```
end
```

```
Theta=alpha_trim+gamma;
```

```
tsim=[14.0 15.8 16.0 19.8 20.0 22.0]';
```

```
usim=[eta eta eta eta eta eta;0 0 1 1 0 0]';
```

```
Theta_0=Theta*d2r;
```

```
Uk_0 = V_t*cos(alpha_trim*d2r);
```

```
Wk_0 = V_t*sin(alpha_trim*d2r);
```

```
H_0=H;
```

APPENDIX B

M-file - Derivatives look-up tables (listing).

% LOOK-UP TABLES

alpha1=[-4.0 -3.0 -2.0 -1.0 0.0 1.0 2.0 3.0 4.0 5.0 6.0 7.0];

alpha2=[-4.12 -3.71 -3.26 -2.81 -2.31 -2.18 -1.90 -1.63 -1.59 -1.23 -0.73 0.00 0.54 0.95 1.58 2.21 3.21 3.80 4.79
6.01 6.69];

alpha3=[-4.0 -3.0 -2.0 -1.0 0.0 1.0 2.0 3.0 4.0 5.0 6.0 7.0];

alpha4=[-6.4 -5.4 -4.4 -3.4 -2.4 -1.4 -0.4 0.6 1.6 2.6 3.6 4.6 5.6 6.6 7.6 8.6 9.6 10.6 11.6 12.6 13.6];

eta1 = [-15.0 -10.0 -5.0 0.0 5.0 10.0 15.0 20.0 25.0];

s= [0 0.1 0.2 0.3 0.4 0.5 0.6 0.7 0.8 0.9 1.0];

%DATCOM table_Cl_alpha1=[0.049 0.128 0.208 0.288 0.369 0.449 0.530 0.611 0.691 0.763 0.828 0.888 0.941
0.987 1.023 1.034];

table_Cl_alpha1=[0.005 0.13 0.24 0.35 0.46 0.57 0.69 0.80 0.90 1.05 1.12 1.20];

%DATCOM table_Cd_alpha1=[0.012 0.013 0.013 0.014 0.015 0.017 0.018 0.021 0.023 0.026 0.028 0.031];

table_Cd_alpha2=[0.0100 0.0100 0.0100 0.0100 0.0105 0.0105 0.0095 0.0095 0.0095 0.0100 0.0110 0.0120
0.0130 0.0135 0.0155 0.0165 0.0190 0.0220 0.0250 0.0315 0.0410];

table_Cm_alpha3=[0.0559 0.0449 0.0339 0.0226 0.0104 -0.0031 -0.0179 -0.0338 -0.0512 -0.0728 -0.0978 -
0.1256];

table_Cl_eta1=[-0.052 -0.036 -0.018 0.000 0.018 0.036 0.052 0.061 0.064];

table_Cm_eta1=[0.2744 0.1875 0.0937 -0.0002 -0.0937 -0.1875 -0.2745 -0.3210 -0.3382];

table_Cd_eta1_alpha1=[8.85E-04 3.01E-04 -1.19E-05 3.49E-07 3.37E-04 9.98E-04 1.91E-03 2.50E-03
2.73E-03

5.65E-04 8.27E-05 -1.21E-04 5.68E-07 4.46E-04 1.22E-03 2.23E-03 2.87E-03 3.12E-03
2.46E-04 -1.35E-04 -2.30E-04 7.86E-07 5.55E-04 1.43E-03 2.55E-03 3.24E-03 3.51E-03
-7.38E-05 -3.53E-04 -3.39E-04 1.00E-06 6.64E-04 1.65E-03 2.87E-03 3.61E-03 3.90E-03
-3.92E-04 -5.71E-04 -4.48E-04 1.22E-06 7.73E-04 1.87E-03 3.19E-03 3.99E-03 4.29E-03
-7.11E-04 -7.88E-04 -5.56E-04 1.44E-06 8.81E-04 2.09E-03 3.50E-03 4.36E-03 4.68E-03
-1.03E-03 -1.00E-03 -6.65E-04 1.66E-06 9.90E-04 2.30E-03 3.82E-03 4.73E-03 5.07E-03
-1.35E-03 -1.22E-03 -7.73E-04 1.87E-06 1.10E-03 2.52E-03 4.14E-03 5.10E-03 5.46E-03
-1.67E-03 -1.44E-03 -8.83E-04 2.09E-06 1.21E-03 2.74E-03 4.46E-03 5.47E-03 5.86E-03
-1.99E-03 -1.66E-03 -9.92E-04 2.31E-06 1.32E-03 2.96E-03 4.78E-03 5.85E-03 6.25E-03
-2.32E-03 -1.88E-03 -1.10E-03 2.53E-06 1.43E-03 3.18E-03 5.11E-03 6.23E-03 6.65E-03
-2.65E-03 -2.11E-03 -1.22E-03 2.76E-06 1.54E-03 3.41E-03 5.44E-03 6.61E-03 7.06E-03];

table_Cl_s=2*0.7104*0.9036*0.2066*[0		-0.2828	-0.5075	-0.5854	-0.6250	-0.6059	-0.5916	-0.5854	-		
0.5185	-0.5308	-0.5239	0	-0.2644	-0.5676	-0.6455	-0.7289	-0.7705	-0.7377	-0.7125	-0.7063
-0.6776	-0.6489		0	-0.2507	-0.5410	-0.6646	-0.7733	-0.8313	-0.8600	-0.8730	-0.8450
-0.8279	-0.7835		0	-0.2493	-0.5069	-0.5936	-0.7384	-0.8416	-0.9065	-0.9413	-0.9420
-0.9543	-0.9276		0	-0.2657	-0.4918	-0.5697	-0.6879	-0.7753	-0.8867	-0.9317	-0.9871
-1.0137	-1.0158		0	-0.2739	-0.4993	-0.5656	-0.6585	-0.7309	-0.8293	-0.8928	-0.9263
-0.9727	-0.9918		0	-0.2910	-0.5232	-0.5820	-0.6899	-0.7384	-0.8231	-0.8689	-0.8955
-0.9413	-0.9891		0	-0.3033	-0.5444	-0.5888	-0.6933	-0.7453	-0.8293	-0.8655	-0.8962
-0.9256	-0.9925		0	-0.3115	-0.5649	-0.6216	-0.7138	-0.7733	-0.8382	-0.8750	-0.9092
-0.9454	-0.9939		0	-0.3245	-0.5868	-0.6339	-0.7405	-0.7897	-0.8580	-0.8914	-0.9283
-0.9515	-0.9994		0	-0.3477	-0.6134	-0.6653	-0.7562	-0.8245	-0.8744	-0.9235	-0.9433
-0.9918	-1.0328		0	-0.3798	-0.6469	-0.6968	-0.7719	-0.8163	-0.8948	-0.9481	-0.9748
-1.0185	-1.0670		0	-0.3928	-0.6831	-0.7302	-0.7972	-0.8511	-0.9256	-0.9591	-1.0014
-1.0315	-1.0916		0	-0.4215	-0.7097	-0.7603	-0.8204	-0.8696	-0.9454	-1.0021	-1.0321
-1.0513	-1.1018		0	-0.4515	-0.7534	-0.7842	-0.8341	-0.9215	-0.9877	-1.0308	-1.0629
-1.0909	-1.1537		0	-0.4741	-0.7589	-0.7978	-0.8662	-0.9338	-1.0192	-1.0417	-1.0834
-1.1250	-1.1517		0	-0.4891	-0.7555	-0.8067	-0.8723	-0.9447	-1.0240	-1.0800	-1.0923
-1.1332	-1.1701		0	-0.4829	-0.7336	-0.7951	-0.8798	-0.9297	-1.0069	-1.0554	-1.0895
-1.1353	-1.1599		0	-0.3935	-0.6517	-0.7070	-0.7862	-0.8402	-0.9229	-0.9659	-1.0117
-1.0267	-1.0697		0	-0.3415	-0.5779	-0.6332	-0.7309	-0.7910	-0.8839	-0.9304	-0.9550
-0.9857	-1.0219		0	-0.2685	-0.5144	-0.5799	-0.6763	-0.7056	-0.8115	-0.8696	-0.8955
0.9133	-0.9488];										

table_Cd_s=2*0.7104*0.9036*0.2066*[0		0.0690	0.1598	0.1776	0.2124	0.2452	0.2616	0.2835			
0.2999	0.3238	0.3525	0	0.0465	0.1516	0.1646	0.1954	0.2261	0.2609	0.2965	0.3019
0.3183	0.3381		0	0.0410	0.1264	0.1475	0.1872	0.2165	0.2343	0.2685	0.2924
0.3101	0.3252										

0.2876	0.2842	0	0.0321	0.1059	0.1230	0.1598	0.1885	0.2193	0.2411	0.2623
0.2603	0.2726	0	0.0287	0.0936	0.1059	0.1434	0.1742	0.2029	0.2302	0.2459
0.2555	0.2568	0	0.0314	0.0854	0.0977	0.1277	0.1578	0.1872	0.2138	0.2445
0.2445	0.2480	0	0.0314	0.0806	0.0861	0.1182	0.1469	0.1715	0.2056	0.2275
0.2343	0.2206	0	0.0280	0.0847	0.0874	0.1052	0.1373	0.1660	0.2001	0.2186
0.2200	0.2193	0	0.0321	0.0806	0.0820	0.1093	0.1271	0.1537	0.1892	0.2104
0.2070	0.2015	0	0.0273	0.0724	0.0799	0.0943	0.1257	0.1503	0.1721	0.1913
0.1913	0.1858	0	0.0246	0.0697	0.0779	0.0936	0.1148	0.1475	0.1667	0.1940
0.1960	0.1803	0	0.0287	0.0690	0.0779	0.0909	0.1264	0.1551	0.1633	0.1756
0.1940	0.1776	0	0.0273	0.0642	0.0731	0.0970	0.1202	0.1394	0.1653	0.1776
0.1906	0.1865	0	0.0253	0.0663	0.0751	0.0936	0.1271	0.1448	0.1626	0.1783
0.1865	0.1769	0	0.0273	0.0663	0.0731	0.1052	0.1161	0.1380	0.1592	0.1762
0.1742	0.1762	0	0.0232	0.0663	0.0779	0.1004	0.1189	0.1325	0.1544	0.1667
0.1878	0.1851	0	0.0266	0.0663	0.0820	0.1079	0.1223	0.1448	0.1503	0.1776
0.1783	0.1810	0	0.0287	0.0704	0.0806	0.1038	0.1271	0.1503	0.1619	0.1735
0.1831	0.1790	0	0.0184	0.0560	0.0745	0.0990	0.1168	0.1291	0.1503	0.1715
0.1646	0.1660	0	0.0130	0.0512	0.0642	0.0799	0.1011	0.1243	0.1428	0.1592
0.1885	0.1851];	0	0.0198	0.0615	0.0772	0.0936	0.1243	0.1394	0.1496	0.1701

table_Cm_s=2*0.7104*0.9036*0.2066*[0			0.1503	0.3258	0.3443	0.3805	0.4344	0.4146	0.4351		
0.4160	0.4324	0.4959	0	0.1086	0.3306	0.3477	0.3928	0.4433	0.4809	0.5376	0.5191
0.5055	0.5157		0	0.1045	0.2623	0.3026	0.4044	0.4611	0.4502	0.5164	0.5383
0.5485	0.5294		0	0.0977	0.2343	0.2500	0.3354	0.3955	0.4761	0.5000	0.5137
0.5526	0.5328		0	0.0943	0.2165	0.2165	0.2801	0.3299	0.4058	0.4570	0.5021
0.5096	0.5513		0	0.1120	0.2261	0.2165	0.2657	0.3006	0.3648	0.4112	0.4440
0.4857	0.5021		0	0.1195	0.2295	0.2165	0.2828	0.3094	0.3450	0.3900	0.4112
0.4440	0.4905										

0.4208	0.4659	0	0.1100	0.2473	0.2261	0.2746	0.3088	0.3450	0.3928	0.4023
0.4324	0.4816	0	0.1271	0.2493	0.2302	0.2903	0.3265	0.3504	0.3846	0.4126
0.4262	0.4631	0	0.1271	0.2500	0.2363	0.2794	0.3279	0.3600	0.3757	0.4105
0.4495	0.4775	0	0.1236	0.2596	0.2507	0.2883	0.3292	0.3648	0.3955	0.4126
0.4365	0.4857	0	0.1387	0.2575	0.2603	0.2828	0.3122	0.3579	0.3887	0.4023
0.4488	0.4946	0	0.1325	0.2794	0.2616	0.3026	0.3299	0.3661	0.4017	0.4187
0.4590	0.5034	0	0.1557	0.2965	0.2951	0.3135	0.3491	0.3805	0.4269	0.4474
0.4604	0.5164	0	0.1612	0.3094	0.2801	0.3019	0.3409	0.3941	0.4201	0.4529
0.4570	0.5048	0	0.1619	0.3135	0.2746	0.3183	0.3552	0.3969	0.4119	0.4467
0.4727	0.5144	0	0.1735	0.2896	0.2801	0.3252	0.3573	0.4003	0.4215	0.4351
0.4659	0.5069	0	0.1605	0.2869	0.2760	0.3122	0.3545	0.3996	0.4256	0.4454
0.4194	0.4754	0	0.1380	0.2514	0.2398	0.2698	0.3088	0.3593	0.3894	0.4174
0.3866	0.4358	0	0.1059	0.2104	0.1844	0.2329	0.2589	0.3286	0.3600	0.3771
0.3696	0.4146];	0	0.0710	0.1885	0.1776	0.2159	0.2418	0.2937	0.3368	0.3436

table_Cl_alphadot_alpha1=[0.7658 0.7716 0.7760 0.7826 0.7889 0.7898 0.7906 0.7806 0.7631 0.7135 0.6639 0.6236];

table_Cm_alphadot_alpha1=[-4.340 -4.373 -4.398 -4.436 -4.471 -4.476 -4.481 -4.424 -4.325 -4.044 -3.763 -3.534];

APPENDIX C

LS 8 CHARACTERISTICS MEASURED BY IDAFLIEG IN 1995

C_L / C_D

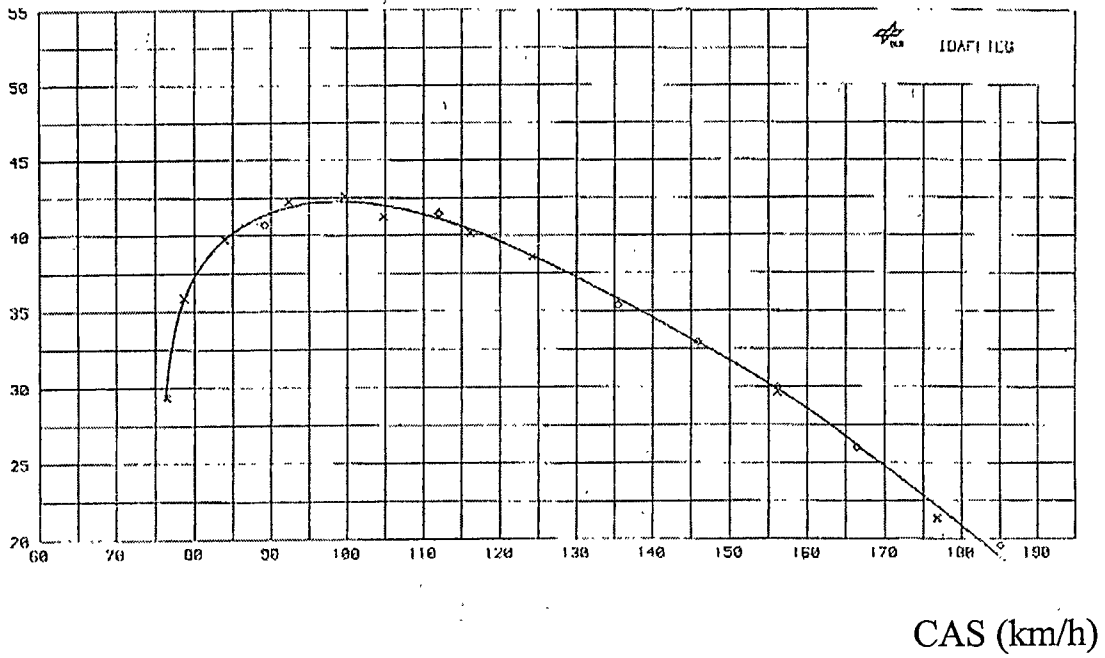
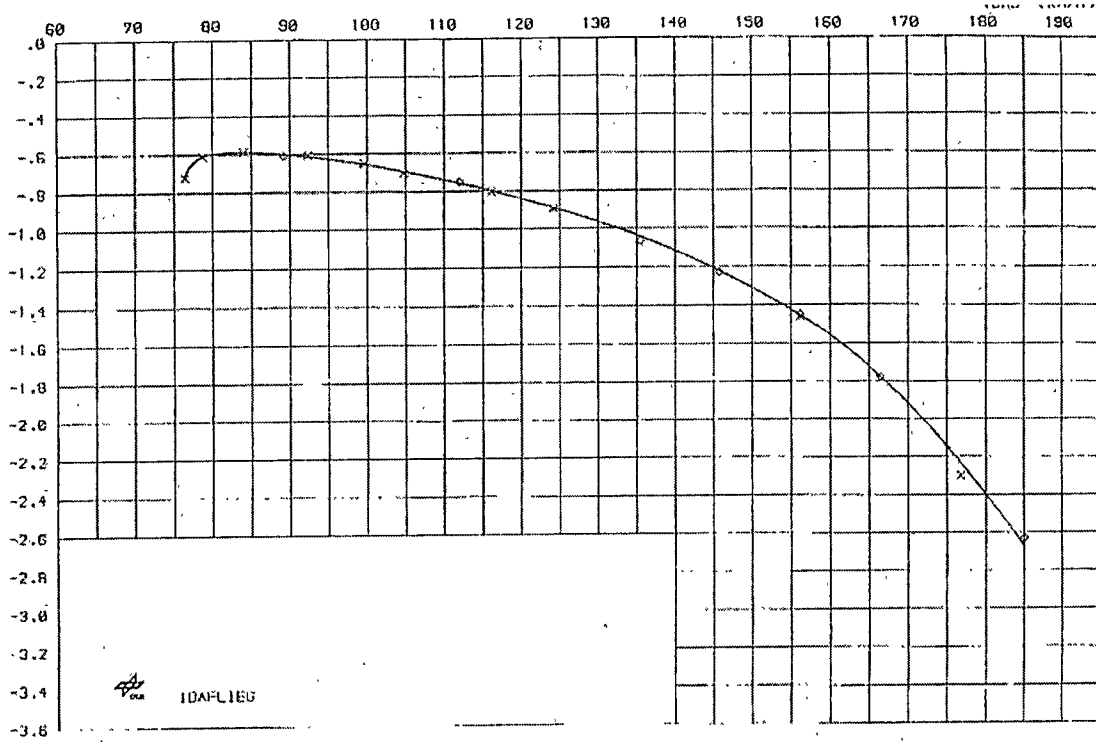


Figure C-1

LS 8 Glide Ratio vs Calibrated Airspeed

CAS (km/h)



Wsink (m/s)

Figure C-2
LS 8 Speed Polar

C_L

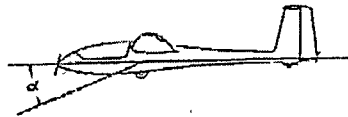
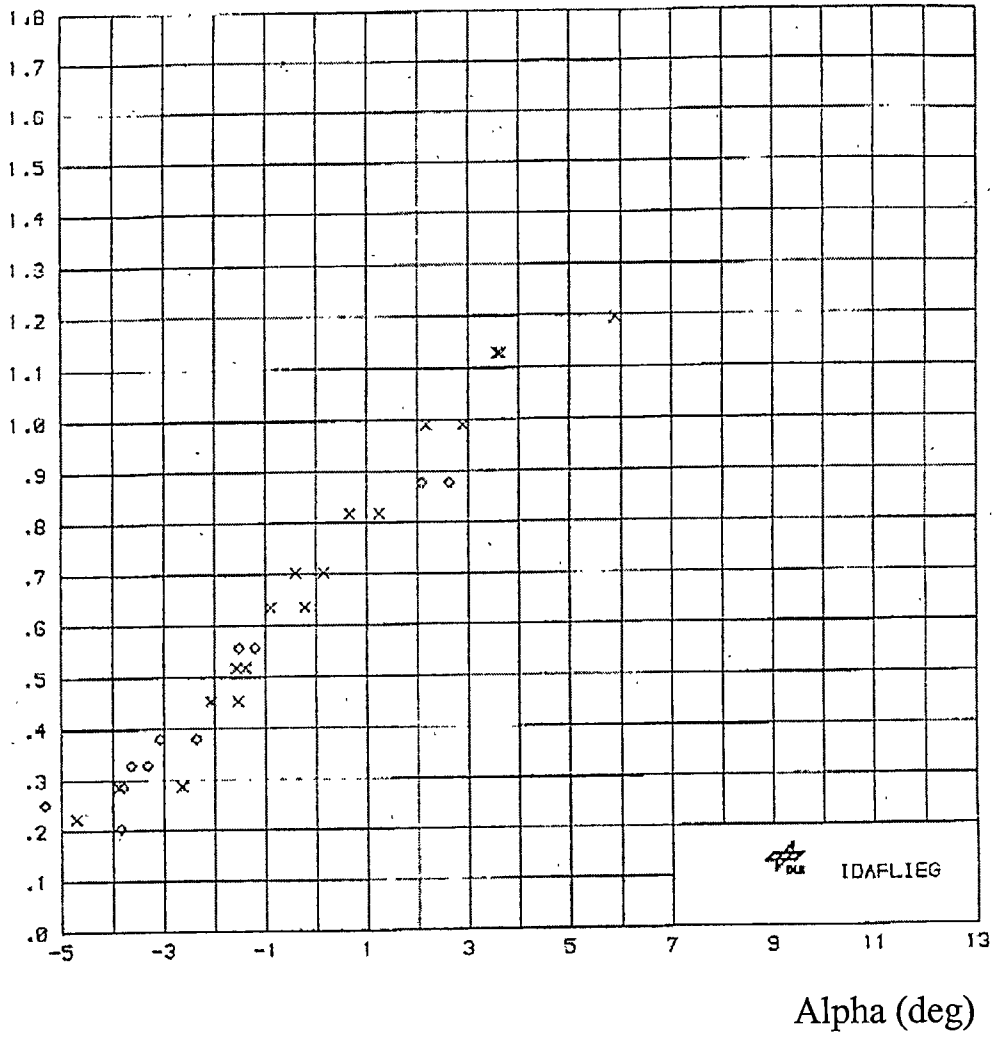
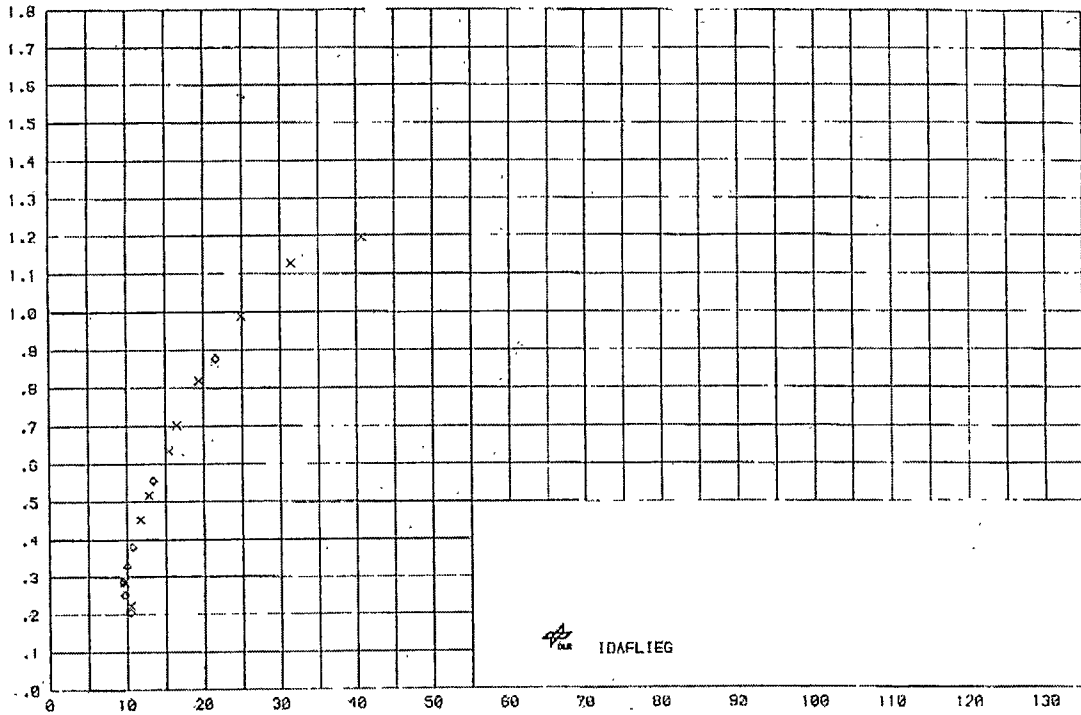


Figure C-3

LS 8 Lift Coefficient vs Fuselage Angle of attack Curve

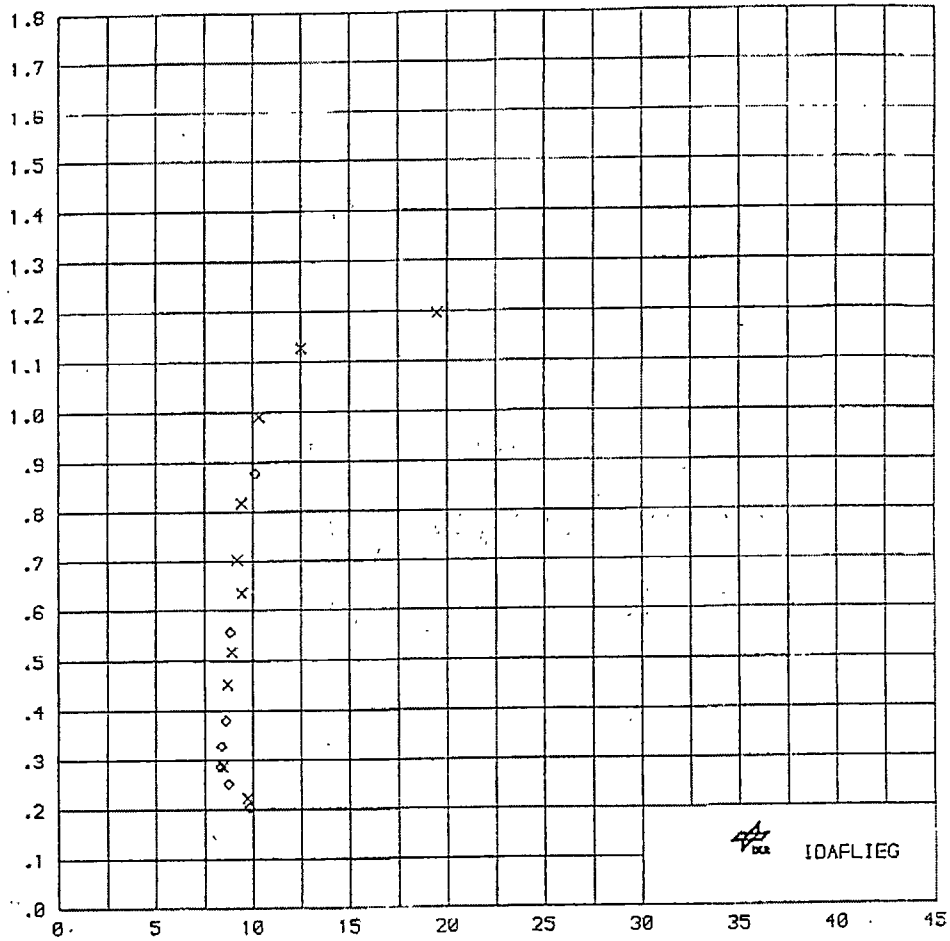
C_L



$C_D * 1000$

Figure C-4
LS 8 Drag Polar

C_L



$(C_D - C_{D1}) * 1000$

Figure C-5

LS 8 Modified Drag Polar

APPENDIX D
LS 8 AIRBRAKE SYSTEM DESCRIPTION

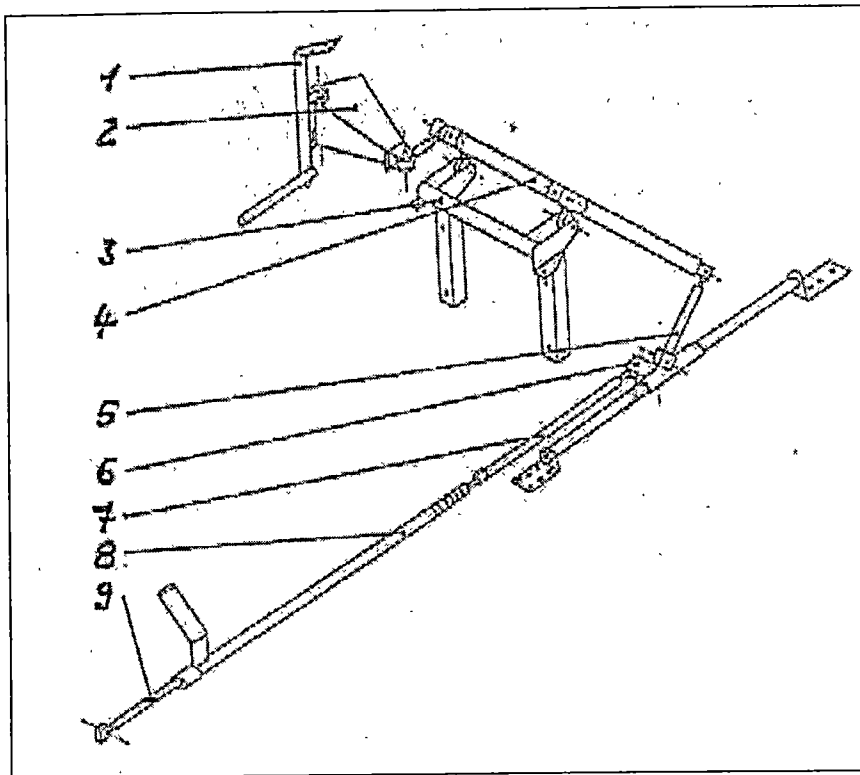


Figure D-1

LS 8 Airbrake Control Mechanism – Fuselage

On the fuselage:

- 1- Bearing for automatic connections
- 2- Automatic connector airbrake-fuselage
- 3- Airbrake connector bearing cage
- 4- Airbrakes lever
- 5- Connection rod
- 6- Ramification
- 7- Pushrod
- 8- Pushrod
- 9- Guiding tube

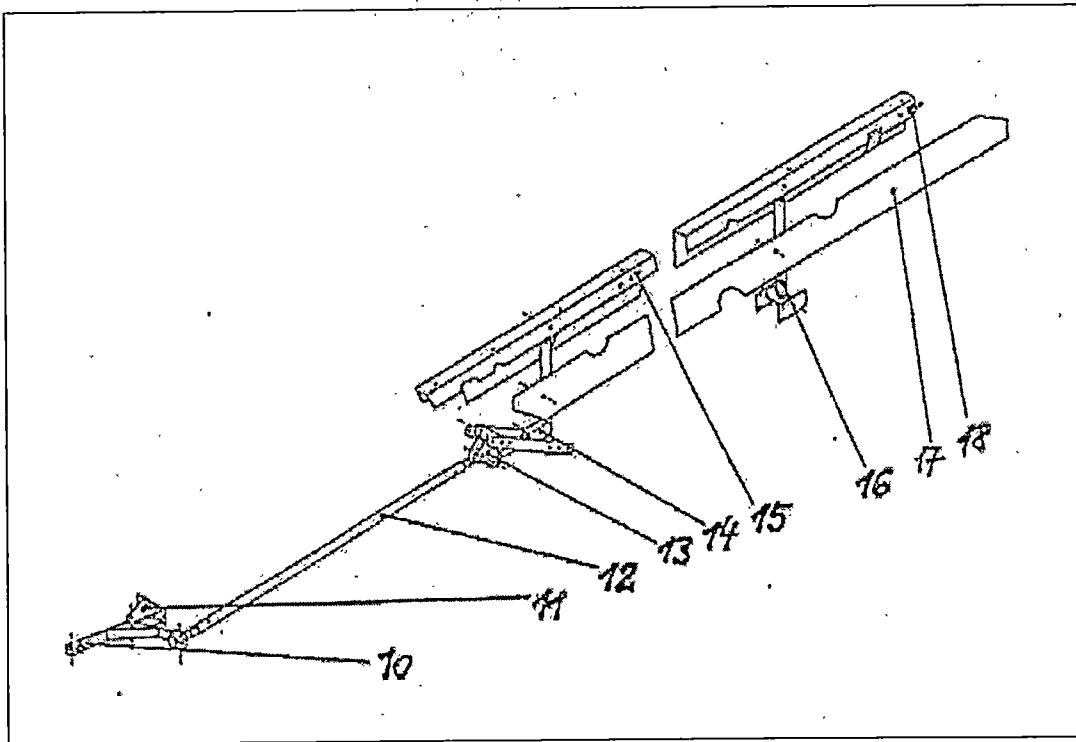


Figure D-2

LS 8 Airbrake Control Mechanism – Wing

On the wing:

- 10- Connector
- 11- Bearing cage
- 12- Push-pull rod
- 13- Locking lever (stop)
- 14- Lever (inner)
- 15- Upper airbrake plate
- 16- Lever (outer)
- 17- Lower airbrake plate
- 18- Friction brake

APPENDIX E

Examples of time histories obtained from the flight tests

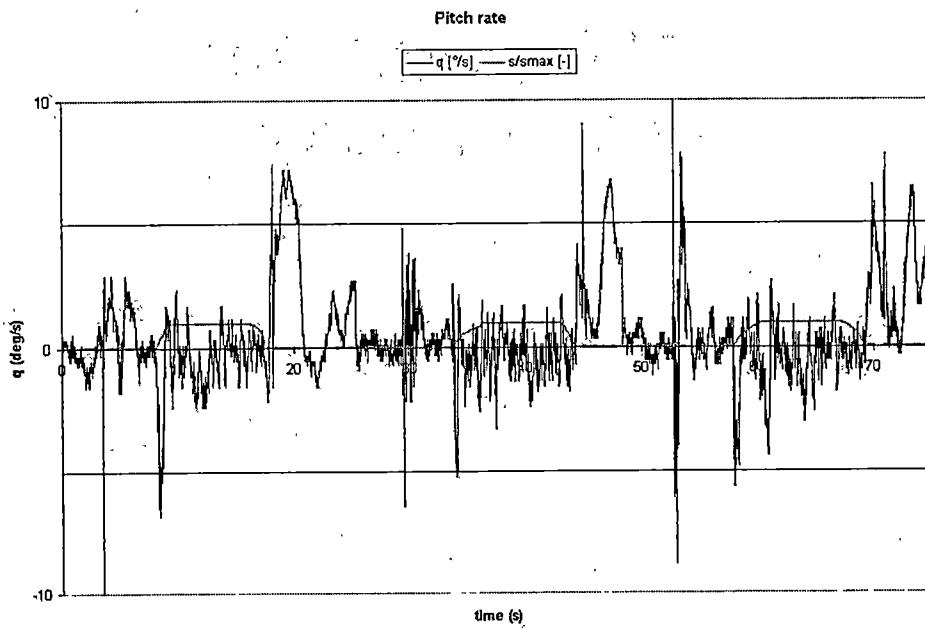
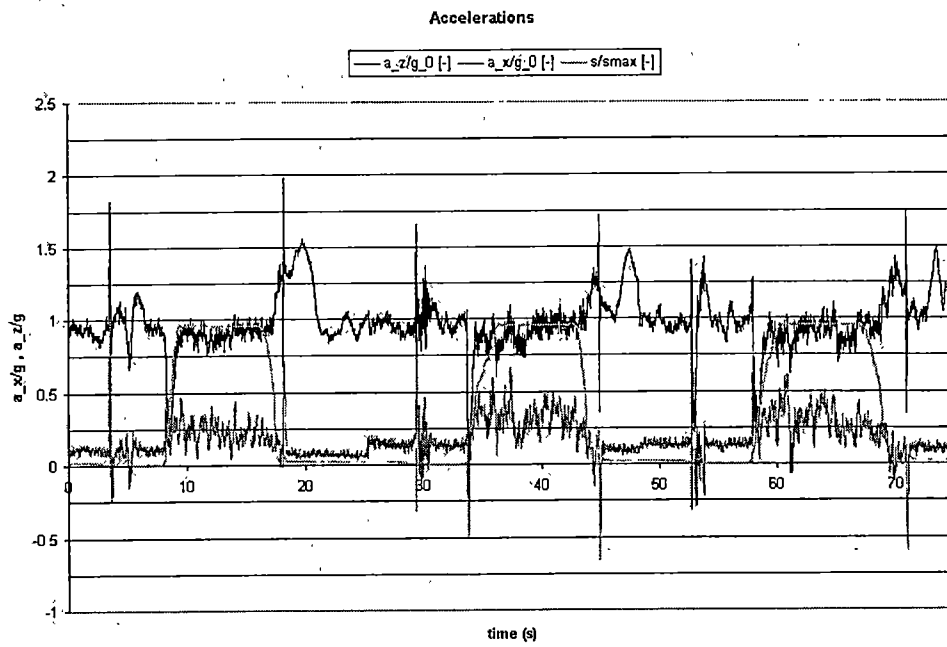


Figure E-1

Flight test Data – Accelerations & Pitch Rate

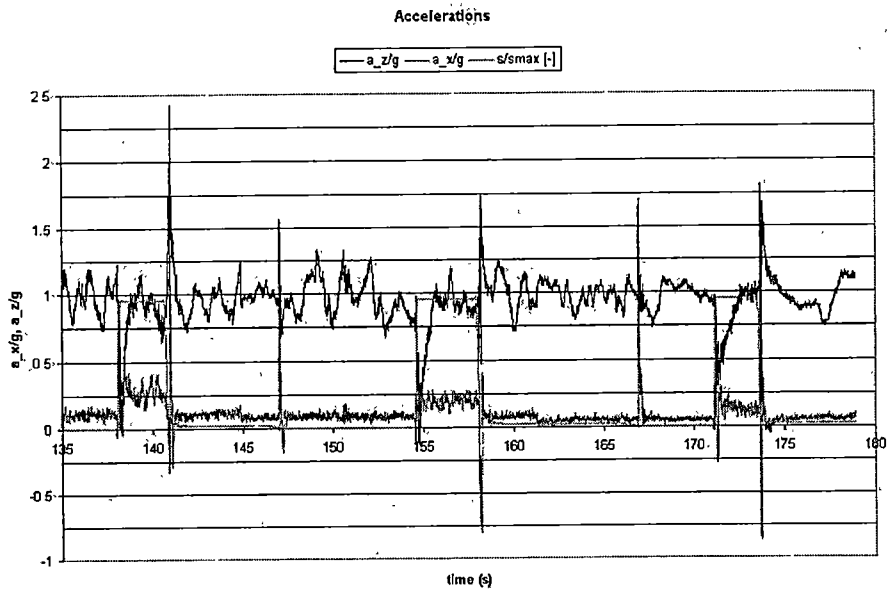
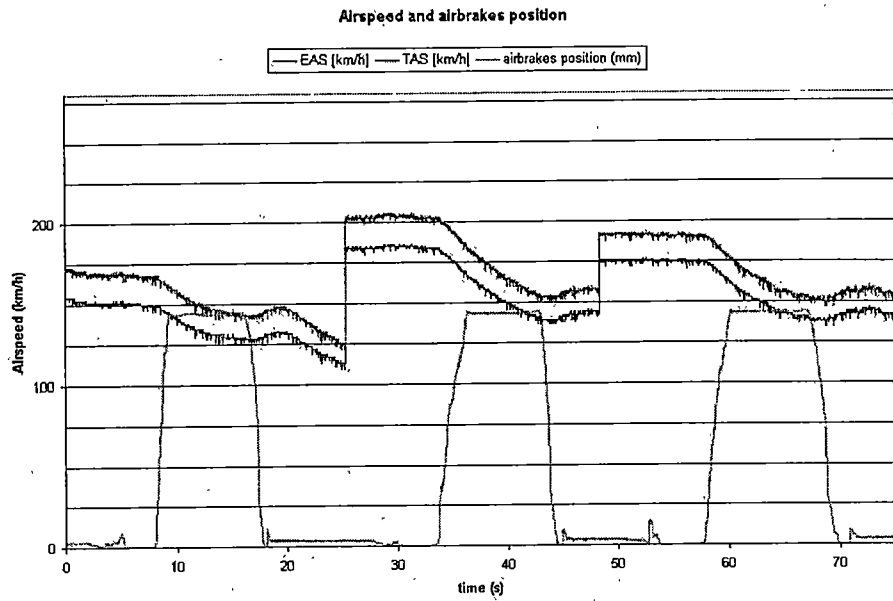


Figure E-2

Flight Test Data – Airspeed, Accelerations and Airbrakes Position

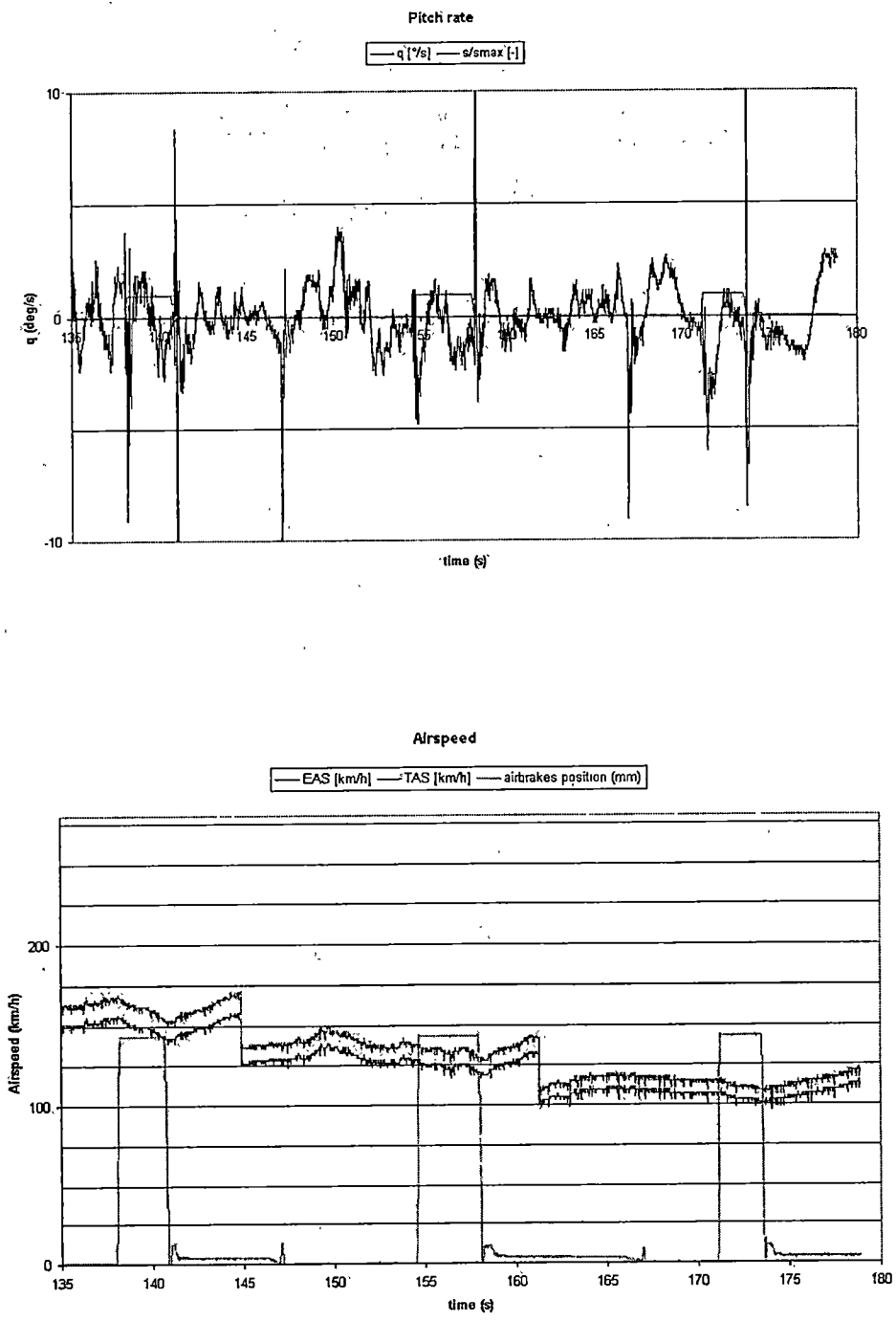


Figure E-3

Flight Test Data – Pitch Rate, Airspeed and Airbrakes Position

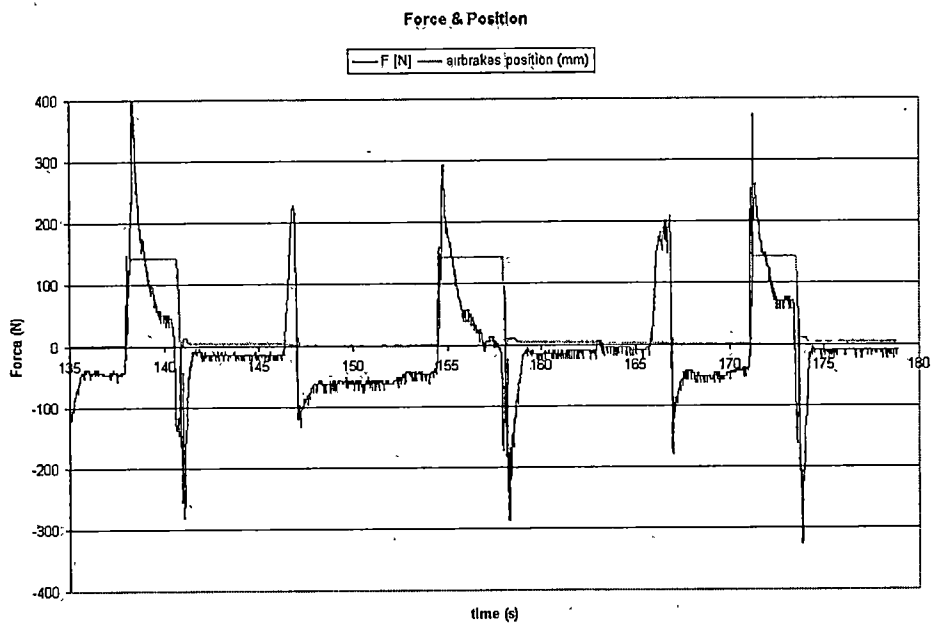


Figure E-4

Flight Test Data – Airbrakes Control Force and Airbrakes Position

VITA

Ignacio Agramunt was born on February 3 1974 in Lima, Peru. He attended Inmaculado Corazon Elementary School and Santa Maria High School, graduating in 1990. He earned a B.S. Degree in Mechanical Engineering from Catholic University of Peru in 1998.

While working at the International Airport of Lima he discovered aviation and decided to pursue a higher level of education that will lead him to work in this industry. After a short work experience in a local factory, he moved to Tennessee to pursue his Master's Degree in Aviation Systems at The University of Tennessee Space Institute (UTSI).

While attending UTSI he got involved with the UTSI Soaring Club, where he learned to fly and ultimately obtained a Private Pilot Glider Certificate. His interest for the sport of soaring and the agreement for partnership between the Institute of Aeronautics and Astronautics of the Technical University of Aachen led him to Germany. He spent the Summer of 2000 in Aachen working in his Master's Thesis.

After completing his Master's Degree in UTSI he will pursue an engineering career in the aeronautical industry.